AD-A129 690 INTERACTION OF THE RADAR WAVES WITH THE CAPILLARY WAVES 1/3
ON THE OCEAN..(U) KANSAS UNIV/CENTER FOR RESEARCH INC
LAWRENCE REMOTE SENSING L.. S BARKESHLI ET AL. MAY 83
UNCLASSIFIED CRINC/RSL-TR-419-1 N00014-79-C-0533 F/G 17/9 NL

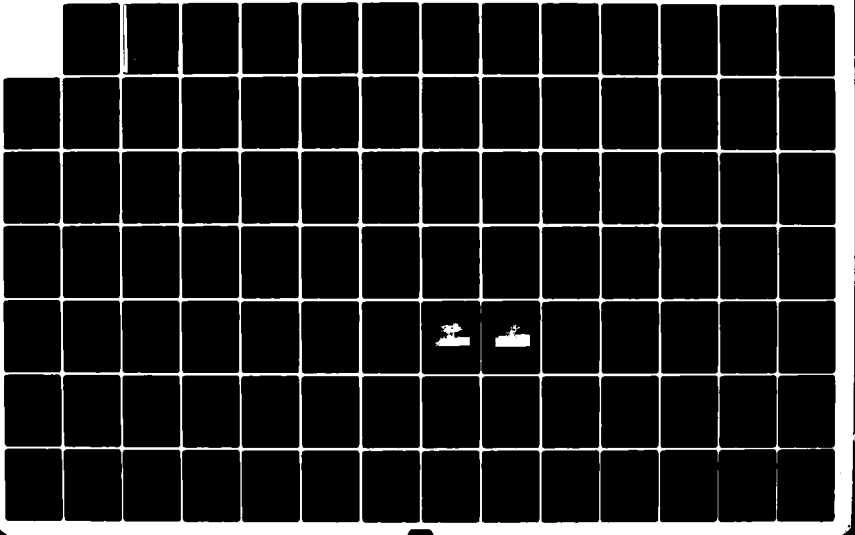

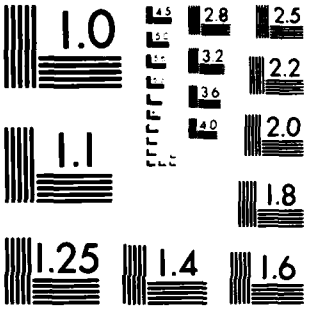

CRINC

REMOTE SENSING LABORATORY

(12)

AD-A129690

DTIC FILE COPY

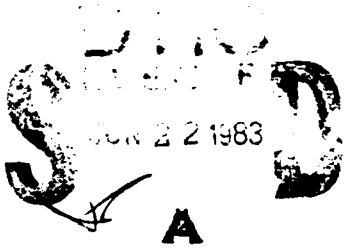

THE UNIVERSITY OF KANSAS CENTER FOR RESEARCH, INC.

2291 Irving Hill Drive—Campus West
Lawrence, Kansas 66045

INTERACTION OF THE RADAR WAVES
WITH
THE CAPILLARY WAVES ON THE OCEAN

by

S. Barkeshli
R.K. Moore

Remote Sensing Laboratory
Center for Research, Inc.
The University of Kansas
Lawrence, Kansas 66045

RSL Technical Report
RSL TR 419-1
May 1983

Supported by:

OFFICE OF NAVAL RESEARCH
Department of the Navy
800 N. Quincy Street
Arlington, Virginia 22213

CONTRACT N00014-79-C-0533

Unclassified

SECURITY CLASSIFICATION OF THIS PAGE (When Data Entered)

REPORT DOCUMENTATION PAGE		READ INSTRUCTIONS BEFORE COMPLETING FORM
1. REPORT NUMBER RSL TR 419-1	2. GOVT ACCESSION NO. AD-A129 690	3. RECIPIENT'S CATALOG NUMBER
4. TITLE (and Subtitle) Interaction of the Radar Waves with the Capillary Waves on the Ocean		5. TYPE OF REPORT & PERIOD COVERED Interim-Technical Report 6. PERFORMING ORG. REPORT NUMBER
7. AUTHOR(s) S. Barkeshli and R.K. Moore		8. CONTRACT OR GRANT NUMBER(s) N00014-79-C-0533
9. PERFORMING ORGANIZATION NAME AND ADDRESS Remote Sensing Laboratory; University of Kansas Center for Research, Inc.; 2291 Irving Hill Drive-Campus West; Lawrence, Kansas 66045		10. PROGRAM ELEMENT, PROJECT, TASK AREA & WORK UNIT NUMBERS
11. CONTROLLING OFFICE NAME AND ADDRESS Office of Naval Research Dept. of the Navy 800 N. Quincy St.; Arlington, Va. 22213		12. REPORT DATE May 1983 13. NUMBER OF PAGES 192
14. MONITORING AGENCY NAME & ADDRESS(if different from Controlling Office)		15. SECURITY CLASS. (of this report) Unclassified 15a. DECLASSIFICATION/DOWNGRADING SCHEDULE

16. DISTRIBUTION STATEMENT (of this Report)

Approved for public release; distribution unlimited

17. DISTRIBUTION STATEMENT (of the abstract entered in Block 20, if different from Report)

18. SUPPLEMENTARY NOTES

19. KEY WORDS (Continue on reverse side if necessary and identify by block number)

20. ABSTRACT (Continue on reverse side if necessary and identify by block number)

Measurements of the radar cross-section of the sea were made from the Noordwijk platform off the Dutch coast during September-November 1979 as part of Project MARSEN using an FM microwave spectrometer over the 8-18 GHz frequency range. A set of techniques for studying the modulation of the capillary waves on the ocean surface was developed for use in analyzing the entire observation set and is presented here as applied to a single set of observations. Thus, the results given here are only of limited oceanographic

DD FORM 1 JAN 73 1473 EDITION OF 1 NOV 65 IS OBSOLETE
S/N 0102-LF-014-6601

Unclassified
SECURITY CLASSIFICATION OF THIS PAGE (When Data Entered)

significance, but illustrate the types of analysis to be performed when these techniques are applied to more data.

Measured scattering coefficient based on instantaneous radar antenna footprint was cross-correlated with wave height and slope for measurements at the Noordwijk tower on 21 September 1979. The scattering coefficient leads the wave height by about 104° and leads the slope by about 77°. A new modulation index concept, $\mu(t)$, the ratio of the measured scattering coefficient (based on instantaneous radar antenna footprint) to the theoretical scattering coefficient (based on uniform capillary modulation and instantaneous resonance with the K-spectrum) has been presented. The RMS value of $\mu(t)$ is 0.876 with standard deviation 0.349 for HH-polarization and 0.673 with standard deviation of 0.044 for VV-polarization. The cross-correlation of $\mu(t)$ and wave height shows that the peak of the modulation leads the wave height by about 153°. Cross-correlation of $\mu(t)$ and slope shows that the peaks of the modulation are located at about the minima of the dominant slope, 165° away from both sides of the maximum. An algorithm for transformation from temporal to spatial domain has been developed, and the modulation transfer function based on Plant's definition [1979] has been calculated.

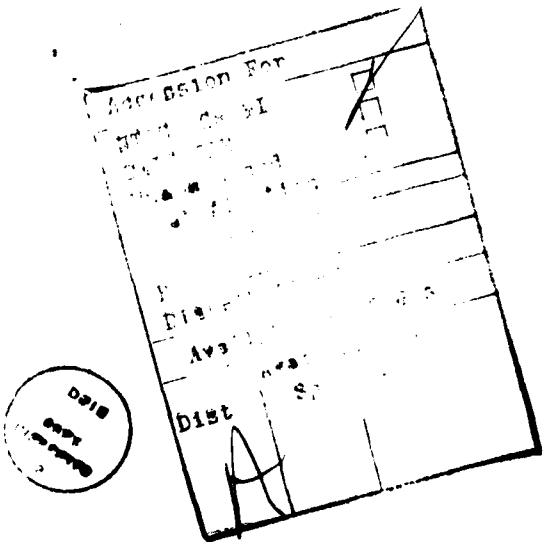

TABLE OF CONTENTS

LIST OF FIGURES

LIST OF TABLES

1.0 ABSTRACT

Measurements of the radar cross-section of the sea were made from the Noordwijk platform off the Dutch coast during September-November 1979 as part of Project MARSEN using an FM microwave spectrometer over the 8-18 GHz frequency range. A set of techniques for studying the modulation of the capillary waves on the ocean surface was developed for use in analyzing the entire observation set and is presented here as applied to a single set of observations. Thus, the results given here are only of limited oceanographic significance, but illustrate the types of analysis to be performed when these techniques are applied to more data.

Measured scattering coefficient based on instantaneous radar antenna footprint was cross-correlated with wave height and slope for measurements at the Noordwijk tower on 21 September 1979. The scattering coefficient leads the wave height by about 104° and leads the slope by about 77°. A new modulation index concept, $\mu(t)$, the ratio of the measured scattering coefficient (based on instantaneous radar antenna footprint) to the theoretical scattering coefficient (based on uniform capillary modulation and instantaneous resonance with the K-spectrum) has been presented. The RMS value of $\mu(t)$ is 0.876 with standard deviation 0.349 for HH-polarization and 0.673 with standard deviaton of 0.044 for VV-polarization. The cross-correlation of $\mu(t)$ and wave height shows that the peak of the modulation leads the wave height by about 153°. Cross-correlation of $\mu(t)$ and slope shows that the peaks of the modulation are located at about the minima of the dominant slope, 165° away from both sides of the maximum. An algorithm for transformation from temporal to spatial domain has been developed,

and the modulation transfer function based on Plant's definition [1979] has been calculated.

2.0 INTRODUCTION

Radar backscatter from the ocean can be used to monitor the wind velocity with a scatterometer that observes at two or more directions relative to the wind vector, to determine wave heights and ocean elevation (and from it currents) with an altimeter, and to monitor features of the wave spectrum, bottom topography, internal waves, ship wakes, and oil spills with an imaging radar. Since the radar backscatter represents a confusing ''clutter'' for radars observing targets such as ships and periscopes, studies of the radar backscatter have been conducted since the early days of radar before the direct applications listed above were developed.

The relatively recent advent of spaceborne scatterometers, altimeters, and synthetic-aperture imaging radars has led to greatly increased interest in the nature of radar backscatter from the sea. Furthermore, the use of these instruments calls for different kinds of understanding (consequently theory and measurements) than those required for earlier clutter measurements. To aid in improving this understanding, several major international measurement programs have been conducted in recent years. Project MARSEN, of which this research is a part, is one of the more recent programs. This program was conducted in the fall of 1979 in two instrumented areas in the North Sea: off the German coast near the Helgoland Bight and off the Dutch coast near Noordwijk. This is a report of part of one of the studies conducted from the Noordwijk platform of the Dutch Department of Water Control.

Measurements of radar backscatter from instrumented towers in the sea are based on the need for observations under more carefully

controlled conditions than are possible with measurements from aircraft and spacecraft, and to study with a greater variety of conditions than can be encountered with measurements from aircraft whose flight times are limited. A goal of measurement programs such as MARSEN is to perform many measurements of different kinds from towers and aircraft so that the synergism of data comparisons may lead to better understanding than would be obtained with isolated measurement programs by small groups of investigators.

Radar measurements were made at the Noordwijk platform by three groups: The University of Kansas, a Dutch group of experimenters from the Physics Research Laboratory of National Defence and the Technical University of Delft, and a French group from the Institut Francaise du Petrole. A JPL group made measurements with a capillary wave gauge and near-surface wind probes, and a British group made measurements of breaking waves with special buoys deployed from the platform. In addition, overflights were made by a NASA aircraft carrying a scatterometer and by several imaging radars from the U.S., Germany, France, and the Netherlands. The object of the aircraft measurements over the Noordwijk platform was to allow comparison with the platform measurements.

Major goals of the University of Kansas measurements, most of which were shared by the other radar investigators on the platform were:

1. To establish the variation of the capillary-wave amplitude over the underlying larger waves, and to establish the portion of the underlying waves contributing the strongest radar signals. This is important because the nature of a synthetic-aperture image of

the larger waves depends on the local velocities associated with the strongest scattering centers, and these velocities are different for different parts of the larger waves. The nature of the University of Kansas radar allowed it to be used as a ''radar wave gauge'' to measure the wave height at the center of the radar beam, so the type of analysis conducted to meet this objective was unique—no other radar measurements have been made where the wave height was measured exactly at the radar observation spot.

2. To establish the variations of the capillary-wave component of the ocean-wave spectrum for different wind speeds and directions relative to that of the wind. This is important because the radar backscatter from the sea at angles of 20° or more from vertical is known to be governed by resonance with these capillary and near-capillary waves. In fact, the determination of the spectrum from the radar measurements is based on this known resonance phenomenon. With the University of Kansas radar's capability of measuring over wavelengths from about 1.7 cm to 3.3 cm and that of the French radar from 3.3 cm to 25 cm, this experiment provided an unparalleled opportunity to observe the capillary spectrum.

3. To determine empirically the variation of radar scattering coefficient from the sea over a wide range of angles of incidence, angles relative to the wind direction, frequencies, and polarizations. This is important in scatterometry, radar design, and clutter rejection studies. Although many previous measurements of this nature have been performed from aircraft and stationary platforms, none has allowed measurements with such a variety of radar parameters at one time. Furthermore, although

aircraft and spacecraft measurements have allowed development of successful wind-vector measurement systems using scatterometers, one of the greatest unknowns is the exact relationship between scattering coefficient and wind speed—the previous measurements have led to considerable scatter in the values of the coefficients in this relationsip.

4. To establish the variation of the quantities determined under objectives 1-3 when an oil spill is present on the surface. Oil is known to damp the shorter components of the ocean-wave spectrum, and this fact is used as the basis for oil-spill monitoring radar systems used by several countries, although quantitative measurements of the effect are scarce.

The study reported here is related to object (1) above, the determination of the modulation of the capillary waves associated with the underlying larger waves. This report is primarily concerned with development of the methodology for a later study of the more complete data set. However, the preliminary results reported for a single set of data have value in their own right.

One of the approaches commonly used for describing this modulation is to calculate a ''modulation transfer function'' (MTF) in the frequency domain. The MTF amplitude shows the underlying-wave frequencies at which the capillary amplitude correlates best with the underlying waves, and the phase indicates the location of the relevant capillary components on the individual frequency components of the underlying waves.

In this report an alternate time-domain approach is presented that is based on the cross-correlation function between the radar signal and

the underlying waves. The cross-correlaton function tends to show the principal effects in a more compact and understandable form than the MTF. So that this relation may be understood better, the cross-correlation function is calculated for the capillary modulation alone by using as an input the ratio of the observed signal to the one that would be observed if the capillary waves were of uniform amplitude (changes in the slope of the underlying wave would cause all variations in the received signal if this were true). This ''instantaneous modulation'' can only be calculated in the time domain.

During the course of the investigation of the data the presence of strong-signal ''events'' was observed. These are presumably the same as the ''sea spikes'' that have been reported by numerous previous investigators. To determine the capillary-wave effects, one must first remove these anomalously large signals from the time series of the signal. Methods for doing this have been devised, and the result of the removal is a significant improvement in the repeatability of the modulation-study results.

This study was intended primarily to develop methodology, so only one data set was used—this was for a wind speed of 8.8 m/sec with the radar looking in the upwind direction. The dominant wave period was 5.8 seconds, and the maximum of the measured scattering coefficient was found to occur 1.8 seconds, or 104°, before the crest of the oncoming wave—it is therefore on the front face of the wave and nearer the trough than the crest. The location of the maximum instantaneous modulation (ratio of observed signal to that predicted if the capillary waves were uniformly distributed) is 153° ahead of the crest, a location almost in the trough. Furthermore, a secondary maximum was

found at 62° behind the crest, or well up on the back face of the wave.

Correlations were also performed between the scattered signal and the instantaneous slope of the waves. The slope spectrum has a higher peak frequency than the wave-height spectrum, so these correlations lead to different separations between maximum of the slope and maximum radar signal than would be observed if a single sine wave were observed. That is, one should be able to obtain the location of the peak signal on the slope of a single sine-wave component from the height record alone, but with a complex wave pattern this is no longer possible. Interpretation of the relation between peak radar scatter and slope remains to be worked out.

Most of the analyses were performed on time records, since the wave heights were measured at the fixed center of the radar footprint as time histories. However, one can determine the spatial picture over a limited distance from a time record by suitably summing a series in distance using the Fourier coefficients of the time series. The method for doing this was also developed here and will be used in future studies of the measurements.

3.0 Background of Theory and Experiment

The phenomenon of sea scatter and its theoretical basis has been of interest since the advent of the practical radar system. It has been generally agreed [Wright (1968), Chan and Fung (1973), Wu and Fung (1972), Long (1974)] that the scattering properties of the sea surface can be explained fairly well in terms of a two-scale slightly rough surface model, where the small-scale capillary waves are assumed to satisfy the small perturbation assumption, and the large-scale waves are assumed to satisfy the Kirchhoff approximation. This theory, verified to a large extent by experiment, indicates that backscatter at microwave frequencies is from those wavelength components of the ocean-wave spectrum that are resonant to the radar probing wavelength (Figure 3.1). In general, the scattering cross-section per unit area, σ^o, depends on the local angle of incidence (Figure 3.2), and also on the small capillary waves which are tilted by the large-scale wave slope. This angle depends on the position of the capillary waves with respect to the large-scale waves. The amplitudes of the small capillary waves are modified by a variety of hydrodynamic interactions with the large-scale waves. The local scattering cross-section depends on this amplitude. In fact, in first-order scattering theory, the cross-section and power spectrum amplitude are proportional(Section 4.3.1). Therefore, it is the modulation of scattering by the large-scale waves which makes them detectable by microwave radar. If the small capillary wave amplitude is modulated, so is the stress. A modulated stress, if of the proper phase, results in larger wave-growth. Table 3.1 shows the list of symbols for the following analysis.

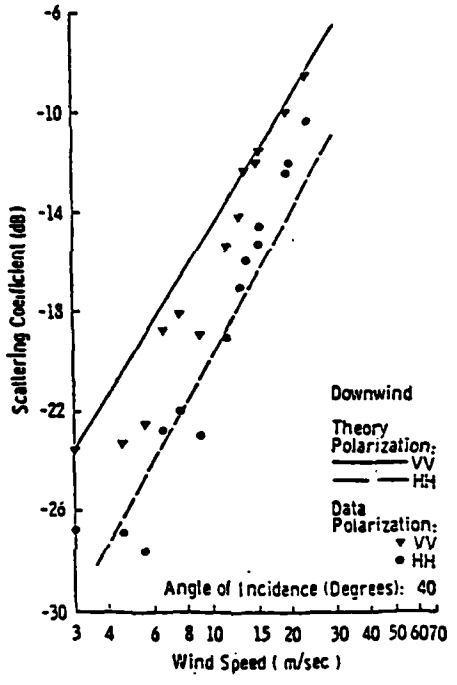

Figure 3.1: Comparison between theoretical and measured σ^{o}_{pp} for vertical and horizontal polarizations at 40° incidence angle for downwind observation with a 13.9 GHz radar. This illustrates close correspondence between experiment and theory based on resonance with capillary waves.

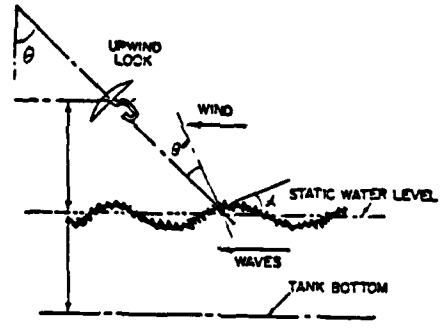

Figure 3.2: Dependence of scattering coefficient on local angle of incidence, θ' and small capillaries which are tilted by the large-scale wave slope.

TABLE 3.1
LIST OF SYMBOLS

u^*	Air friction velocity
θ	Angle of incidence (angle between vertical and radar-wave direction)
k_x	Component of wave number in x direction
cg, cg°	Group speed of wind-generated wave with and without plunger-generated wave
u	Horizontal component of orbital velocity of plunger-generated wave
e(t)	Linearly-detected, rectified, received signal
θ'	Local angle of incidence (angle between normal to local surface and radar-wave direction)
M	Measured fractional modulation
r	Measured peak-peak modulation of R(0)
k_o	Microwave number
P	Modulation index of received signal
u_o	Modulation of u
u(t)	Periodic constituent of e(t)
f,(k)	Perturbation of surface displacement spectrum
ϕ	Phase angle
C	Phase speed of plunger-generated wave
C_o	Phase speed of wind-generated wave in absence of plunger-generated wave
k	Plunger-generated wave number
S	Plunger-generated wave slope
ω	Radian frequency of plunger-generated wave
Ω	Radian frequency of wind-generated wave
f(t)	Random (wind-generated) constituent of e(t)
P	Received power
P_o	Received power in absence of plunger
γ	Straining constant
B	Straining function
D	Straining function
τ	Time lag
β	Wind-generated wave growth rate
β_r	Wind-generated wave relaxation rate
H	Wind-wave interaction functional
F, F_o	Wind-wave surface displacement spectrum

Keller and Wright [1975] suggested a two-scale scattering theory called 'the relaxation time model,' and state that the small capillary waves, if perturbed from equilibrium, will relax back at an exponential rate called 'the relaxation rate.' The relaxation rate is a function of the small capillary-wave spectrum.

They found that these waves grew exponentially over several orders of magnitude in spectral intensity. The energy influx from the wind to a wave of given wave number must be balanced by transfer to other wave numbers for dissipation or growth of the wave. The transport equation gives this balance. In the case of growth along a single cartesian coordinate x in the direction of the wind, it may be written:

$$\frac{\partial F}{\partial t} + c_g \frac{\partial F}{\partial x} = \beta F + H(F, k, u^*) \qquad (3.1)$$

where F(k,x,t) is the surface displacement spectrum, cg is the group velocity, β is the exponential growth rate, H(F,k,u*) is a function which accounts for nonlinear transfer to other waves and non-linear dissipation, all evaluated at wave number k. The quantities $\frac{\partial F}{\partial x}$ and F may be obtained directly in wave-tank experiments from the intensities of the first-order Bragg line in the Doppler spectra (Figure 3.3a). β is the initial temporal growth rate, provided nonlinear interactions are negligible in the initial stages of growth [Keller and Wright, 1975]. The quantities $\frac{\beta F}{F_m}$, (c_g/F_m) and $\frac{S_{nl}}{F_m} = (c_g(\frac{\partial F}{\partial x}) - \beta F)/F_m$, where F_m is the maximum value of F observed under the conditions of the measurement, are shown in Figure 3.3b for some cases reported by Plant and Wright [1977]. The difference $c_g(\frac{\partial F}{\partial x})/F_m - \beta F/F_m$ can be matched, for the cases shown, by values of

S_{nl}/F_{max} calculated from the second-order gravity-capillary wave-wave interaction. When the nonlinear interactions bring the wave to a steady state or equilibrium, the vertical flux βF from the wind is large compared to horizontal flux $c_g\left(\frac{\partial F}{\partial x}\right)$. The difference is dissipated either by the breaking of the wave itself or by the transfer to other wave numbers for subsequent dissipation, but in either case, the equilibrium is spatially localized. It is the perturbation of this equilibrium by the fluid motions associated with the large waves which modulates the small-wave amplitude, and in consequence, the scattering cross-section.

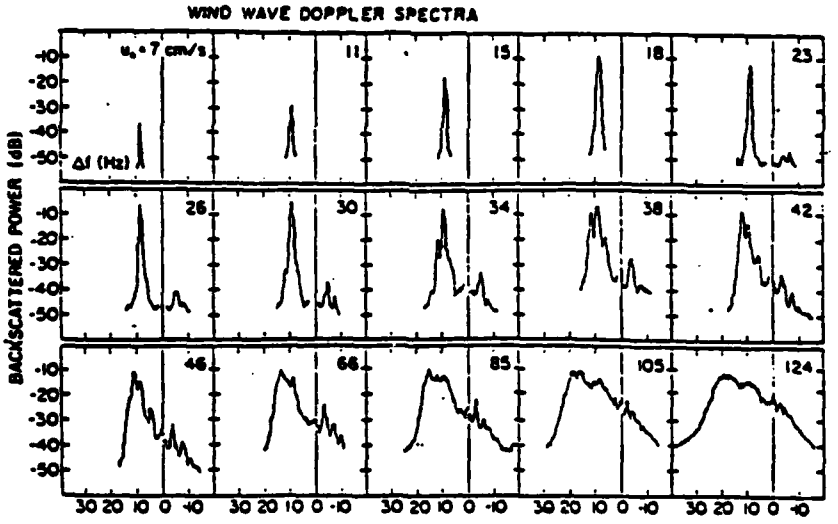

Figure 3.3a
Evolution of Doppler spectra of backscattered microwaves with increasing wind speed at fixed fetch. The wavelength was 6.9 cm (f = 4.35 GHz), the depression angle was 30°, and the Bragg wavelength was 4.05 cm.

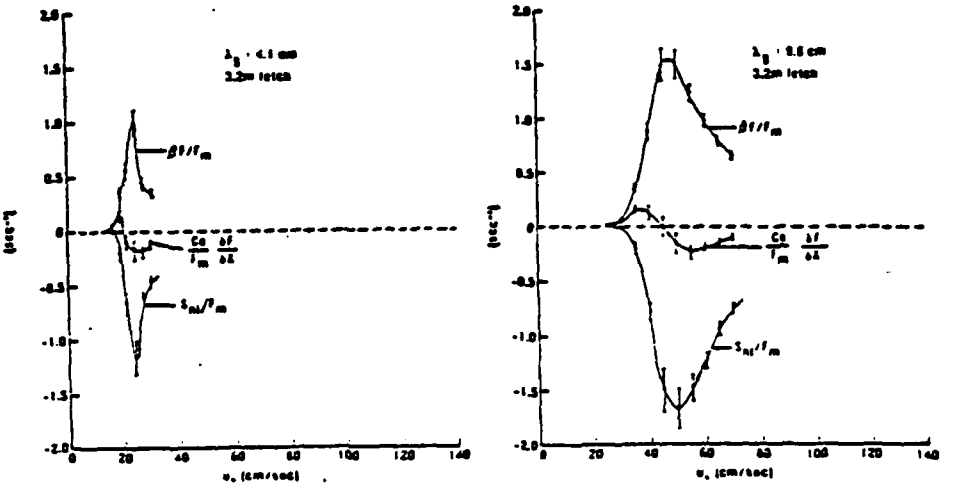

Figure 3.3b
Terms in the equilibrium transport equation for gravity-capillary waves. The curve labeled S_{nl}/F_m is the difference of the other two curves, i.e., $S_{nl}/F_m \equiv (C_g(\partial F/\partial x) - \beta F)/F_m$. The Bragg wavelength is denoted by λ_B.

A phenomenological model of the perturbation of this equilibrium by the horizontal component of orbital speed of a large wave [Keller and Wright, 1975] can be constructed after including the effect of the horizontal current u(x,t) in the transport equation

$$\frac{\partial F}{\partial t} + c_g \frac{\partial F}{\partial x} - \frac{\partial \omega}{\partial x}\frac{\partial F}{\partial k} = \beta F + \gamma(k) F \frac{\partial u}{\partial x} + H(F, k, u^*) \qquad (3.2)$$

where:

$$\omega = \omega_0 + \vec{k} \cdot \vec{u} \qquad (3.3)$$

$$c_g = \frac{\partial \omega}{\partial k} \tag{3.4}$$

The quantity is the angular freqency of the small wave under consideration. The term on the right containing (k), the straining constant, is called the radiation stress and

$$\gamma(k) = 1 - c_g^0/c^0 \tag{3.5}$$

where c_g^0 and c^0 are the group and phase speed, respectively, of the small wave in the absence of the current u.

Let $F_0(k,x)$ be the surface displacement spectrum in the absence of the current u(x,t) which we now assume to have the form

$$u(x,t) = u_0 e^{i(kx - \Omega t)} \tag{3.6}$$

This is the current which perturbs the equilibrium spectrum. In consequence we expand the resultant surface displacement spectrum in a perturbation series in (u_0/c), where $c = \Omega/k$ is the phase speed of the large wave.

$$F = F_0 + (u_0/c) f_1(k) e^{i(kx - \Omega t)} + \ldots\ldots \tag{3.7}$$

The key assumption is that the increment in the nonlinear transfer can be written:

$$\delta H = \left(\delta H/\delta F \right)_{F=F_0} (u_0/c) f_1 \tag{3.8}$$

This is called the relaxation time appproximation. It is now straightforward to solve (3.2) and (3.7) to first order in (u_0/c)

$$\frac{f_1}{F_0} = \frac{-\left(\frac{\Omega}{\beta_r}\right)^2 (1 - c_g^0/c)\left(\frac{k}{F_0}\frac{\partial F_0}{\partial k} - \gamma\right) + \frac{\Omega}{\beta_r}\frac{1}{kF_0}\frac{\partial F_0}{\partial x}}{1 + (1 - c_g^0/c)^2 (\Omega/\beta_r)^2} -$$

$$\gamma \frac{(\Omega/\beta_r)\left(\frac{k}{F_0}\frac{\partial F_0}{\partial k} - \gamma\right) + (\Omega/\beta_r)^2 (1 - c_g^0/c)\frac{1}{kF_0}\frac{\partial F_0}{\partial x}}{1 + (1 - c_g^0/c)^2 (\Omega/\beta_r)^2} \qquad (3.9)$$

where the relaxation rate

$$\beta_r \equiv \left(\delta H/\delta F\right)_{F=F_0} - \beta \qquad (3.10)$$

has been introduced [Wright, 1977].

The first order in (u_0/c) terms in the expansion adequately describes the response of the wind-generated waves for winds of less than 7 to 8 m/sec and $u_0/c < 0.1$.

Modulation of backscattering cross-sections have been measured at 9.35 GHz and depression angle of 45 degrees (Bragg wavelength = 2.3 cm) by Keller and Wright [1975, 1976]. The linearly detected signal, proportional to the scattered electromagnetic field was ratified and filtered to remove frequency a and phase modulation and cross-correlated.

The measured auto-covariance function, $R(\tau)$ exhibited a spike at $\tau = 0$, due to the longer short-gravity waves of the wind-generated wave system, a mean value proportional to the square of the mean scattered field and a periodic portion due to modulating plunger-generated wave:

$$R(\tau) = \frac{1}{T_a} \int_0^{T_a} e(t)\, e(t+\tau)\, dt \qquad (3.11)$$

$$e(t) = f(t) + p\bar{f}\, u(t) \qquad (3.12)$$

$$R(0) = \overline{f^2(t)} \qquad (3.13)$$

If $$u(t) = \cos(\Omega t) \qquad (3.14)$$

$$R(\tau) = \frac{1}{T_a} \int_0^{T_a} f(t) f(t+\tau)\, dt + \frac{p^2}{2} (\bar{f})^2 \cos(\Omega\tau) \qquad (3.15)$$

The ratio of the peak-to-peak amplitude of the periodic portion of $R(\tau)$, r, to R(0), which latter quantity is proportional to the main scattered power is called the fractional modulation, m (Figure 3.4). So

$$r = p^2 (\bar{f})^2 \qquad (3.16)$$

and

$$M = \frac{r}{R(0)} \qquad (3.17)$$

where M is fractional modulation.

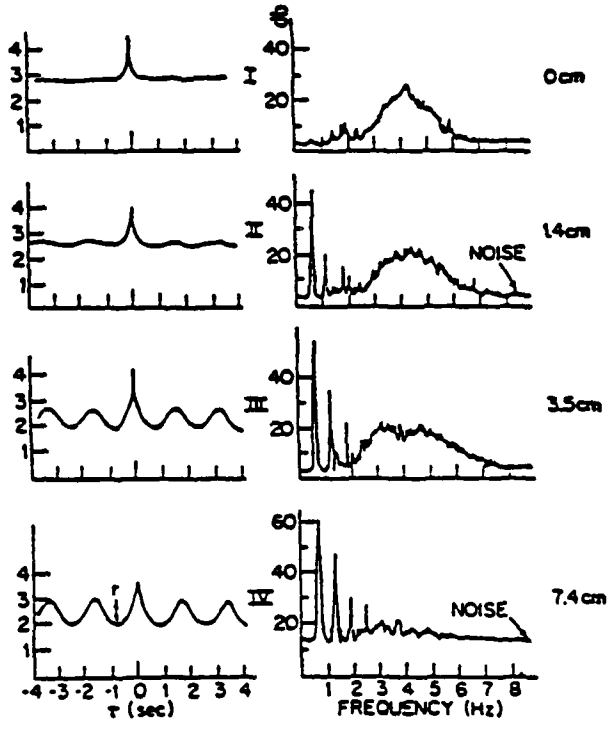

Figure 3.4
Autocorrelation functions of the microwave return (left) and wind-wave spectra (right) for various wave amplitudes at u* = 16.5 cm sec-1

If we represent p, power return as

$$P = P_o (1 + m \cos(\Omega t + \phi) \tag{3.18}$$

where

$$m = (B^2 + D^2 + T^2 \pm 2DT)(4_o/C) \tag{3.19}$$

and

$$\phi = \tan^{-1}((D \pm T)/B) \tag{3.20}$$

then

$$M = \left(\frac{m^2}{4}\right)\left(\frac{\overline{\chi^2}}{(\bar{\chi})^2}\right) \tag{3.21}$$

or

$$M = \left(\frac{m^2}{4}\right)\left(\frac{R(o)}{(\bar{\chi})^2}\right) \tag{3.22}$$

Positive and negative signs refer to upwind and downwind-looking antenna orientations, respectively.

The calculated theoretical curves and fractional modulation, are nonetheless an excellent fit to the measured value for winds of less than 8 m/sec and $u_0/c < 0.1$. For these winds, larger wave amplitudes, the fractional modulations saturated, i.e., they ceased to increase with increasing modulation wave amplitude, (Figures 3.5a,b).

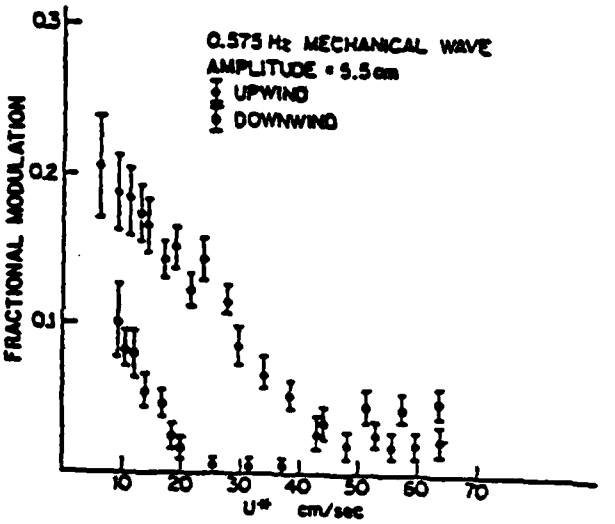

Figure 3.5a
Fractional modulation vs. air friction velocity for 0.575 Hz wave, $U_o/C = 0.091$; solid circles, upwind; open circles, downwind

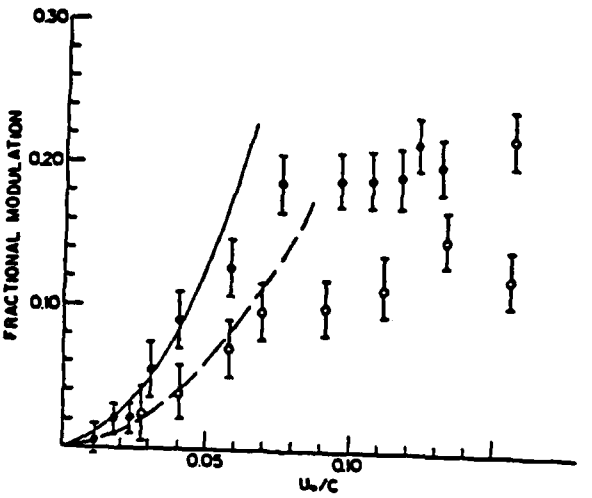

Figure 3.5b
Comparison of theoretical and measured fractional modulations looking upwind vs orbital velocity of 0.575 Hz waves. Solid data points and solid line are for $u^* = 16.5$ cm sec^{-1}. Open data points and dashed line are for $u^* = 30$ cm sec^{-1}.

Keller and Wright [1976] stated that at the higher wind speed there is definitely another phenomenon present unaccounted for by the relaxation theory. They believe that, at present, the theory is phenomenological and the relaxation rate is an adjustable parameter. The reasons for choosing certain values for this and other incompletely known parameters become clearer upon consideration of relaxation of a pair of waves which simulate short gravity waves coupled to capillary waves by the second-order resonant interaction [Valenzuela and Laing, 1972, Plant and Wright, 1977, Plant 1979].

In a consequent study of sea surface backscatter phenomena, Plant, Keller and Wright [1978] conducted an experiment to measure the modulation of small capillary wind-generated waves by those with typical ocean wave periods. They stated that the horizontal component of the orbital velocity of shoaling waves much exceeds the vertical component exception in the region near the wave crests. Hence the relative importance of modulation due to tilting is much reduced over most of the large-scale wave, so the shoaling waves beyond the surf zone provide easily understood modulating conditions. The power spectra of e(t), rectified scattered field strength e(t), and the line-of- sight speed v(t), here show contributions both from the crests and low-amplitude quasi-periodic portions of the waves. The narrow peaks in the spectra were used to obtain quantitative measurements of the modulation. They also were used to calculate 'fractional modulation M' (Figures 3.6a,b and c).

In the most recent work by Plant et al. [1980] the modulation transfer function is calculated.

Let p(t), the square of the homodyne-detected [King, 1978]

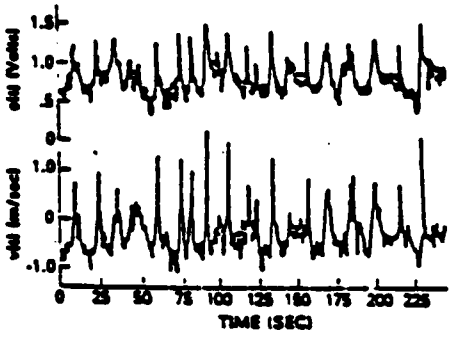

(a)

Processed microwave return from shoaling waves. The top trace is the rectified signal amplitude e(t), while the lower trace is the line-of-sight speed v(t), delayed by 1.25 s from the top trace. Both signals have been low-pass-filtered with a 0.6 Hz cutoff.

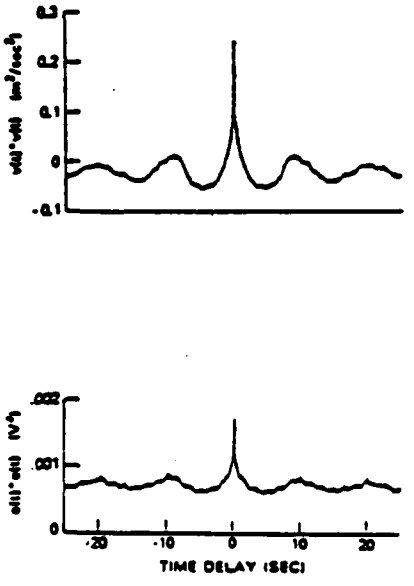

(b)

Autocovariance functions of line-of-sight speed v(t) and rectified backscattered signal amplitude e(t).

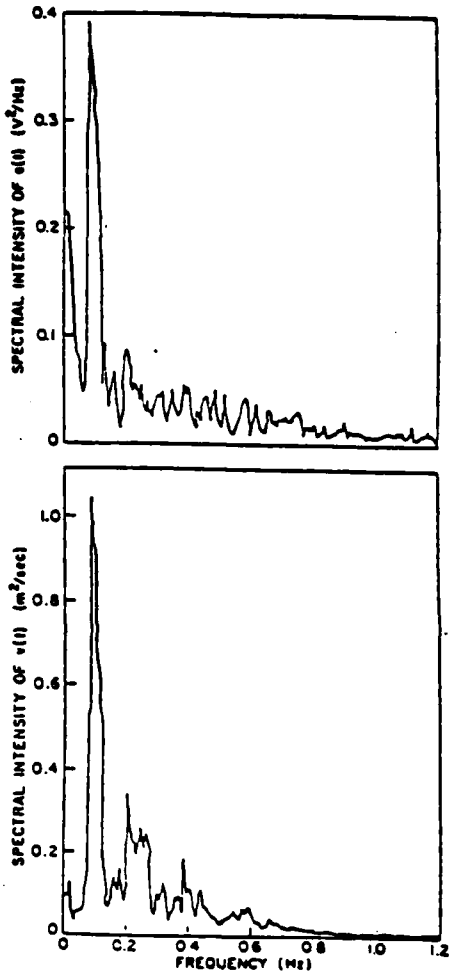

(c)

Power spectra of rectified back-scattered signal amplitude e(t) and line-of-sight speed v(t).

Figure 3.6

microwave voltage, which in turn is proportional to the backscattered electromagnetic field, be called the instantaneously received power. Let v(t) be the instantaneous line-of-sight speed. If G_{pv} is the cross-spectrum of instantaneously received power and instantaneous line-of-sight speed and G_{vv} is the autospectrum of the latter, define

$$m(\Omega) = \frac{C(\Omega)}{\bar{\rho}} \frac{G_{pv}(\Omega)}{G_{vv}(\Omega)} \tag{3.23}$$

The phase speed $C(\Omega)$ and mean received power $\bar{\rho}$ normalize the modulation transfer function, $m(\Omega)$ making it dimensionless. $G_{pv}(\Omega)$ is, of course, complex. To fix ideas, suppose the plane of incidence (the plane containing the microwave propagation vector) and the normal to the undisturbed ocean surface, also contain the direction of a monochromatic, modulating surface wave of frequency Ω and wave number K, propagating in water of depth D, and the depression angle is θ, then:

$$V(t) = V_o \cos(\Omega t + \varphi_s) \tag{3.24}$$

$$\tan(\varphi_s) = \tanh(KD)\tan(\theta) \tag{3.25}$$

$$V_o/u_o = \left(\sin^2\theta + \cos^2\theta \tanh^2(KD)\right) \tag{3.26}$$

and

$$\rho = \bar{\rho}\left(1 + m(u_0/c)\cos(\Omega t + \varphi)\right) \qquad (3.27)$$

where φ_s is the phase angle by which the line-of-sight speed leads the horizontal component of orbital speed, $u = u_0 \cos(\Omega t)$ (Figure 3.7).

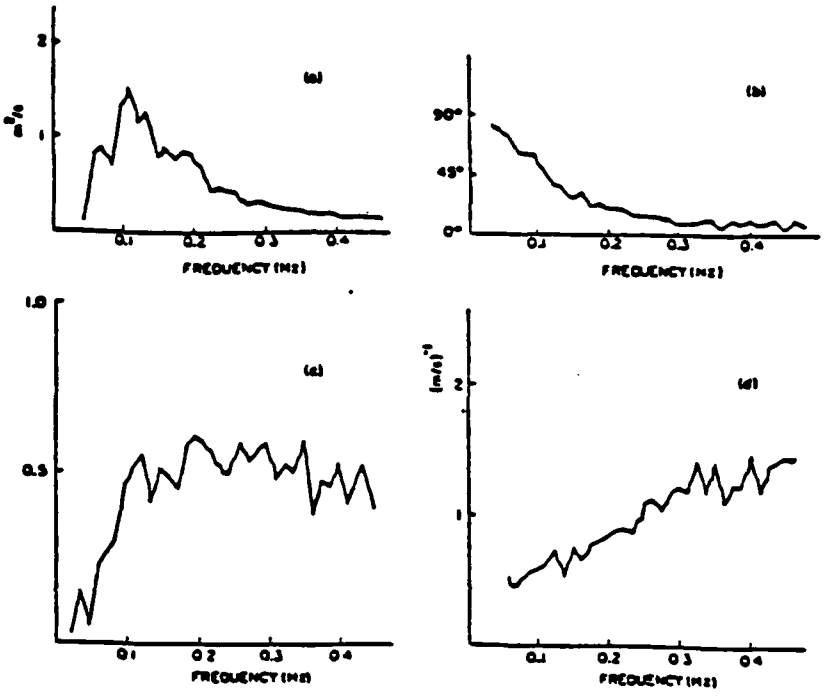

Figure 3.7
Modulation spectra of the demodulated return of the 9.375 GHz radar. Wind speed = 7.5 m/s.
(a) Line-of-sight component of orbital speed;
(b) phase of the modulation transfer function;
(c) coherence;
(d) modulus of the modulation transfer function divided by the ocean wave phase speed, m/c.

The transfer functions and their phase shown in Figures 3.8 to 3.11 are referred to the line-of-sight velocity as defined by (3.24). The transfer function which refers to the horizontal component of orbital speed (a more useful quantity for interpretive purposes) is obtained by multiplying m by V_0/u_0 given by (3.26). Although the transfer function, before averaging over the wind speed bands, exhibited scatter as large as a factor of 2, the finally averaged

modules (Figure 3.12a) and phase (Figure 3.12b) show smooth, stable dependence on modulating frequency and wind speed.

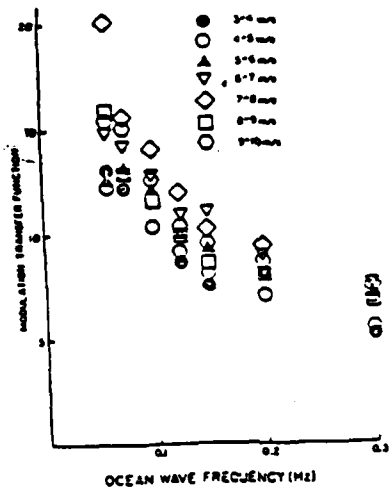

Figure 3.8
Modulus of the 1.5 GHz (Bragg wavelength = 13 cm) transfer functions.

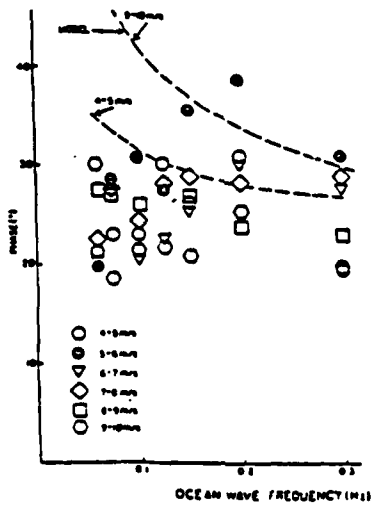

Figure 3.9
Phase of the 1.5 GHz (Bragg wavelength = 13 cm) transfer functions. Phases are measured from wave crests and are positive leading the crest. Dashed lines are theoretical predictions assuming modulation caused solely by straining. [Plant, Keller and Wright, 1980]

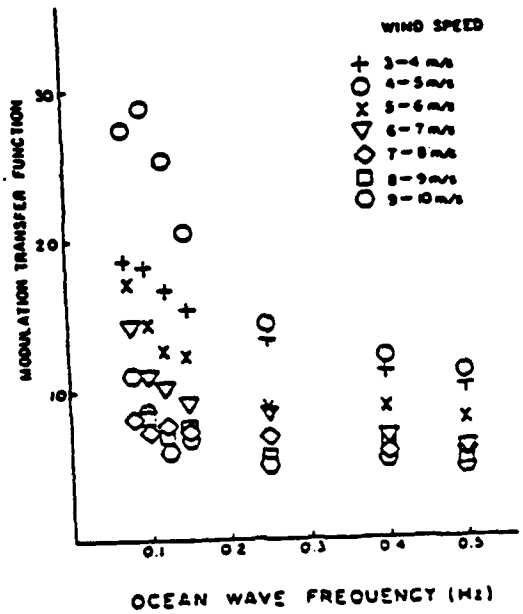

Figure 3.10
Modulus of the 9.375 GHz (Bragg wavelength = 2.3 cm) transfer functions

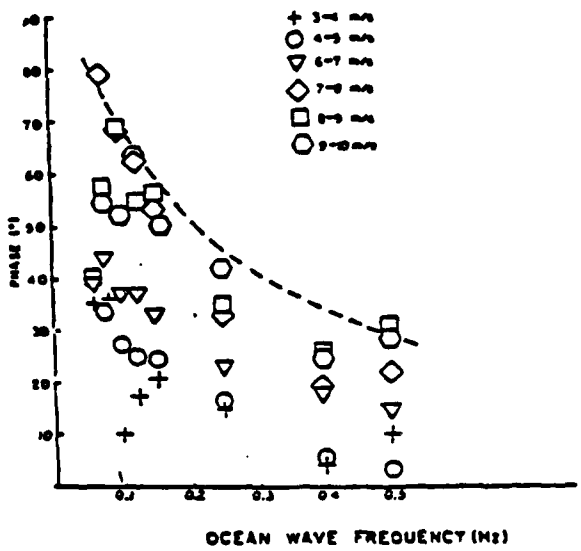

Figure 3.11
Phase of the 9.375 GHz (Bragg-wavelength = 2.3 cm) transfer functions. Phases are measured from wave crests and are positive leading the crest. Dashed line is a theoretical prediction assuming modulation caused only by straining.

Although the total averaged MTF looks very smooth and corresponds reasonably well with the theory, we believe the MTF concept is especially difficult for radar theorists who are not involved in pure theoretical hydrodynamics and fluid mechanics equations. We think that 'modulation index', $\mu(t)$, (Section 4.4.2), would, if it could be treated well, be an easily interpreted concept that could be used to make a simple statement about phase relationships between the peak of capillary and large-scale waves.

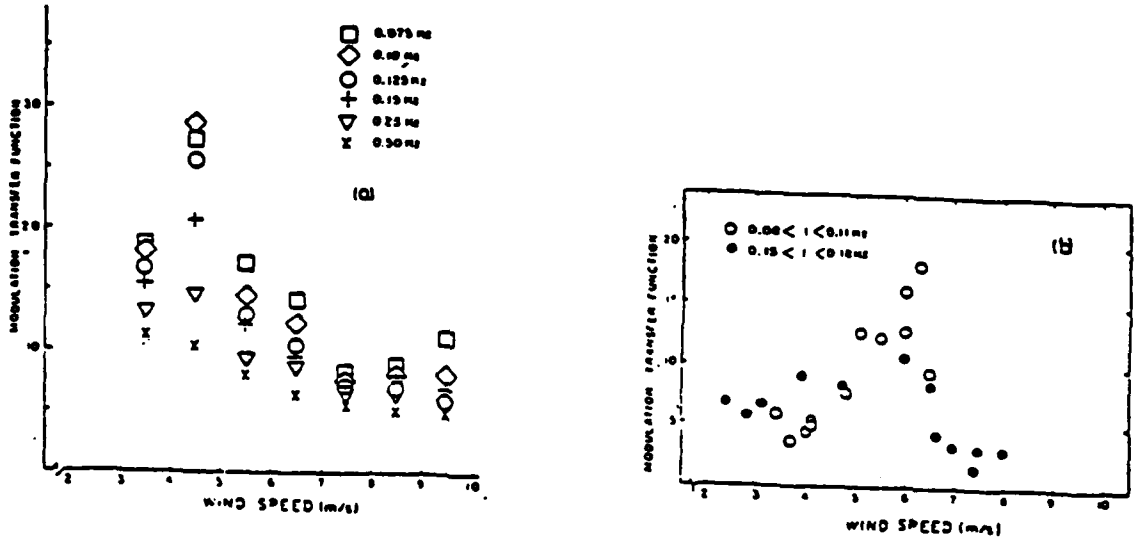

Figure 3.12
Wind speed dependence of 9.375 GHz modulation transfer functions. (a) NOSC tower; (b) Nags Head, North Carolina [Plant et al., 1978].

4.0 THEORY OF OCEAN WAVES

4.1 Ocean Wave Phenomena

4.1.1 The Theory of Wave Motion

Waves on the actual ocean are extraordinarily complex phenomena. A distinction must be made between the idealized classical wave motions of hydrodynamics and the much more complex (and far less well understood) wave motions that occur in nature. There is a distinction between deep water and shallow water waves depending on the ratio between wavelength and water depth.

4.1.2 Definition of Periodicity

The solution of the classical equations for ocean waves takes the form of a sum of periodic functions (Section 4.1.3). A function f(t) is periodic of period T if and only if f(t) = f(t+T) for all t. Records of the rise and fall of the water surface as a function of time at a fixed point on the ocean surface do not satisfy the above definition. Water waves in nature are not periodic. Hence, the sum is in principle infinite and representable by a continuous spectrum.

For all types of truly periodic traveling-wave motion

$$\lambda = CT \tag{4.1}$$

where λ is the distance between the crests of the waves, C is the speed with which the crests move and T is the time required for the water surface to go through one complete oscillation at a fixed point.

The period and length of a wave are rather cumbersome notations and it is possible to replace them by the concepts of wave number and angular frequency.

$$k = \frac{2\pi}{\lambda} \tag{4.2}$$

$$\omega = \frac{2\pi}{T} \tag{4.3}$$

4.1.3 General Gravity, Large-Scale Wave Theory

The simplest wave motion is that of a simple harmonic long-crested traveling wave in the +x direction whose equation would be given by

$$h(x,t) = a\cos\left(\frac{2\pi x}{\lambda} - \frac{2\pi}{T}t\right) \tag{4.4}$$

It is possible to write

$$h(x,t) = a\cos\left((x-ct)\frac{2\pi}{\lambda}\right) \tag{4.4a}$$

In the following derivation it is assumed that the earth is flat, that the water is of constant depth h, that the Coriolis force is negligible, that the density of the air can be neglected compared with the density of the water, that the water is of constant density, that the body of water is infinite in extent and completely covered by waves, and that the viscosity and surface tension can be neglected. Moreover, it is assumed that there is no variation in wave propagation

in the y direction. The equations are unsolvable in closed form, as they are nonlinear. A perturbation technique must be employed to linearize these equations and to obtain a useful result.

Assume that the unknown functions in hydrodynamic equations can be expanded in powers of a small dimensionless parameter ϵ, so that the solution is a power series in ϵ that will converge if enough terms are taken. These expansions are substituted into the equations, and all terms to the same power in ϵ are collected. It is possible, in general, to obtain terms to zero power in ϵ, to the first power in ϵ, to the second power in , and so on. Depending upon the power of ϵ used in the expansion, successively higher and more nearly correct approximations to the solution of the complete equation are obtained [Neumann and Pierson, 1966].

The steady, time-independent wave equation can be shown to be

$$g a \cos(Kx) - \frac{a C_o^2 \cosh(kh)}{\sinh(Kh)} K \cos(Kx) = 0 \qquad (4.5)$$

where

$$C_o^2 = \frac{g}{k} \tanh(Kh) \qquad (4.6)$$

where g is the gravitational acceleration (9.8 m/sec).

Equation (4.6) relates the phase speed C to the wave number K and the depth of the water h. For a given depth there is only one possible value for the wave speed given the wavelength (or the wave number).

Equation (4.6) can be simplified for two situations with reference to the values of h and K. The hyperbolic tangent of a function varies between zero and 1 for positive values of the argument. The hyperbolic tangent approaches the value 1 very closely for values of the argument that are very large Thus, if the product of K and h is such that the hyperbolic tangent is essentially 1, (4.6) reduces to the much simpler form given by

$$C_o^2 = \frac{g}{k} \tag{4.7}$$

The waves that satisfy this simplified form of the equation are called short waves, or 'deep water' waves. The second approximation occurs if the product of K and h is very small. Under these circumstances the hyperbolic tangent of Kh is approximately equal to Kh and if this substitution is made, (4.6) will be

$$C_o^2 = gh \tag{4.8}$$

Waves that satisfy this equation, relating the phase speed to the depth since the length of the wave no longer determines the phase speed, are called long waves, or 'shallow-water' waves.

Table 4.1 shows the various relations for deep-water waves between the different parameters.

	L	C_0	T	ω	k	C_g
L	L	$(gL/2\pi)^{1/2}$	$(2\pi L/g)^{1/2}$	$(2\pi g/L)^{1/2}$	$2\pi/L$	$\frac{1}{2}(gL/2\pi)^{1/2}$
C_0	$2\pi C_0^2/g$	C_0	$2\pi C_0/g$	g/C_0	g/C_0^2	$C_0/2$
T	$gT^2/2\pi$	$gT/2\pi$	T	$2\pi/T$	$4\pi^2 g/T^2$	$gT/4\pi$
ω	$2\pi g/\omega^2$	g/ω	$2\pi/\omega$	ω	ω^2/g	$g/2\omega$
k	$2\pi/k$	$(g/k)^{1/2}$	$2\pi/(gk)^{1/2}$	$(gk)^{1/2}$	k	$\frac{1}{2}(g/k)^{1/2}$
C_g	$8\pi C_g^2/g$	$2C_g$	$4\pi C_g/g$	$g/2C_g$	$g/4C_g^2$	C_g

Table 4.1
Relationship between wavelength, phase speed, period, angular frequency wave number, and group velocity for deep water linear periodic gravity waves. Read down to express the quantity in the top row in terms of the quantity in the left-hand column [Neumann and Pierson (1966]

4.1.4 General Solution for Large-Scale Gravity Waves

The linear solution that has been obtained can be used as a basis for second-order solutions. One could proceed to third and even higher orders. In general one can show

$$h(x) = \sum_i a_i \cos(k_i x + \varphi_i) \qquad (4.9)$$

It is possible to transform the solution to the form in which the presence of a current to produce the steady motion is eliminated. The general solution for the moving wave profile would then be given by

$$h(x,t) = \sum_i a_i \cos(k_i(x + C_i t) + \varphi_i) \qquad (4.10)$$

It is worthwhile to mention that C_i in general <u>is not</u> equal to $C_0 = \sqrt{\frac{g}{k}}$. C_i and C_0 have nonlinear relations, but it is very difficult to find the exact nonlinear relationships. In the following analysis we assume a linear relationship between C_i and C_0, where:

$$C_i = C_o \tag{4.11}$$

4.2 Capillary Waves

4.2.1 Capillary Phenomena

If the surface tension of the water is important, as it is for very short waves, additional restoring force due to curvature of the free surface enters the Bernoulli equation.

In linearized theory, the equation for the phase speed is:

$$C_o = \left(\frac{g}{k} + \frac{TK}{\rho} \right)^{1/2} \tag{4.12}$$

where ρ is the sea water density. Perturbation techniques were applied to the problem by Pierson and Fife [1961]. In general, waves have a phase speed that increases with increasing wave amplitude. However, in linear theory the speed and amplitude are independent.

When capillary waves interact with large-scale waves the capillaries appear at times to be concentrated on the forward face of the large-scale wave just before the sharp crest. In this case, perturbation techniques are rather difficult to apply, because the effect of surface tension is not uniform over the whole disturbed surface. Longuet-Higgins [1963] introduced surface tension as a perturbation effect on large-scale waves in the region of the sharp crest and has shown the reason for the occurrence of this phenomenon.

4.2.2 Capillary Generation by Wind

One of the universal features of wind-generated wave systems is

the modulation of velocity and amplitude of small capillary waves by large-scale gravity waves. These modulations are of practical importance. For example, the imaging properties of microwave radars used for remote-sensing of ocean waves depend on the modulation of surface scatterer density, amplitude, and velocity. Furthermore, the short gravity and capillary waves can support the entire stress of the wind on the water [Larson and Wright, 1975]. If the large-scale waves modulate the small capillary wave amplitudes, they also modulate the stress. The component of this modulation stress which is in phase with the horizontal component of orbital speed of the large-scale wave will work on the large-scale wave and cause it to grow. The mechanism of energy transfer between short and long waves, discussed by Hasselman [1971] also depends on the phase and amplitude of this modulation.

4.2.3 Sources of Modulations

At least three sources of modulation have been noted so far: modulation of the orientation of small capillary waves (called tilting), modulation of the amplitude of the small capillary waves exemplified by the straining of the capillary waves by the horizontal component of the orbital velocity of the large-scale waves [Longuet-Higgins and Stewart (1964), Phillips (1966)], and modulation due to wave-induced airflow. The last type of modulation, wave-induced airflow, is a principal result in the recent work of Wright, Plant and Keller [1980]. The dependence of modulation on modulating ocean wave frequency and, partially, upon wind speed are qualitatively consistent with wave-induced airflow as a modulator, but positive identification of the modulation sources remains to be made.

4.3 Current Theory of Scattering from the Ocean

4.3.1 History and Basis of Equations

The current scatter theory is a refinement of the two-scale model developed in the 1960's [Bass and Fuks (1968), Fuks (1969), Valenzuela (1967, 1968)]. The success of such a theory in explaining dependence on wind speed, wind direction, angle of incidence and frequency depends almost exclusively upon the adequacy of knowledge of the sea spectrum.

The derivation of the average backscattering coefficient for the sea surface involves two major steps: (1) compute the backscattering coefficient for the capillary waves using standard perturbation techniques [Valenzuela (1967), Wright (1966)] and (2) account for the tilting effect of the large-scale waves. The expression for the polarized scattering coefficients from step (1) is well known [Valenzuela (1967), Chan and Fung (1973)] and is

$$\sigma^{0}_{pp}(\theta, \varphi) = 8k^4 |\alpha_{pp}|^2 W(\theta, \varphi) \qquad (4.13)$$

where for horizontal polarization p=h and for vertical polarization p=v, k is the electromagnetic wave number, θ is the incidence angle, is the aspect angle relative to the upwind direction, and $W(\theta, \varphi)$ is the roughness spectrum of the sea surface. The coefficients, α_{pp}, for different polarization states are defined as

$$\alpha_{hh} = R_h \cos(\theta) \qquad (4.14)$$

$$\alpha_{vv} = R_v \cos^2(\theta) + (k'^2 - k^2) T_v^2 \sin^2\theta / 2k'^2 \qquad (4.15)$$

where θ is the incidence angle, φ is the aspect angle relative to the upwind direction, k' is the wave number in sea water, R_h,R_v are Fresnel reflection coefficients for horizontal and vertical polarizations, respectively, and T_v=1+R_v. The depolarization scattering coefficient is also known [Valenzuela, 1967].

$$\begin{aligned}\alpha_{hv}(\theta,\varphi) &= \alpha_{vh}(\theta,\varphi) \\ &= \frac{2}{\pi} k^4 \left| (k'^2 - k^2)(R_v - R_h)\cos\theta \right|^2 \\ &\iint_{-\infty}^{\infty} mn\, W(m^+,n^+)\, W(m^-,n^-) |D|^{-2} dm\, dn\end{aligned} \qquad (4.16)$$

where:

$$D = k^2 (k'^2 - m^2 - n^2)^{1/2} + k'^2 (k^2 - m^2 - n^2)^{1/2} \qquad (4.17)$$

$$m^{\pm} = n \sin(\varphi) + (m \pm k \sin\theta)\cos(\varphi) \qquad (4.18)$$

$$n^{\pm} = n \cos(\varphi) - (m \pm k \sin\theta)\sin(\varphi) \qquad (4.19)$$

To account for the tilting effect of large-scale waves, it is necessary to identify polarization changes due to tilting and then to

average the resulting expression for the scattering coefficient of the capillary waves over the slope distribution of the large-scale waves. The concept involved in considering polarization changes can be described in terms of two sets of coordinates: (1) the reference coordinates in which the scatter problem is posed, and (2) the local coordinates in which scattering due to capillary waves is computed. Let $\hat{v}$, $\hat{h}$, be the unit vertical and horizontal polarization vectors in the reference frame and $\hat{v}'$, $\hat{h}'$ be the corresponding unit vectors in the local frame. Let the incident field be $\mathcal{E}_o$. Then components of the local incident fields are:

$$\mathcal{E}^i_{h'} = \hat{h}'_o \cdot \vec{\mathcal{E}}_o \tag{4.20}$$

and

$$\mathcal{E}^i_{v'} = \hat{v}'_o \cdot \vec{\mathcal{E}}_o \tag{4.21}$$

Upon scattering by the capillary waves, each of the above incident field components is depolarized so that the scattered fields are

$$\mathcal{E}^s_{v'} = S_{v'h'} \mathcal{E}^i_{h'} + S_{v'v'} \mathcal{E}^i_{v'} \tag{4.22}$$

and

$$\mathcal{E}^s_{h'} = S_{h'h'}\,\mathcal{E}^i_{h'} + S_{h'v'}\,\mathcal{E}^i_{v'} \tag{4.23}$$

where S_{pq} is the scattering function for the capillary waves. The scattered fields in the reference frame become

$$\mathcal{E}^s_v = (\hat{v}\cdot\hat{h}')\,\mathcal{E}^s_{h'} + (\hat{v}\cdot\hat{v}')\,\mathcal{E}^s_{v'} \tag{4.24}$$

$$\mathcal{E}^s_h = (\hat{h}\cdot\hat{h}')\,\mathcal{E}^s_{h'} + (\hat{h}\cdot\hat{v}')\,\mathcal{E}^s_{v'} \tag{4.25}$$

It is clear from (4.13) that to compute the scattering coefficient for horizontal polarization the local vertically-polarized scattered field is needed and vice versa. Furthermore, there is a term involving the product of $\mathcal{E}^s_{h'}$ and $\mathcal{E}^s_{v'}$.

Special cases where $S_{h'v'}$, $S_{v'h'}$ are zero and tilt angles are small have been treated by Wright [1968], and cases where the tilt angle is restricted to the plane perpendicular to the plane of incidence have been studied by Valenzuela [1968]. Note that Valenzuela did not average over the tilt angles as Wright did. Thus, his results show the effect of polarization changes. The study of these special cases indicates that the polarization effects due to tilting are unimportant for vertical polarization. The same statement can be made for horizontal polarization when the incidence angle is restricted to less than about 70°. Hence, when averaging is included, the scattering coefficient for polarization scattering is approximately

$$\sigma^{\circ}_{pp}(\theta,\varphi) = \int_{-\infty}^{\infty}\int_{-\cot\theta}^{\infty} \sigma^{\circ}_{pp}(\theta';\varphi)\, P_{\theta}(Z_{x'}, Z_{y'})\, dZ_{x'}\, dZ_{y'} \quad (4.26)$$

where $\sigma^{\circ}_{pp}(\theta',\varphi)$ is given (4.1), θ' is the local angle of incidence, $P_0(Z_{x'},Z_{y'})$ is the slope distribution of the large-scale waves as viewed at an incidence angle, θ, and is defined in the prime coordinate whose x' axis is parallel to the wind direction. $Z_{x'},Z_{y'}$ are partial derivatives of Z. It is assumed that the plane of incidence is the x-z plane and that the angle between the x axis and the x' axis is φ, (Figure 4.1) so that an upwind observation occurs when φ=0. The relations between the primed and unprimed coordinates are

$$Z_{x'} = Z_x \cos(\varphi) - Z_y \sin(\varphi) \quad (4.27)$$

$$Z_{y'} = Z_y \cos(\varphi) - Z_x \sin(\varphi) \quad (4.28)$$

The cross-polarized scattering coefficient, including polarization and averaging effects for small tilts, is approximately

$$\sigma^{\circ}_{hv}(\theta,\varphi) = \int_{-\infty}^{\infty}\int_{-\cot\theta}^{\infty} \left[\sigma^{\circ}_{hv}(\theta',\varphi) + \sigma^{\circ}_{hv}(\theta',\varphi)\right] P_{\theta}(Z_{x'}, Z_{y'})\, dZ_{x'}\, dZ_{y'} \quad (4.29)$$

where

$$\sigma^{\circ}_{hv}(\theta',\varphi) = 8\, k^4 \left| Z_y (\alpha_{vv} - \alpha_{hh})/\sin\theta' \right|^2 W(\theta',\varphi) \quad (4.30)$$

and $\sigma^{\circ}_{hv}(\theta',\varphi)$ is given by (4.1).

The relation between the slope and density function $P_{\theta}(Z_{x'},Z_{y'})$ and function $P_{\theta}(Z_{x'},Z_{y'})$ defined by Cox and Munk [1954] is

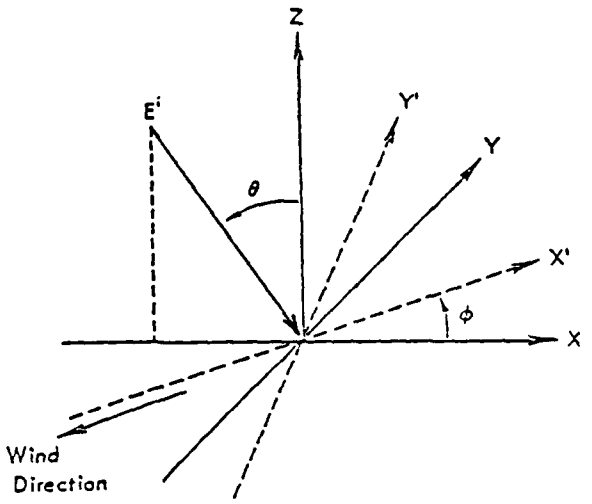

Figure 4.1
Diagram of the relation between
(Z,X,Y) and (Z,X',Y') coordinates.
[Chan and Fung, 1977]

$$P_\theta(z_{x'}, z_{y'}) = (1 + z_x \tan\theta) P(z_{x'}, z_{y'}) \qquad (4.31)$$

The form of $P(Z_{x'},Z_{y'})$ has been found to be a Grom-Charlier series [Cox and Munk (1954), Longuet-Higgins (1963), Pierson (1975)]. However, the values of the slope-variance parameters in the function require further studies. The slope variances, σ_u^2, σ_c^2, given by Cox and Munk [1954] are not restricted to large-scale waves. It is not clear at the present time how the slope variances for the large-scale wave alone can be obtained at a given microwave frequency. It has been suggested that one possible way to compute these slope variances is to integrate the low-frequency portion of the slope spectrum of the sea surface [Chan and Fung, 1977]. If we assume that some suitable slope variance parameters can be found, then all the quantities in the scattering coefficient have been discussed except the sea spectrum for the sea spectrum $W(\theta, \phi)$ to be discussed in the following section.

4.3.2 The Sea Spectrum

The high-frequency portion of the sea spectrum has undergone intense study in recent years [Pierson (1973), Mitsuyasu and Honda (1974), Afarani (1975)]. The general form of the directional sea spectrum is

$$S(K,\varphi) = S(K)\left(a_0 + a_1\cos(2\varphi)\right) \qquad (4.32)$$

when higher order terms in φ are neglected [Pierson, 1973]. The quantity determined from measurement is S(K). One form for S(K) proposed by Pierson [1975] for the fully-developed sea is as follows: [The large-K regions are based on wave-tank measurements. It should be noted that further revision of S(K) is being contemplated [Pierson, 1978].]

$$S(K) = S_i(K) \qquad K_{i-1} < K < K_i \qquad (4.33)$$

$$S_1(K) = \frac{a}{k^3}\exp\left[-\frac{0.749^2}{k^2 u(u^*)^4}\right] \qquad 0 < K < K_1 \qquad (4.34)$$

$$S_2(K) = a K_1^{-1/2} K^{-5/2} \qquad K_1 < K < K_2 \qquad (4.35)$$

$$S_3(K) = S_4(K_3)(K/K_3)^{\beta} \qquad K_2 < K < K_3 \qquad (4.36)$$

$$S_4(K) = 0.438(2\pi)^{\beta-1}\frac{g + 3gk^2/13.1769}{(9K + 9k^3/13.1769)^{\beta+1/2}} \qquad K_3 < K < K_4 \qquad (4.37)$$

$$S_5(K) = 1.473\times10^{-4} u^{*3} k_m^6 K^{-9} \qquad K_4 < K < \infty \qquad (4.38)$$

K_4 can be found numerically by setting $S_4(K_4)$ equal to $S_5(K_4)$. Other parameters are as follows:

u^* = friction velocity $u^* > u^*_m$

K_m = (13.1769)

$q = \log[S_8(K_2)/S_4(K_3)]/\log[K_2/K_3]$

$p_1 = 5.0 - \log u^*$

$Z_o = 0.684/u^* + 4.28 \times 10^{-5} u^{*2} - 4.43 \times 10^{-2}$

$u(u^*) = u^*/0.4\ \mathrm{Ln}(Z/Z_0)$ cm/sec.

$a = 4.05 \times 10^{-3}$

$g = 980$ cm/sec.

$u^*_m = 12$ cm/sec.

Note that this sea spectrum shows that the capillary waves (i.e., $S_4(K)$) grow with the wind and that the higher the K value the faster the growth. The parameters a_0 and a_1 have been derived by Chan and Fung [1977] and the relation between $W(\theta', \varphi)$ in (2) and (3) and $S(K, \varphi)$ has been found to be:

$$W(\theta', \varphi) = \frac{S(K)}{2\pi K}\left[1 + 2\left(\frac{1-V}{1+V}\right)\cos(2\varphi)\right] \qquad (4.39)$$

where $K = 2k\sin\theta'$, $V = \sigma_{ct}^2/\sigma_{ut}^2$, σ_{ct}^2, σ_{ut}^2 are the slope variances of the sea surface along the crosswind and upwind directions. A possible way of estimating V is to use the slope variance parameters given by Cox and Munk [1954] for their clean sea model. Note that $W(\theta', \varphi)$ is resricted to that portion of the sea spectrum which satisfies the assumptions in the perturbation theory. Thus, the value of K has a lower bound which is a function of the electromagnetic wavelength.

With the sea spectrum given in the preceding section, the sea-scatter model given by (4.14) can be evaluated. Figure 4.2 shows a comparison of the theoretical σ^o versus azimuth angle curves with experimental data taken on two different AAFE RADSCAT flights [Jones,

Schroeder and Mitchell, 1977, 1978]. Figure 4.3 illustrates the relation between scattering coefficient and wind speed at three angles for horizontal polarization and 13.9 GHz frequency, along with experimental points obtained with the AAFE RADSCAT instrument. The lines on the figures are theoretical values based on the σ° model and spectrum of Section 4.3.2.

Our following analysis for determination of theoretical scattering coefficient $\sigma^{\circ}_{\text{theory}}$, is based on having instantaneous slope. One can derive instantaneous local angle of incidence, θ', and also roughness spectrum $W(\theta', \varphi)$ and directly calculate the instantaneous

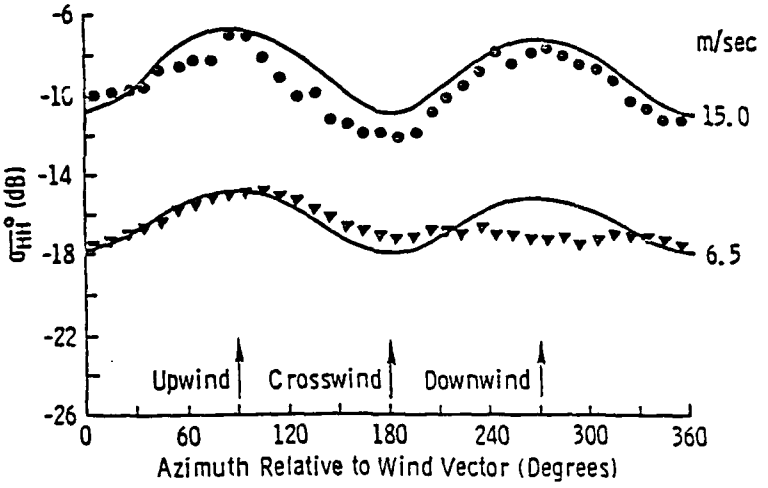

Figure 4.2
Comparison of theoretical results with a sample AAFE run [Chan and Fung, 1977].

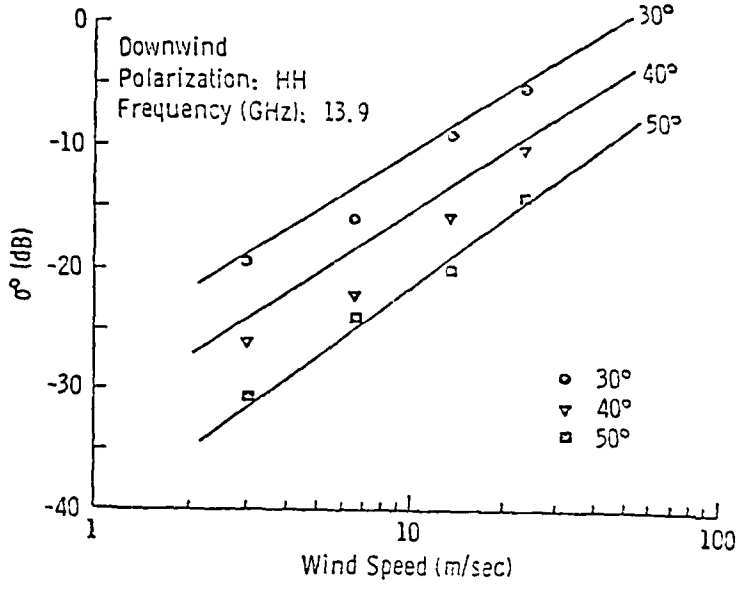

Figure 4.3
Example of theoretical and observed values of σ° plotted versus wind speed. AAFE Radscat data.

theoretical scattering coefficient, σ°_{theory}, Section 6.2.

$$\sigma^{\circ}_{pp}(\theta', \varphi) = 8k^4 |\alpha_{pp}|^2 W(\theta', \varphi) \qquad (4.40)$$

Note that α_{pp} and K are also functions of local angle of incidence, and that the above theory assumes that the shorter waves are uniformly distributed over the longer waves. When modulation of the amplitude of the shorter waves takes place, the analysis must be modified.

4.4 Theoretical Basis of Capillary Modulation Distribution

4.4.1 Modulation Phenomena

Short gravity-capillary waves, the equilibrium excitation of the ocean surface, are spatially and temporally modulated by large-scale ocean waves. Remote sensing of ocean waves by microwave radar depends

on these modulations [Wright, 1977] which may also induce transfer of substantial energy between short capillary and long large-scale waves.

An FM radar, such as that used by K.U., is a self-contained two-scale wave probe. The measure of the large-scale waves (several meters in length) is the instantaneous wave height, which is obtained from time-delay of the received signal (slant range) (Section 5.3). At appropriately chosen viewing angles the primary scatterers are capillary waves, a few centimeters in length. Hence the amplitude modulation of the received signal is a measure of the modulation of the capillary waves. Two important sources of modulation of scattered microwave power have been noted: modulation of the orientation of the capillary waves, called tilting, and modulation of the amplitude of the capillary waves, exemplified by the straining of the short capillary waves by the horizontal component of orbital velocity of the large waves.

If one assumes that the capillary wave amplitudes are uniform over the large-scale waves, the modulation of the received signal is completely governed by the variation of the local angle of incidence (tilting effect) caused by slope changes. Note that the instantaneous large-scale wave slope can easily be derived from the instantaneous wave height time profile, provided a long-crested assumption is made.

If one knows the spectrum of the capillary waves S(K) and the slope of the large-scale waves, the scattering coefficient can also be established (Section 6.2). Since the capillary wave amplitudes are not the same at all points on the large-scale waves, due to modulation, one of the major goals is to establish their distribution. This task can be done by comparing the radar signals calculated as mentioned above with the actual radar signal observed. The difference must be due to a

change in the amplitude of the capillary waves at the Bragg-resonant wavelength. When the variation of this amplitude difference is cross-correlated with the height or slope of the large-scale waves, an estimate of the phase relations of the peak of the distribution of 'apparent' capillary wave amplitude (with the crest of the wave or point of maximum slope) can be obtained (Section 8.0).

The term 'apparent' is used because interactions between the larger wavelength ocean waves and the capillary wave can result in stretching or compressing a persistent train of capillary waves, so that the wavelength associated with a particular pair of wave crests may be different, depending upon their position on the large-scale wave. Since the Bragg resonant condition for the radar can not follow these expansions and contractions of the wavelengths for a wave train, the signal observed might actually come from different wavelets, depending upon their position on the large-scale waves, even if the local angle of incidence were to remain the same.

4.4.2 Definition of the Modulation Index

Note that the scattering coefficient, σ°_{total}, can be resolved into the two components: contribution of backscattering due to orientation modulation (tilting) σ°_{tilt}, and contribution of backscattering due to amplitude modulation, σ°_{mod}. Hence

$$\sigma^{\circ}_{total} = \sigma^{\circ}_{tilt} + \sigma^{\circ}_{mod} \tag{4.41}$$

but

$$\sigma^{\circ}_{Theory} = \sigma^{\circ}_{tilt} \tag{4.42}$$

so

$$\sigma^{\circ}_{total} = \sigma^{\circ}_{Theory}\left(1+\frac{\sigma^{\circ}_{mod}}{\sigma^{\circ}_{Theory}}\right) \tag{4.43}$$

Let

$$\mu = \frac{\sigma^{\circ}_{mod}}{\sigma^{\circ}_{Theory}} \tag{4.44}$$

so

$$\sigma^{\circ}_{total} = \sigma^{\circ}_{Theory}(1+\mu) \tag{4.45}$$

where μ is called the 'modulation index.'

The concept of the modulation index is fairly straightforward. It is simply the ratio of the contribution of amplitude modulation to the contribution of tilting to the backscatter. The phase relations of the modulation index with respect to the crest and slope are discussed in Section 8.0.

5.0 EXPERIMENTAL SET-UP, MEASUREMENT TECHNIQUES AND 'EVENT' SOLUTION

5.1 Experimental Set-Up and System Description

The University of Kansas system was an FM radar operated over the band from 8-18 GHz, Ku-band. The block diagram of the system is shown in Figure 5.1. The platform near the Dutch coast was instrumented with both microwave and ocean-wave equipment for measurement of waves, currents and tides (Figures 5.2a and 5.2b).

5.2 Basis of Experiment

The microwave antenna was mounted just below the helicopter deck of the platform (Figures 5.3a and 5.3b). It illuminated a portion of the ocean surface that was small in comparison with the wavelength of any modulating (large-scale) ocean wave of interest. The short capillary waves, the predominant microwave scatterers are advected about by the large waves. The backscatter field caused by Bragg-resonant phenomena was measured at the receiver. From the frequency difference between transmitted and received signals, the slant range between the radar and the centroid of the illuminated area could be found and converted to wave height. From the signal return and the instantaneous area of the observed spot, the scattering coefficient could be determined. The result of these conversions would be a sample time profile of wave height in the center of the scattering-measurement area which is comparable with that obtained by a wave gauge at the tower and a simultaneous time history of the scattering coefficient. Brief remarks on radar equations and calculation of scattering coefficients and range follow. Note that the simplification of the radar equation when the radar parameters remain

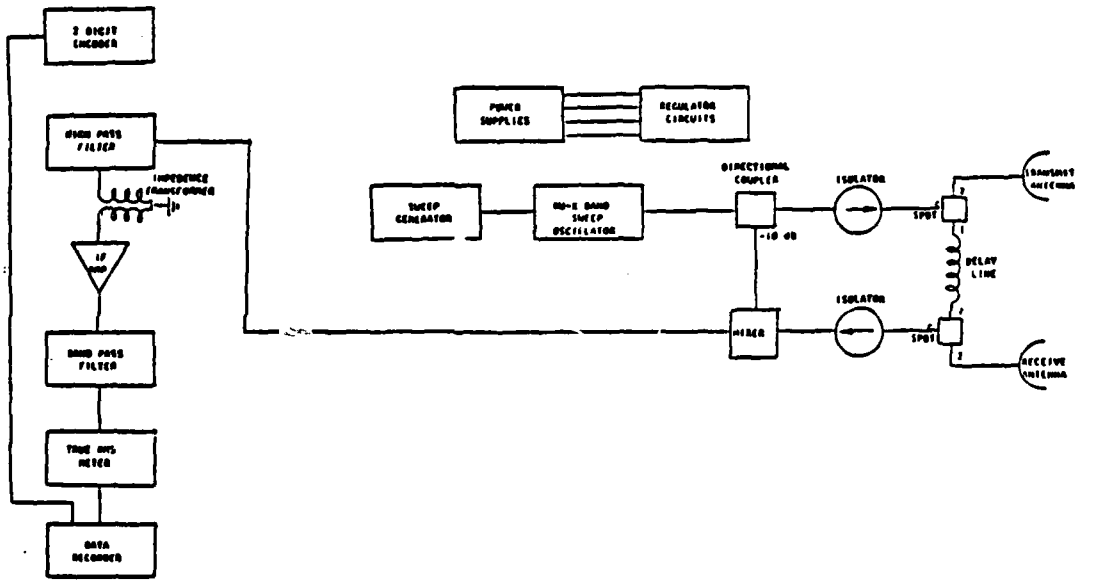

Figure 5.1
The block diagram of the radar system (TRAMAS)
used in the Noordwijk experiment

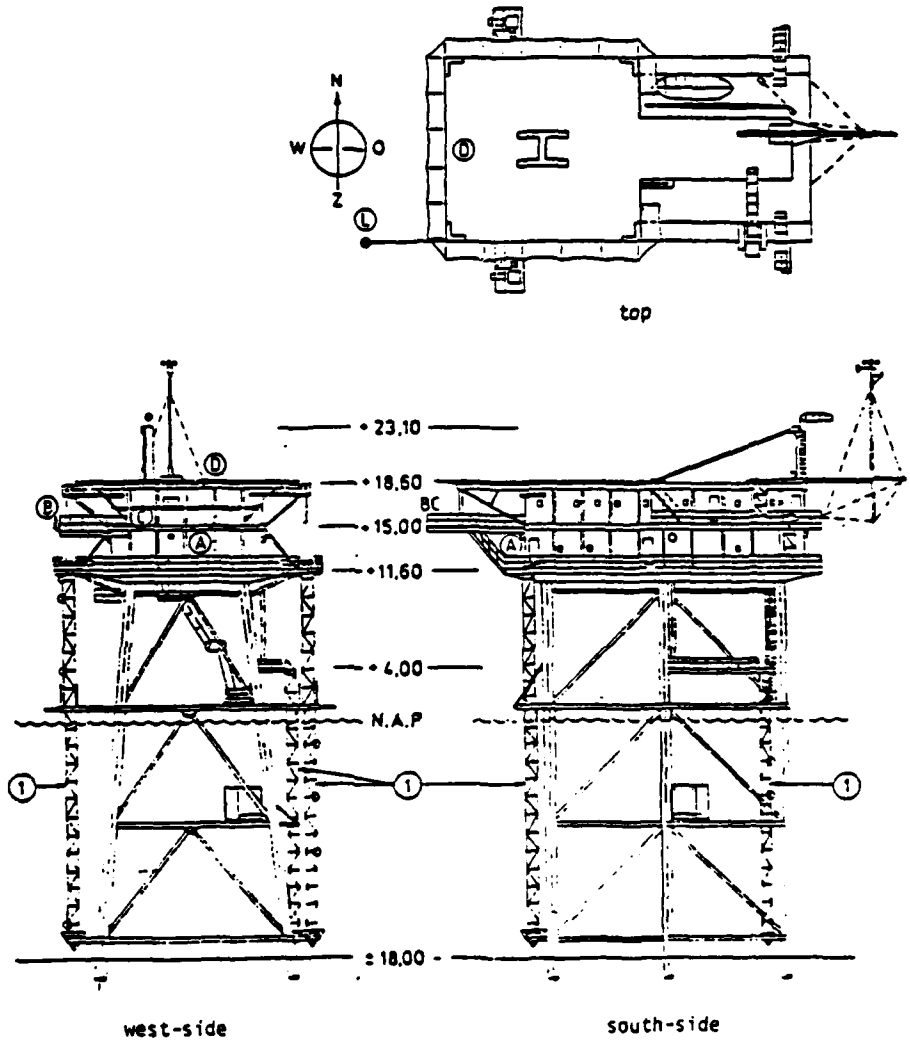

1. poles with oceanographic sensors
A. place of FM/CW measuring radar in 1977
B. ditto in 1978
C. place of French RAMSES system
D. place of 8 mm navigation radar
L. luneberg lens, protruding from helicopter deck (calibration)

Figure 5.2a
Measurement platform Noordwijk

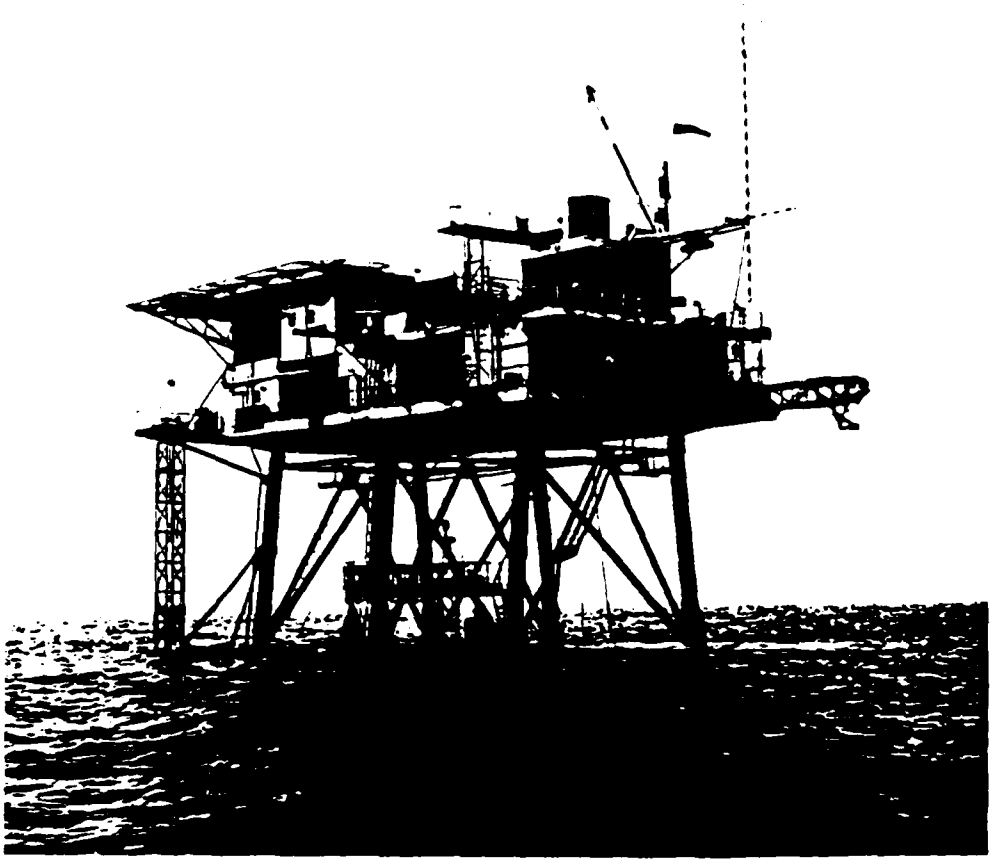

Figure 5.2b
Platform Noordwijk

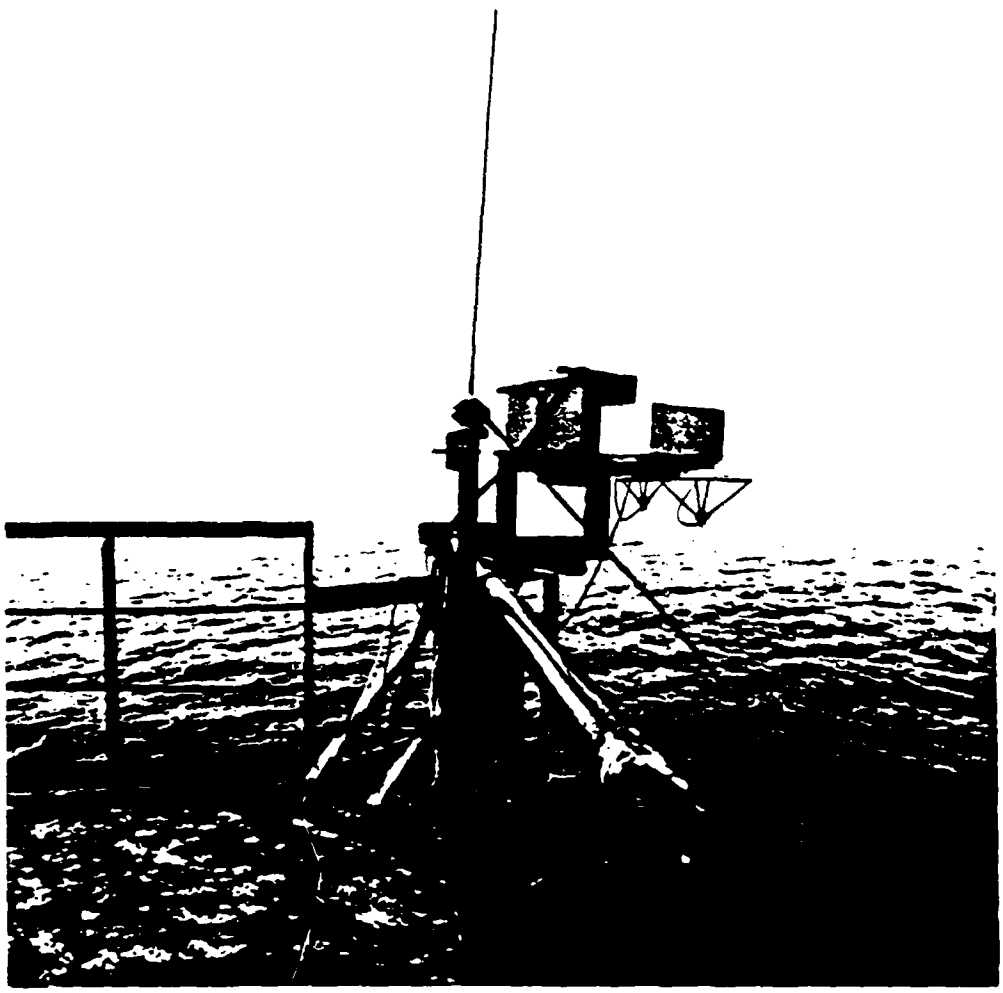

Figure 5.3
Illustration of antenna mounted at the top
of the Noordwijk Tower

essentially unchanged can be represented by

$$P_r = \frac{P_t G_t G_r \lambda^2 \sigma^\circ A_{ill}}{(4\pi)^3 R_t^4} \qquad (5.1)$$

where:

P_r = received power

P_t = transmitted power

G_t = transmit antenna gain

G_r = receive antenna gain

λ = wavelength

σ° = scattering coefficient (scattering cross-section per unit area)

A_{ill} = illuminated area

R = slant range to centroid of observation spot

The return power is measured by use of a square-law detector. The power measured by the detector may be related to the returned power at the receive-antenna terminal through an unknown constant K_t, which represents the effects of attenuation and conversion losses between antenna and detector. P_{dt}, the detector power, is therefore related to the returned power by

$$P_{dt} = K_t^2 \left[\frac{P_t G_t G_r \lambda^2 \sigma^\circ A_{ill}}{(4\pi)^3 R_t^4} \right] \qquad (5.2)$$

Immediately before and after recording the return from the ocean, a coaxial delay line of loss L is switched into the circuit at the antenna ports to replace the path through the transmit antenna to the surface and back through the receive antenna.

The power (through the delay line) after square-law detection is given by

$$P_{DLT} = K_t^2 P_t L \tag{5.3}$$

Taking the ratio of equations (5.2) and (5.3)

$$\frac{P_{dt}}{P_{DLT}} = \left[\frac{G_t G_r \lambda^2 \sigma^\circ A_{ILL}}{(4\pi)^3 R_t^4 L}\right] \tag{5.4}$$

To complete calibration of the system, the returns from a standard target of a known radar cross-section are measured. The Luneberg lens of the Dutch group was used as a standard target. The returned power of standard radar targets is given by

$$P_{LENS} = K_c^2 \left[\frac{P_t G_t G_r \lambda^2 \sigma_{SRT}}{(4\pi)^3 R_c^4}\right] \tag{5.5}$$

where:

K_c = system constant k at time of calibration

R_c = range to standard radar target

σ_{srt} = scattering coefficient of standard target

The power detected through the coaxial delay line at the time of calibration using the standard radar target is given by

$$P_{DLL} = K_c^2 P_L L \tag{5.6}$$

The ratio of equations (5.5) and (5.6) is given by:

$$\frac{P_{LENS}}{P_{DLL}} = \frac{G_t G_r \lambda^2 \sigma_{SRT}}{(4\pi)^3 R_c^4 L} \tag{5.7}$$

Combining equation (5.4) with (5.7) and solving for :

$$\sigma^o = \frac{P_{dt} P_{DLL} R^4 \sigma_{SRT}}{P_{DLT} P_{LENS} R_c^4 L} \tag{5.8}$$

Note that the radar cross-section of the Luneberg lens was supplied by the manufacturer, but a recalibration was performed at the University of Kansas [Kim, 1982].

The illuminated area was calculated using the geometry shown in Figure 5.4. The projection of the radar beam as seen on the flat

surface is a skewed ellipse. The area of the ellipse was calculated using

$$A = \frac{\pi}{4}\left(M_{axis}\right)\left(m_{axis}\right)$$

where M_{axis} is the major axis and m_{axis} is the minor axis.

From the geometry of Figure 5.4, the expressions for the major and minor axes were derived.

$$M_{axis} = R\cos\theta\left[\tan\left(\theta+\frac{\beta_E}{2}\right)-\tan\left(\theta-\frac{\beta_E}{2}\right)\right] \qquad (5.9)$$

$$m_{axis} = 2\left[R\tan\left(\frac{\beta_A}{2}\right)\right] \qquad (5.10)$$

where:

M_{axis} = major axis

m_{axis} = minor axis

R = range to center of target

θ = pointing angle of antennas off vertical

β_E = effective gain-product (for receiving and transmitting antennas) beamwidth in elevation plane

β_A = effective gain-product beamwidth in the azimuthal plane

For a given target at range R, the time that returned signals are delayed is

$$\Delta t = \frac{2R}{c} \qquad (5.11)$$

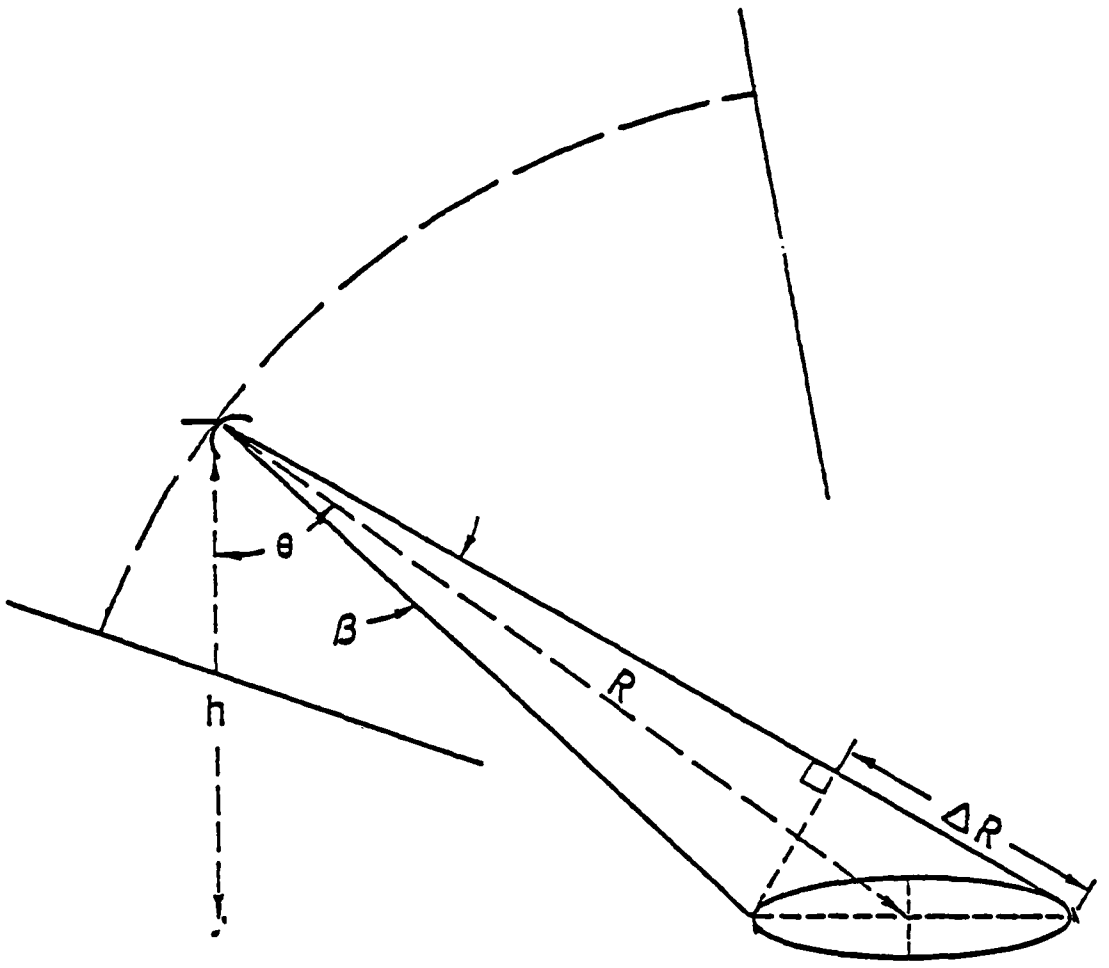

Figure 5.4
Parameters used in determining illuminated area.

An illustration of the frequency relationship between the transmitted and received signal is shown in Figure 5.5. It can be shown that

$$\frac{\Delta t}{F_{IF}} = \frac{1/4 F_M}{\Delta f/2} \tag{5.12}$$

so

$$R = \frac{F_{IF} c}{4(\Delta f) F_M} \tag{5.13}$$

where:

c = speed of light

F_{IF} = intermediate frequency

F_M = sweep rate

Δf = sweep frequency width

In this system, F_{IF} was fixed at 50 kHz and Δf was fixed at 1 GHz. F_M is adjusted by a tracking loop to center the target return at 50 kHz.

5.3 Measurement Techniques

Measurements were made at angles of incidence, θ, from 10^{o} to 80^{o} (Figure 5.6), with both vertical and horizontal polarizations. Frequencies for the measurements were at 1 GHz intervals from 9 to 17 GHz. Measurements were made at various angles relative to the wind direction with a large number of measurements in the upwind and downwind direction, a smaller number of measurements in the cross-wind

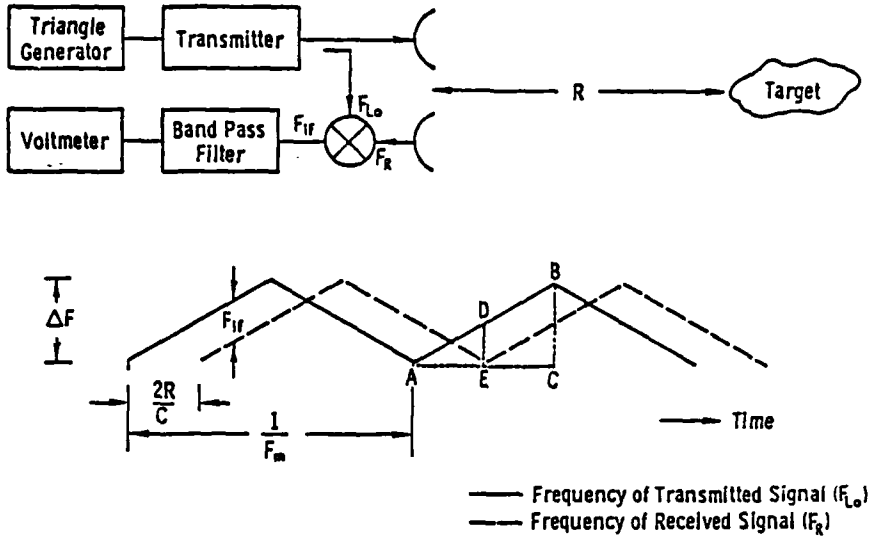

Figure 5.5
Frequency relationship between the transmitted and received signal for an FM radar

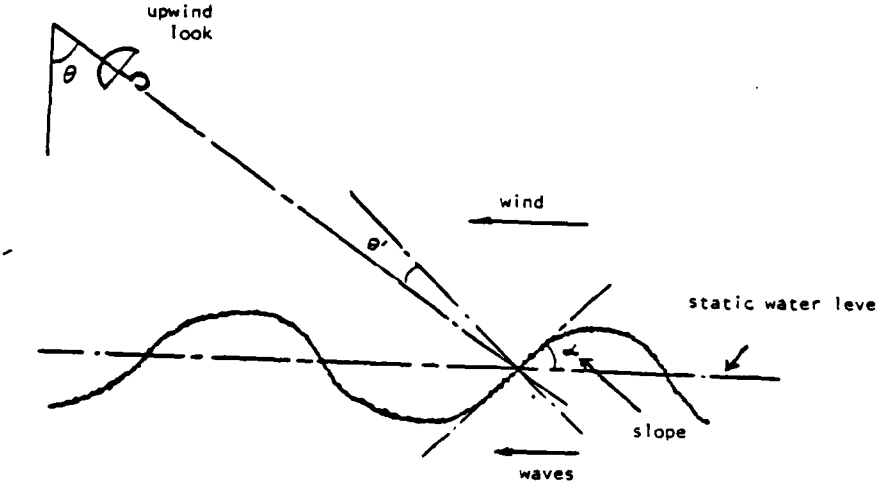

Figure 5.6
Angle of incidence, θ, varies between 10° and 80°. Note that the local angle of incidence θ' is modified by the slope α of the large-scale wave.

direction and a few measurements in which the azimuth angle was varied during collection of a single set of data.

Sampling rate was 1 Hz (one sample per second) so the maximum frequency one expected to see was 0.5 Hz. For both convenience and assurance that aliasing would be prevented, the wave height time series were low-pass filtered to a cutoff frequency of 0.35 Hz. This should not eliminate significant information in the wave height time series, since one expects about 95 percent of signal energy to be distributed between 0.1 and 0.2 Hz in normal climate conditions for wind speed less than 20 m/sec. Each set of experiments usually took 10-15 minutes. At the start of a set, the wind speed, polarization and azimuth were recorded and, in each set, the instantaneous slant range (actually F_M), wave gauge record, and power return were recorded on the cassette tape.

Examination of the reduced data showed that a very large number of successful measurements was made, but that many of the measurements contained errors due to such causes as lack of proper tracking of the illuminated area by the range-tracker circuitry and poor signal-to-noise ratio.

Although measurements were made at frequencies separated by only 1 GHz, many of the data sets were obtained at only two frequencies -- 10 and 15 GHz. This was done to permit longer sampling intervals than would have been possible if both angle of incidence and frequency had been changed over the entire range of parameters. Because of the variation of the Bragg-resonant wavelength with angle of incidence, a nearly complete set of the possible Bragg-resonant conditions was obtained with the two-frequency measurements.

5.4 'Specular Events' Observation

Interesting phenomena that were observed in the time history of radar return records were designated 'specular events'. Study of the time history of radar returns indicates that most of the time the signal fades about a mean level associated with the local angle of incidence. Occasionally certain 'events' occur in which the signal is much larger. This has been noted particularly at angles of incidence near grazing [Kalmykov and Pustovoytenko, 1976], but has also been observed at other angles of incidence. An example of this type of behavior is shown in Figure 5.7 that contains six noncontiguous 128-second samples of the time series of scattering coefficient. Notice the generally small fluctuation about the varying mean level with the occasional events, where the signal increases greatly. No corresponding events occur for decreasing signal, so these large signals appear to be caused by different phenomena than the normal fading. These phenomena were observed by Kwoh and Lake [1981] in a wave tank, where they identified two classes of events. In one class, both polarizations gave the same return, and the laser sensor indicated that specular reflection was possible. In the other class, the vertically polarized returns were larger than the horizontal returns. These were attributed to edge diffraction from sharp edges where waves approach the breaking point.

The capillary-wave return power is proportional to the square of the number of scatterers within the footprint, because their backscattered fields add coherently, whereas the mean return from the events is proportional to the average number of events per footprint. Since the events are randomly located, their backscattered fields add

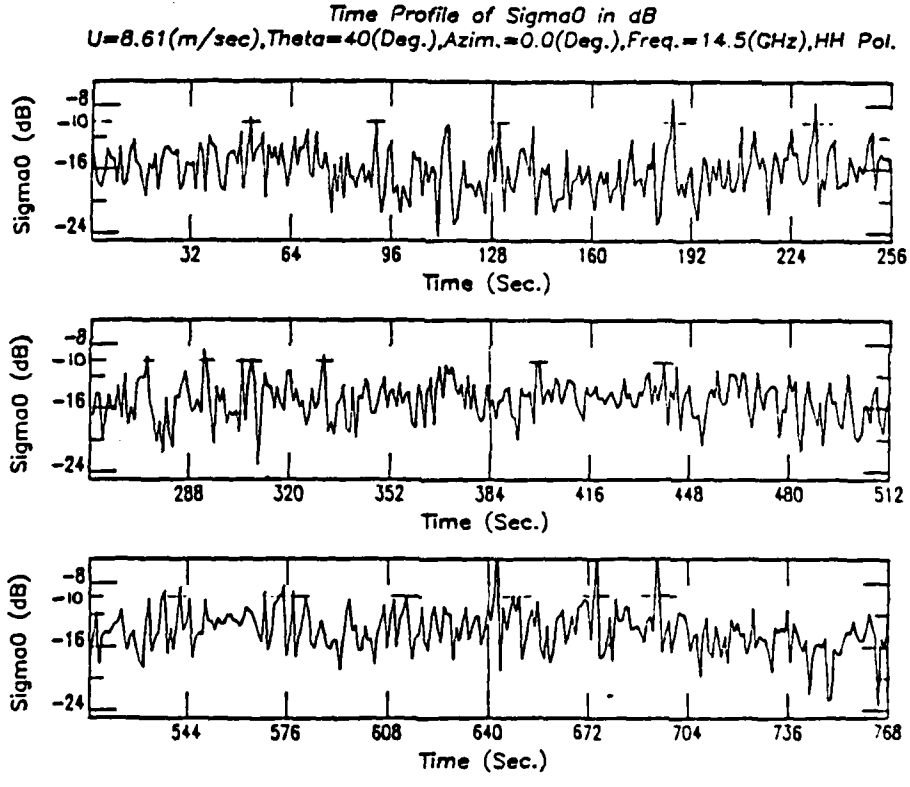

Figure 5.7
Sample of time profile of σ^0 (dB), illustrating the specular events. Each 128-sec record is from a different time.

noncoherently. The significant differences which have been reported between the scattering coefficient of the ocean measured by radars in aircraft and spacecraft and those measured by radars on towers may be explainable with this theory. The larger footprints mean a larger capillary contribution relative to the event contribution. Therefore, the specular and other (perhaps edge diffraction) events cause a much larger modification to the Bragg-scatter signal strength for the low altitude (where the footprint is smaller) than for the high altitude (where the footprint is large). The derivation of this conclusion is shown in Appendix B.

6.0 THE BASIS OF THE CALCULATIONS

6.1 Slope Calculation

The height of the large-scale gravity waves for a finite record length can be written as follows (Section 4.1.5):

$$h(x,t) = \sum_i a_i \cos(k_i (x + c_o t) + \varphi_i) \quad (6.1a)$$

$$= \sum_i a_i \cos(k_i x + \omega_i t + \varphi_i) \quad (6.1b)$$

where:

a_i = the amplitude of the i^{th} component of the wave

ω_i = angular frequency of the i^{th} component

K_i = i^{th} wave number

The water at Noordwijk is about 20 m deep. This is close enough to the condition for use of a deep-water dispersion relation (Section 4.1.4) that such a relation can be used with little error. Here we used the deep-water form:

$$k_i = \omega_i^2 / g \quad (6.2)$$

where g is the gravitational constant 9.81 m/sec^2.

Another simplifying assumption made here is that the wave is sufficiently long-crested that its slope may be considered to be in the direction of wave travel in the -x direction. Making this assumption, slope s(x,t) is given by:

$$s(x,t) = \frac{\partial h}{\partial x}(x,t) = -\sum_i a_i k_i \sin(\omega_i t + k_i x + \varphi_i) \quad (6.3)$$

During the Noordwijk experiment two measurements of H(t) were made (Section 5.3), one with a wave gauge at the tower and the other by measuring the slant range between the radar and the observed spot on the surface. The latter measurement amounts to locating a wave gauge at the centroid of the observed region. If we assume that this point is at x=0, the slope at that point will be, on an instantaneous basis:

$$S(0,t) = -\sum_i a_i k_i \sin(\omega_i t + \varphi_i) \qquad (6.4a)$$

$$= -\sum_i a_i \frac{\omega_i^2}{g} \sin(\omega_i t + \varphi_i) \qquad (6.4b)$$

This slope, however, is also the tangent of the slope angle so that we write:

$$S(0,t) = \tan(\alpha(0,t)) \cong \alpha(0,t) \qquad (6.5)$$

where the approximation has been made that the slopes are small. The maximum slopes observed are on the order of 12°, at least for the lower wind speeds, so that this is a reasonable assumption. Figure 8.8 (Section 8.0) shows sample slope distribution. Combining (6.4b) and (6.5) the slope angle can be approximated by:

$$\alpha(0,t) \cong -\sum_i a_i \frac{\omega_i^2}{g} \sin(\omega_i t + \varphi_i) \qquad (6.6)$$

6.2 Scattering Coefficient Calculation

The Bragg-resonant wavelength is a function of the instantaneous angle of incidence. The angle of incidence, normally assumed to be the pointing angle θ_p for a radar, is modified by the slope of the underlying, large-scale wave (Figure 5.7). Thus we may write for the Bragg-resonant condition:

$$K = 2k \sin(\theta_p - \alpha) \tag{6.7}$$

where k is the radar wave number and θ_p is the pointing angle, measured from vertical for the radar antenna.

Let the local angle of incidence be θ', where

$$\theta' = \theta_p - \alpha \tag{6.8}$$

so the instantaneous theoretical scattering coefficient $\sigma^\circ_{theory}(\theta', \varphi)$ would be (Section 4.3.1):

$$\sigma^\circ_{pp}(\theta', \varphi) = 8k^4 |\alpha_{pp}|^2 \sigma_1^2 W(\theta', \varphi) \tag{6.9}$$

where for horizontal polarization

$$\alpha_{hh} = R_h \cos^2(\theta') \tag{6.10a}$$

R_h being the Fresnel reflection coefficient for horizontal polarization:

$$R_h = \frac{\cos\theta - \sqrt{\mu_r(\epsilon' - j\epsilon'') - \sin^2\theta}}{\cos\theta + \sqrt{\mu_r(\epsilon' - j\epsilon'') - \sin^2\theta}} \qquad (6.10b)$$

For vertical polarization

$$\alpha_{vv} = R_v \cos^2(\theta') + (k'^2 - k^2) T_v^2 \sin^2(\theta)/2k'^2 \qquad (6.11a)$$

R_v and T_v being the Fresnel reflection and transmission coefficients. For vertical polarization:

$$R_v = \frac{\mu_r(\epsilon' - j\epsilon'')\cos\theta - \sqrt{\mu_r(\epsilon' - j\epsilon'') - \sin^2\theta}}{\mu_r(\epsilon' - j\epsilon'')\cos\theta + \sqrt{\mu_r(\epsilon' - j\epsilon'') - \sin^2\theta}} \qquad (6.11b)$$

$$T_v = 1 + R_v \qquad (6.11c)$$

In α_{pp}, k is the radar wave number in air, k' is the radar wave number in sea water, and θ' is the local angle of incidence.

$W(\theta', \varphi)$ is the normalized anisotropic sea spectrum, and σ_1^2 is the varisance of the small-scale, capillary waves as shown by Fung and Chan [1977].

$$\sigma_1^2 W(\theta', \varphi) = \frac{S(K)}{2\pi K}\left[1 + 2\left(\frac{1-R}{1+R}\right)\cos(2\varphi)\right] \qquad (6.12)$$

where $R = \sigma_{ct}^2/\sigma_{ut}^2$ is the ratio of slope variance at crosswind, σ_{ct}^2, to slope variance at upwind, σ_{ut}^2, and $K = 2k\sin(\theta')$.

Determination of S(K), the spectrum of the small capillary wave is based on a modification of Pierson and Stacy's [1973] sea spectrum (Section 4.3.2). The region of their spectral model that we are

interested in is the capillary region, $S_4(K)$, where

$$S_4(K) = 0.438(2\pi)^{f_1-1} \frac{g + 3gk^2/13.1769}{(gk + gk^3/13.1769)^{f_1+1/2}} \qquad (6.13)$$

The parameters which have been used in this model have been described in Section 4.3.2. Even though the model looks very cumbersome, the instantaneous sea spectrum $S(K(\theta'(t)))$, based on instantaneous local angle of incidence and windspeed, can easily be determined.

In the part of the experiment reported here the antenna pointed to upwind (φ =0°), downwind (φ =180°), or crosswind (φ =90°), so the scattering coefficient would be considered only local-angle-of-incidence, θ', dependent. Hence

$$\sigma_{pp}(\theta') = \frac{2k^3}{\pi \sin(\theta')} |\alpha_{pp}|^2 S(2k \sin\theta') \left[1 + 2\left(\frac{1-R}{1+R}\right)\right] \qquad (6.14)$$

It is worthwhile mentioning that the last factor in the numerator, [1+2(1-R/1+R)]is constant for a specific, given windspeed u, so one can state

$$\sigma_{pp}(\theta'(t)) = \frac{2k^3}{\pi} |\alpha_{pp}|^2 S(2k \sin\theta') A(u) / \sin(\theta') \qquad (6.15a)$$

$$= B_{pp}(\theta'(t), u) A(u) \qquad (6.15b)$$

where:

A(u) is constant at a given windspeed

For determination of instantaneous scattering coefficient, $\sigma^{\circ}(\theta'(t))$, we normalized the instantaneous calculated value of $_{pp}B(\theta'(t),u)$ to $\bar{B}_{pp}/\bar{\sigma}^{\circ}_{pp\,total}$, where $\bar{B}_{pp}$ is mean of $_{pp}B(\theta'(t),u)$ and $\bar{\sigma}_{pp\,total}$ is mean of actual, measured scattering coefficient (Section 5.2). This type of normalization, here called theoretical scattering coefficient calibration, not only takes care of A(u),[1+2(1-R/1+R)] but also compensates for any other scaling factor that we did not take into account (Section 5.4). The theoretical scattering coefficient is therefore defined as $\sigma^{\circ}_{Theory}(\theta'(t))$, with

$$\sigma^{\circ}_{Theory}(\theta'(t)) = B_{pp}(\theta'(t),u) \Big/ (\bar{B}_{pp}/\bar{\sigma}^{\circ}_{pp\,total}) \qquad (6.16)$$

6.3 Modulation Index Calculation

As discussed in Section 4.3, if no amplitude modulation of the capillaries were present, the only source of modulation in backscatter from the sea surface is tilting, but it has been shown very clearly by several investigators (Section 3.0) that the amplitude modulation of the capillary waves does indeed exist and has very important contributions to actual scattering coefficient. Therefore we may write

$$\sigma_{total}(\theta'(t)) = \sigma^{\circ}_{tilt}(\theta'(t)) + \sigma^{\circ}_{mod}(\theta'(t)) \qquad (6.17)$$

where:

$\sigma^{\circ}_{tilt}(\theta'(t))$ is instantaneous scattering coefficient contribution due to tilting effect.

$\sigma^{\circ}_{mod}(\theta'(t))$ is instantaneous scattering coefficient contribution due to capillary wave modulation.

Then

$$\sigma^{\circ}_{total}(\theta'(t)) = \sigma^{\circ}_{tilt}(\theta'(t))\left(1+\frac{\sigma^{\circ}_{mod}(\theta'(t))}{\sigma^{\circ}_{tilt}(\theta'(t))}\right) \qquad (6.18)$$

Note that $\sigma^{\circ}_{tilt}(\theta'(t))$ is the same as $\sigma^{\circ}_{Theory}(\theta'(t))$, the theoretical scattering coefficient (Section 4.3), so

$$\sigma^{\circ}_{total}(\theta'(t)) = \sigma^{\circ}_{Theory}\left(1+\frac{\sigma^{\circ}_{mod}(\theta'(t))}{\sigma^{\circ}_{Theory}(\theta'(t))}\right) \qquad (6.19)$$

Here we define the modulation index

$$\mu(t) = \frac{\sigma^{\circ}_{mod}(t)}{\sigma^{\circ}_{Theory}(t)}$$

So, from (6.19)

$$\mu(t) = \frac{\sigma^{\circ}_{total}}{\sigma^{\circ}_{Theory}} - 1 \qquad (6.20)$$

$\mu(t)$ is the ratio of the contribution of backscatter due to amplitude modulation of capillary waves to the contribution of backscatter due to orientation of capillary waves over the large-scale waves.

6.4 Cross-Correlation Calculation

Cross-correlation of modulation index, $\mu(t)$ with wave height, $h(o,t)$ can readily show the phase relationships between the peak of capillary amplitude and the crest of the large-scale wave (Section 8.0). Analytically,

$$d(\tau) = \left[\frac{1}{T}\int_0^T \mu(t)\, h(o, t+\tau)\, dt\right] \Big/ \left(\bar{\mu}^2 \bar{h}^2\right)^{1/2} \quad (6.21a)$$

Numerically, Section 8.0

$$d(m) = \frac{1}{2N} \sum_0^{2N} \mu(n)\, h(o, n+m) \Big/ \left(\bar{\mu}^2 \bar{h}^2\right)^{1/2} \quad (6.21b)$$

With the cross-correlation of modulation index, $\mu(t)$, with slope, $s(o,t)$ one can determine the phase relationships between peak of capillary modulation and peak of the slope. Analytically

$$\ell(t) = \left[\frac{1}{T}\int_0^T \mu(t)\, S(o, t+\tau)\, dt\right] \Big/ \left(\bar{\mu}^2 \bar{S}^2\right)^{1/2} \quad (6.22a)$$

Numerically, Section 8.0:

$$\ell(m) = \frac{1}{2N} \sum_0^{2N} \mu(n)\, S(o, n+m) \Big/ \left(\bar{\mu}^2 \bar{S}^2\right)^{1/2} \quad (6.22b)$$

6.5 Modulation Transfer Function Calculation

Consider the backscattered signal to a microwave radar which illuminates an area of sea surface, at least one dimension of which is much smaller than the wavelength of the dominant surface wave. The

backscattered power is found to fluctuate with time and may be represented by Fourier series

$$\mathcal{P}(t) = \sum_{0}^{\infty} \mathcal{P}_n \cos(2\pi n f t + \varphi_n) \qquad (6.23a)$$

$$= \mathcal{P}_0 \cos(\varphi_0) + \mathcal{P}_1 \cos(2\pi f_0 t + \varphi_1) + \ldots\ldots \qquad (6.23b)$$

In many cases, harmonics of the ocean wave frequency are not found in the return power. Furthermore, it is found that the amplitude of the fluctuation in the power increases with the height of the ocean wave [Plant, 1980]. To incorporate these observations in $\mathcal{P}(t)$, let

$$\bar{\mathcal{P}} = \mathcal{P}_0 \cos(\varphi_0) \qquad (6.24a)$$

$$\mathcal{P}_1 = \bar{\mathcal{P}} |R| A \qquad (6.24b)$$

$$\varphi_1 = \varphi \qquad (6.24c)$$

$$\mathcal{P}_n = 0 \qquad (6.24d)$$

where $\bar{\mathcal{P}}$ is mean backscattered power, A is wave amplitude and R is a coefficient describing the power modulations with these definitions.

$$\mathcal{P}(t) = \bar{\mathcal{P}} \left[1 + |R| A \cos(2\pi f_0 t + \varphi)\right] \qquad (6.25)$$

Let the surface displacement be $h(x,t)$

$$h(x,t) = A\cos(Kx - 2\pi f_o t) \tag{6.26}$$

The wave slope is given by

$$\frac{\partial h}{\partial x} = -KA\sin(KA - 2\pi f_o t) \tag{6.27}$$

We may therefore write the magnitude of the wave slope as

$$\left|\frac{\partial h}{\partial x}\right| = KA = U_o/C \tag{6.28}$$

where C is the phase speed of the ocean wave, $\frac{2\pi f_o}{K}$, and

$$U_o = \left|\frac{\partial h}{\partial t}\right| \tag{6.29}$$

is the magnitude of the horizontal component of orbital velocity. Thus,

$$P(t) = \bar{P}\left[1 + |m|\frac{U_o}{C}\cos(2\pi f_o t + \varphi)\right] \tag{6.30}$$

where

$$|m| = \frac{|R|}{K} \tag{6.31}$$

If we write this in complex notation, we have

$$P(t) = \bar{P}\left[1 + |m|\left(\frac{U_o}{C}\right)e^{i2\pi f_o t}\right] \tag{6.32}$$

where m is now a complex quantity whose phase is positive if it leads the wave crest. Since m may depend on ocean wave frequency, it is called the modulation transfer function. It is a dimensionless quantity and is related to R, which has dimensions of inverse length, by

$$m = \frac{R}{k} \tag{6.33}$$

The modulation transfer function may be evaluated by cross-correlating with either wave height or horizontal component of orbital velocity. In our case we evaluate MTF by cross-correlating with wave height. Correlating $p(t)$ and $h(0,t)$,

$$p(t) * h^{*}(0,t) = \frac{1}{2} \bar{P} R A^{2} e^{i 2\pi f_0 \tau} \tag{6.34}$$

where τ is the time lag. But,

$$h(0,t) * h^{*}(0,t) = \frac{1}{2} A^{2} e^{i 2\pi f_0 \tau} \tag{6.35}$$

so

$$p(t) * h^{*}(0,t) = \bar{P} R \left(h(0,t) * h^{*}(0,t) \right) \tag{6.36}$$

Transforming the equation to Fourier domain,

$$P(f) H^{*}(f) = \bar{P} R(f) \left| H(f) \right|^{2} \tag{6.37}$$

so

$$R(f) = \frac{\langle P(f) H^{*}(f) \rangle}{\langle \bar{P} \, | H(f)|^{2} \rangle} \qquad (6.38)$$

The plots of R(f), MTF and $P(f)$ and $H(f)$ versus frequency are shown in Figures 8.22 through 8.27 (Section 8.0).

6.6 Coherence Function Calculation

The last quantity that we have calculated is coherence function, defined by

$$C^{2}(f) = \frac{\left\{ E\left[P(f) H^{*}(f) \right] \right\}^{2}}{E\left[|P(f)|^{2} \right] E\left[|H(f)|^{2} \right]} \qquad (6.39)$$

The coherence function has a maximum of one at any given frequency.

Values less than one indicate either: (1) noisy signal, (2) $P(f)$ and $H(f)$ are not linearly dependent, or (3) $P(f)$ is due to sources in addition to $H(f)$. The discussion about coherence function is in Section 8.0. Figures 8.28 and 8.29 (Section 8.0) show the plot of coherence vs frequency.

7.0 TRANSFORMATION FROM TEMPORAL TO SPATIAL DOMAIN

7.1 Problem Description

Measurement of wave height was made with both the wave gauge and the FM radar capability of TRAMAS (Section 5.3). These point measurements of time history are interesting, but many of the features of the waves that are desired are spatial rather than temporal, i.e., distribution of capillary wave amplitude over large-scale wave. In the following we discuss the means to convert the temporal information into spatial information on the assumption that waves are long-crested (Section 4.0), and that observations are made in an upwind or downwind direction. If we know the spectrum of the capillary waves S(K), and the slope of the large-scale waves, as a function of distance, the theoretical scattering coefficient may also be established as a function of distance. Furthermore, if one could prove that the transformation of information from temporal to spatial domain is a linear process, the direct conversion of the scattering coefficient or any other quantity of interest from temporal to spatial domain would be possible.

Since the capillary wave amplitudes are not the same at all points on the large-scale wave (Section 3.0), one of the major goals is to establish their distribution. To establish the spatial distribution of capillary wave amplitude over the large-scale wave, one must convert the waveheight-time profile to a waveheight-distance profile. Because of the nonlinear relationship between the wave number K and the angular frequency , this is not as trivial a task as one might suppose. In the following, we undertake to lay the basis for the calculation.

7.2 Discrete Form

Consider a wave traveling in the -x direction. It may be represented by a series of the form (Section 4.1.5):

$$h(x,t) = \sum_i a_i \cos(\omega_i t + k_i x + \varphi_i) \tag{7.1a}$$

or

$$h(x,t) = \mathrm{Re} \sum b_i e^{j(\omega_i t + k_i x)} \tag{7.1b}$$

where b_i is a complex amplitude.

$$b_i = a_i e^{j\varphi_i} \tag{7.2a}$$

In deep water the relation between K and ω is (Section 4.1.4)

$$k_i = \frac{\omega_i^2}{g} \tag{7.2b}$$

In the radar or wave-gauge measurement, we observe the height h(0,t) where it is assumed that the measurement is made at x=0 (Section 5.3). To express this in terms of Fourier series for a measurement of duration T, we may write

$$b_i = \int_{-T/2}^{T/2} h(0,t) e^{-j\omega t} dt \tag{7.3}$$

where

$$\omega_i = \frac{2\pi i}{T} \tag{7.4}$$

Recovering the time variation of height from the Fourier series then consists merely of evaluating

$$h(o,t) = \mathrm{Re} \sum_i b_i e^{j\omega_i t} \tag{7.5}$$

If somehow we could observe, at a single instant, the height as a function of distance h(x,0) we would obtain the Fourier coefficient for this function by

$$b_n = \int_{-x/2}^{x/2} h(x,o)\, e^{-jk_n x} \tag{7.6}$$

where

$$k_n = \frac{2\pi n}{x} \tag{7.7}$$

We could regain the function of height by

$$h(x,o) = \mathrm{Re} \sum_n b_n e^{jk_n x} \tag{7.8a}$$

where

$$k_n = \left(\frac{2\pi}{T}\right)^2 / g \tag{7.8b}$$

also

$$h(x,o) = Re\sum b_i e^{j\frac{(n\omega)^2}{g}x} \tag{7.8c}$$

Note, however, that the terms in (7.8) are uniformly spaced in K, whereas the terms in (7.5) are uniformly spaced in ω. The Fourier coefficients are different even though the values b_i and b_n are samples of the same continuous spectra. It is this difference that causes problems in using the coefficients obtained by (7.3) to evaluate (7.8a).

The slope might be obtained easily by differentiating the series of (7.1), that is

$$\frac{\partial}{\partial x} h(x,t) = \sum_i j b_i k_i e^{j(\omega_i t + k_i x)} \tag{7.9}$$

so either $\frac{\partial h(o,t)}{\partial x}$ or $\frac{\partial h(x,o)}{\partial x}$ can be recovered by multiplying terms in the appropriate series by jK.

7.3 Continuous Form

It is instructive to consider what happens with continuous frequency and K functions rather than Fourier series, particularly since the FFT algorithms, although actually involving Fourier series, are addressed as if they were for continuous functions.

In continuous form we may write the time series as

$$h(o,t) = \int_{-\infty}^{\infty} H(\omega) e^{j\omega t} \frac{d\omega}{2\pi} \tag{7.10}$$

or the spatial series as

$$h(x,0) = \int_{-\infty}^{\infty} H(\omega(K)) e^{jKx} \frac{dK}{2\pi} \tag{7.11}$$

where

$$\omega = \sqrt{Kg}$$

so

$$h(x,0) = \int_{-\infty}^{\infty} H(\sqrt{Kg}) e^{jKx} \frac{dk}{2\pi} \tag{7.12}$$

The two integrals (7.10) and (7.12) obviously are not the same because K and ω are related by $\omega = \sqrt{Kg}$. Note that H(u) and H($\sqrt{kg}$) are generally not equal.

One can also find the slope in either the time or the frequency domain by differentiating the appropriate functions obtaining

$$\frac{\partial}{\partial x} h(0,t) = \int_{-\infty}^{\infty} j\frac{\omega^2}{g} H(\omega) e^{j\omega t} \frac{d\omega}{2\pi} \tag{7.13}$$

$$\frac{\partial}{\partial x} h(x,0) = \int_{-\infty}^{\infty} jK H(\sqrt{Kg}) e^{jKx} \frac{dk}{2\pi} \tag{7.14}$$

7.4 Numerical Evaluation

The difficulty with converting the formal solution into a numerical one has to do with the way in which the FFT provides the values for the function H(ω). Clearly the inverse FFT requires samples of H($\sqrt{Kg}$) spaced uniformly in K, but the uniform spacing in ω means that the values are non-uniformly spaced in K. Thus, one cannot directly feed the outputs of the FFT of h(0,t) into an inverse FFT in K

to get h(x,0).

If the function were smoothly varying in both amplitude and phase, one could use an interpolation routine to obtain values of the function at uniformly spaced points on the K axis, but unfortunately the values of the Fourier coefficients fluctuate widely. So the interpolation is not possible.

The straightforward way to evaluate the function is simply to sum the series of (7.1a) with t=0 and K given by (7.2b). This can be done in the computer, but not with the inverse FFT routine. Hence, the nonuniformly spaced trigonometric functions themselves must be evaluated, which is time-consuming. For handling masses of data, this means that a table must be generated of the appropriate trigonometric values, so that multiplication can be substituted for the repeated evaluation of numerous trigonometric functions by selecting a standard record length, such as 128 or 256 samples.

Before considering the setting-up of such a table, we must consider the apropriate ranges of X and T. We can write the phase for a component of the surface as

$$\theta = \omega t + \frac{\omega^2}{g} x \tag{7.15}$$

If we are to use values of X and T that correspond to comparable maximum phase shifts, we have

$$T = 2\pi f_m X / g \tag{7.16a}$$

where T is the sample length in time domain and f_m is the maximum

frequency used. Since we start with a time record of limited duration, X must be expressed in terms of

$$X = 9T/2\pi f_m \tag{7.16b}$$

which means that we should not try to reproduce h(x,0) over a larger range than this. That is, we must keep

$$X \leq 9T/2\pi f_m \tag{7.17}$$

Reasonable record lengths to use with the MARSEN data are 64, 128 and sometimes 256 seconds. If we continue to limit the maximum frequency used to .35 Hz, this means that x should be less than 225, 570 or 1140 m, respectively. The predominant wavelength is of the order of 54.0 m, so a 64-second record would only have 5 cycles of this wave and even fewer cycles of the low-frequency components, so correlation achieved with individual records would be very noisy. Accordingly, the minimum record length that should be used is 128 seconds. An analytical experiment was performed to determine the validity of this procedure.

8.0 PRELIMINARY RESULTS

A very large data set (about 115 cassette tapes) was collected during the experiment. The raw cassette-tape data were converted into files in the University of Kansas Honeywell computer system. The files were edited to insert headers and eliminate bad runs. Software was written to produce scattering coefficients, radar wave heights and other quantities of interest. Preliminary calculations have been made on all the basic quantities.

Figures 8.1 and 8.2 illustrate some processed 'raw data' records. Figure 8.1 shows a sample set of versus time, and Figure 8.2 shows the measured wave height both from slant-range measurement and wave staff. The power spectrum for the wave height profile has been calculated both from radar and wave-staff measurements. Figures 8.3 and 8.4 illustrate samples of these spectra. They agree very well. Both have a single peak at about 0.17 Hz. This agreement gave some confidence for further analysis. The sampling rate of the experiment was 1.0 Hz. For slope determination, wave height data set has been low-pass filtered with maximum frequency of 0.35 Hz. This reduces the possibility of aliasing. Figure 8.5 shows a sample histogram of calculated slope for a wind of 12.5 m/sec, obtained from a filtered wave-height measurement. The standard deviation is about 10 degrees. For wind speed cases, say, between 8 and 10 m/sec, one would not expect such a high value of standard deviation. Figure 8.6a illustrates a sample set of measured scattering coefficients with an average windspeed 8.61 m/sec. Note that any point which is greater than 6.0 dB above the mean is called specular 'event' (Section 5.4). Figure 8.6b illustrates the same sample set of scattering coefficients, replacing

the specular events by a seven-point triangularly-weighted average of the adjacent samples. The expected dependence of scattering coefficient on the windspeed has been observed, and is illustrated in Figure 8.7. This dependence is due to the fact that the capillary wave amplitude depends on windspeed (Section 4.3.2) and the amplitude of the capillary spectrum directly governs the backscattered power (Section 4.3.1).

Two samples of measured scattering coefficient for VV- and HH-polarization as a function of incidence are shown in Figure 8.8. The scattering coefficient is inversely proportional to the incidence angle. If the effect of the large-scale wave slope on capillary-wave amplitude could be neglected, the Bragg-wave number, K, would be completely governed by the angle of incidence. Figure 8.9 shows a sample preliminary estimate of the measured spectrum in the Mitsuyasu-Honda range, $S_4(K)$, based on average incidence angle (the pointing angle). The measured values are compared with theoretical K spectra (lines on the figure). Note that tne K-spectrum decreases rapidly with increasing Bragg-wave number, K. Since the scattering coefficient is directly governed by K-spectrum, one would expect the smaller value of scattering coefficient for larger incidence angle. Note that Bragg-wave number K is proportional to angle of incidence.

One of the major goals of this analysis is to estimate the modulation of the capillary waves over the large-scale waves, both temporally and spatially. If the capilary wave spectrum S(K) and the instantaneous slope of the large-scale wave are known, one can calculate the theoretical instantaneous scattering coefficient based on uniform capillary distribution (Section 4.3). The RMS value of

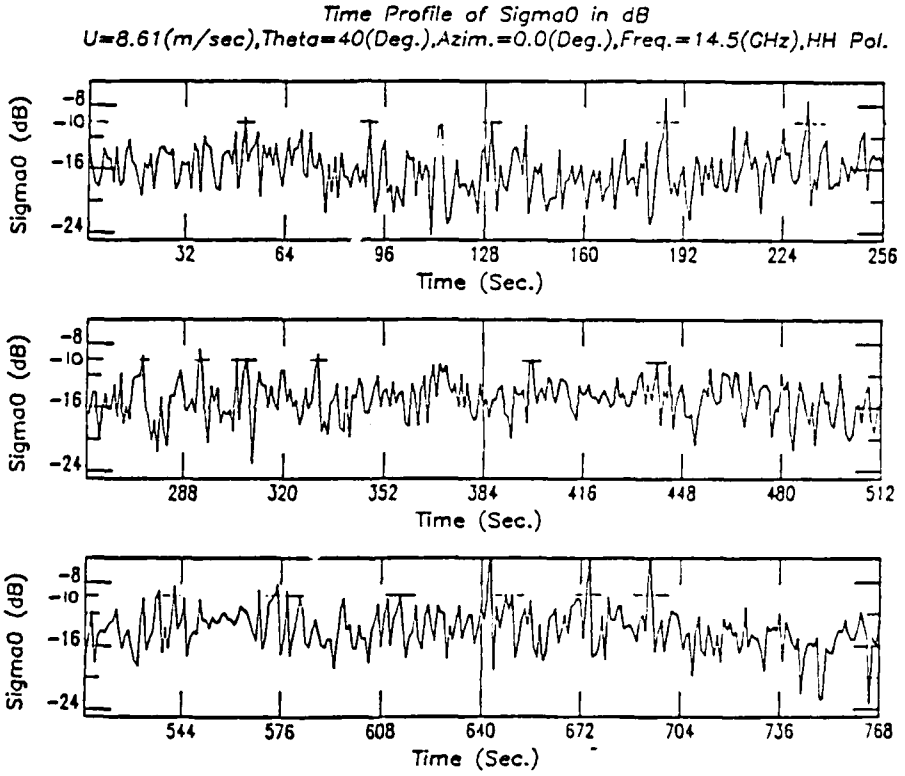

Figure 8.1
Sample of processed σ^{o} (dB), from the radar return, showing the "event" threshold. Each 128-sec record is from a different time.

AD-A129 690 INTERACTION OF THE RADAR WAVES WITH THE CAPILLARY WAVES 2/3
ON THE OCEAN..(U) KANSAS UNIV/CENTER FOR RESEARCH INC
LAWRENCE REMOTE SENSING L.. S BARKESHLI ET AL. MAY 83
UNCLASSIFIED CRINC/RSL-TR-419-1 N00014-79-C-0533 F/G 17/9 NL

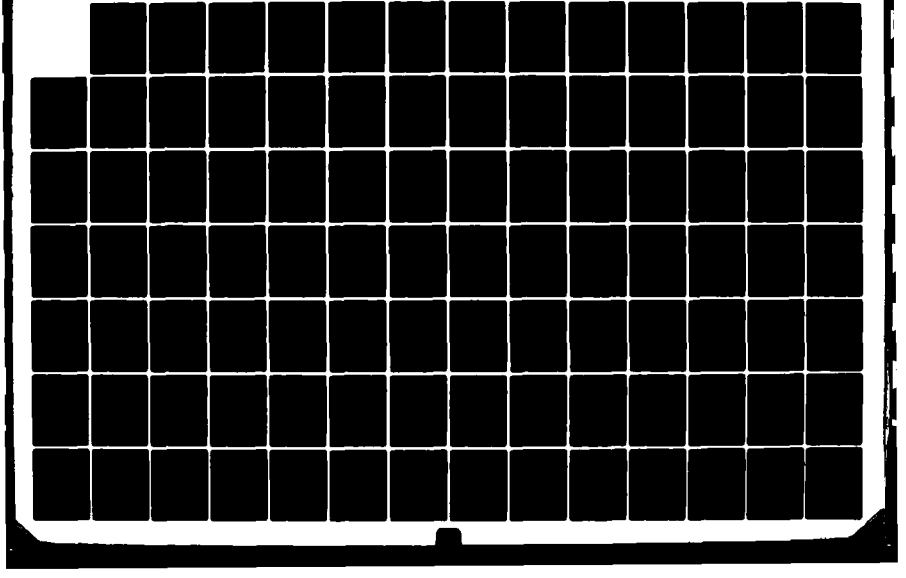

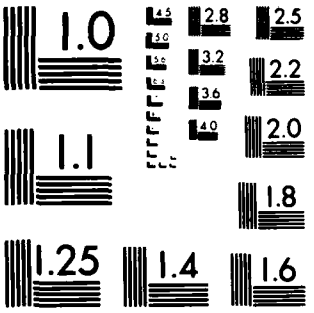

MICROCOPY RESOLUTION TEST CHART
NATIONAL BUREAU OF STANDARDS-1963-A

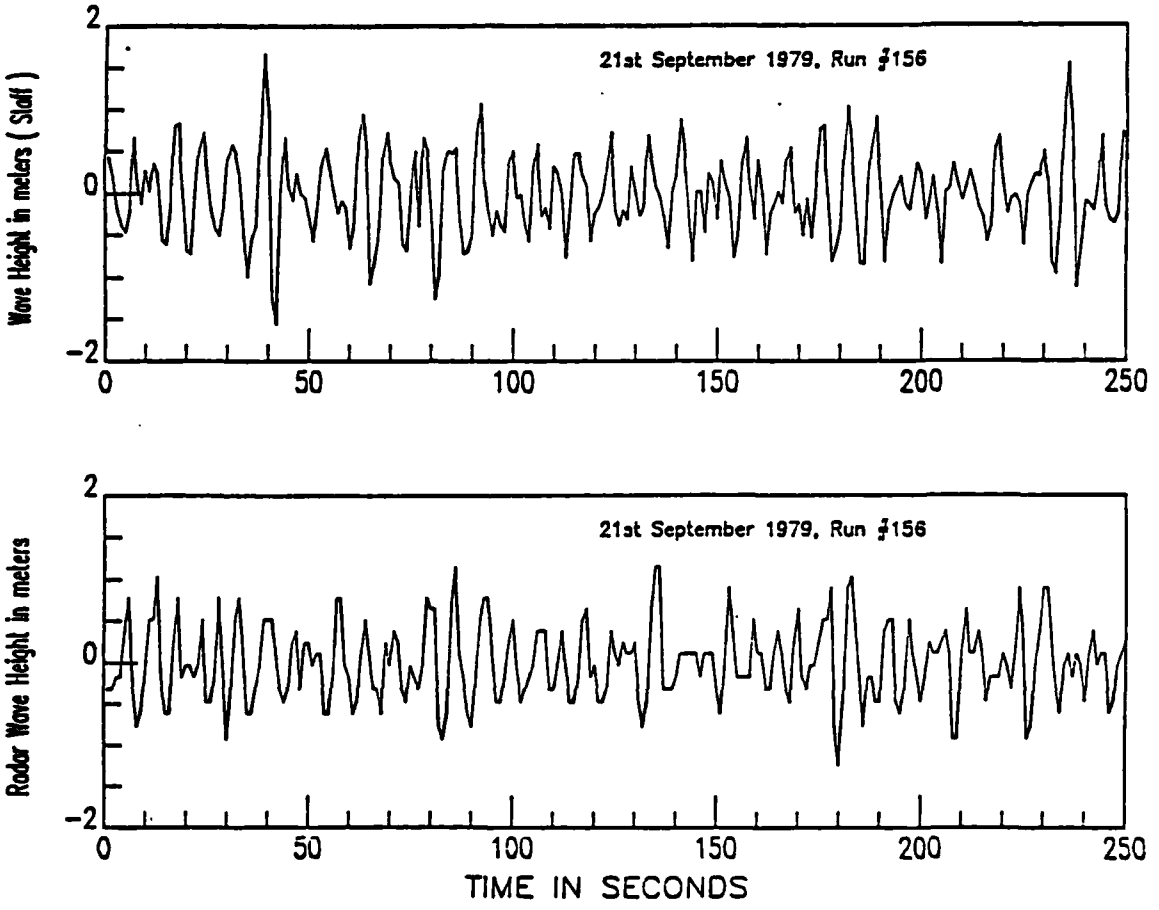

Figure 8.2
Sample comparison of wave staff and radar wave heights.
Wave staff was separated about 11 meters from
Radar Observation.

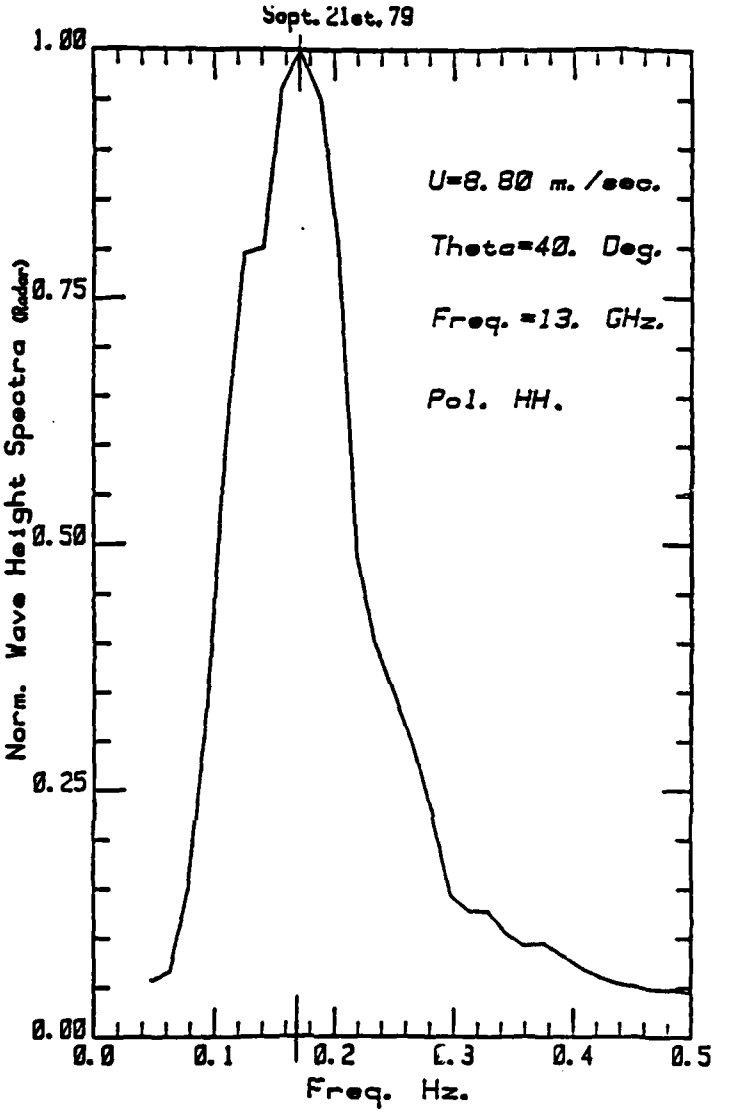

Figure 8.3
Normalized wave-height spectrum (radar);
single peak at 0.17 Hz.

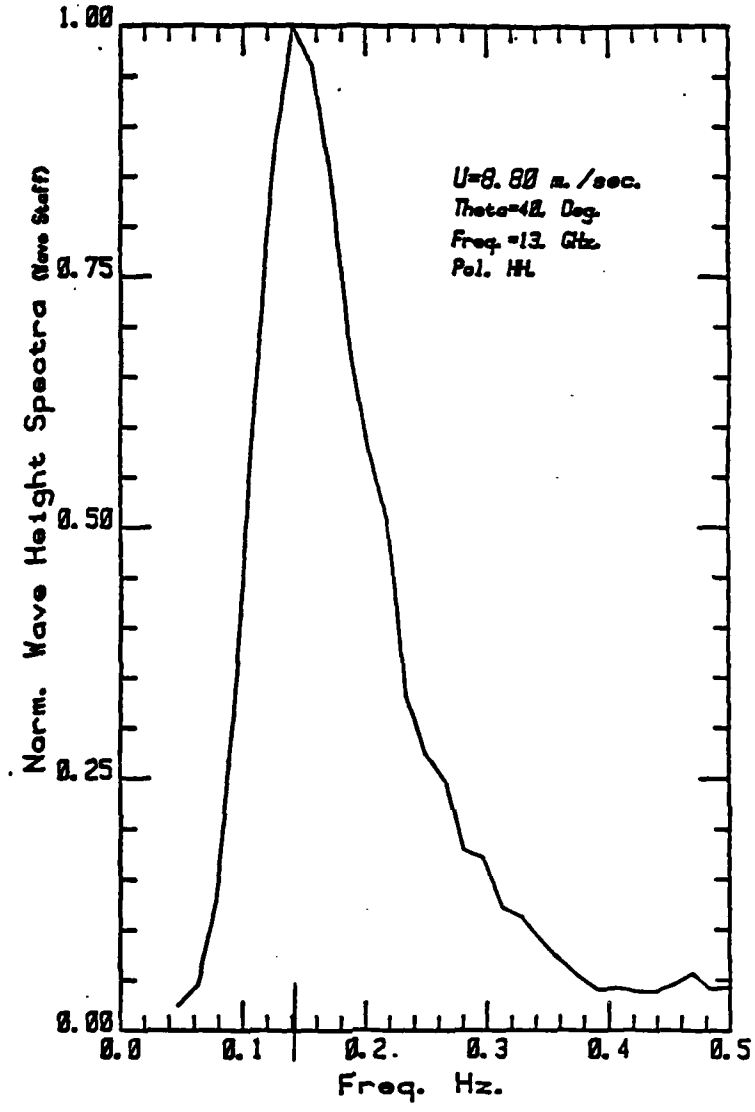

Ave. Of 5, 64Pt. Subruns & 5Pt. Moving Ave.

Figure 8.4
Normalized wave-height spectrum (wave staff);
single peak at 0.16 Hz.

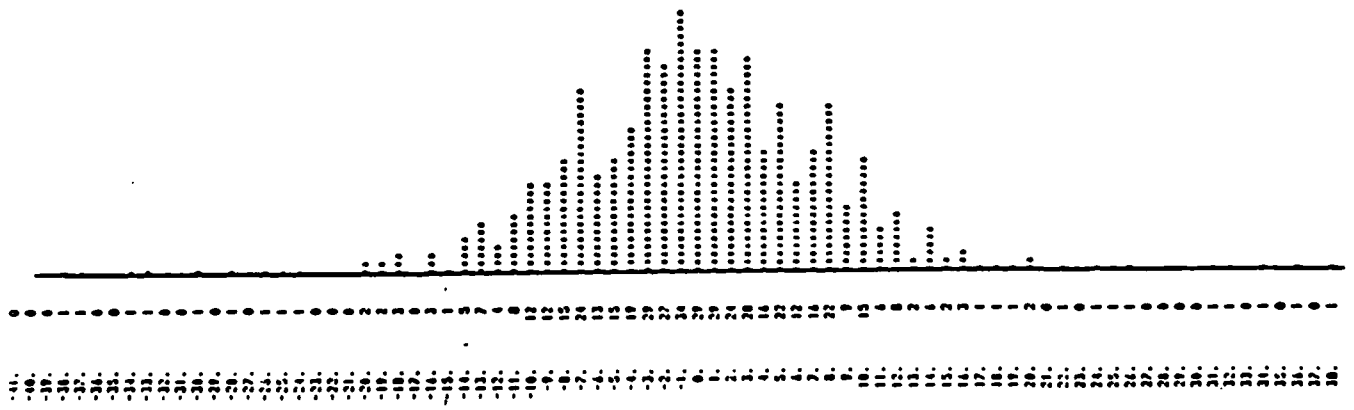

Figure 8.5
Sample slope distribution obtained from instantaneous slopes derived from radar wave-height measurement. Standard deviation 10°. Wind speed 12.5 m/s. Scale on Figure: Number of observations (upper list of numbers). Slope in degrees (lower list of numbers).

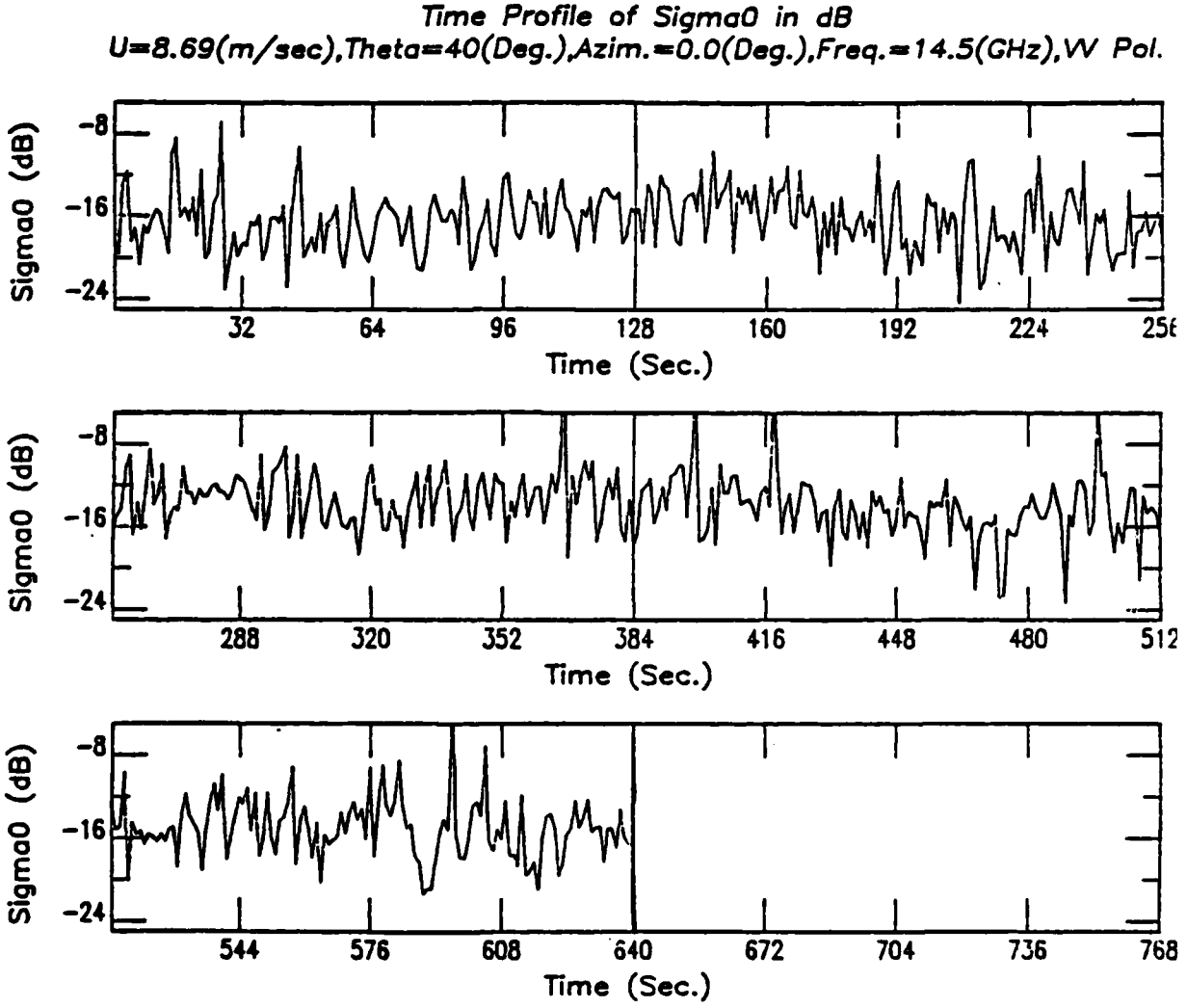

Figure 8.6a
Sample of σ^{o} (dB), illustrating numerous specular events.
Each 128-sec record is from a different time.

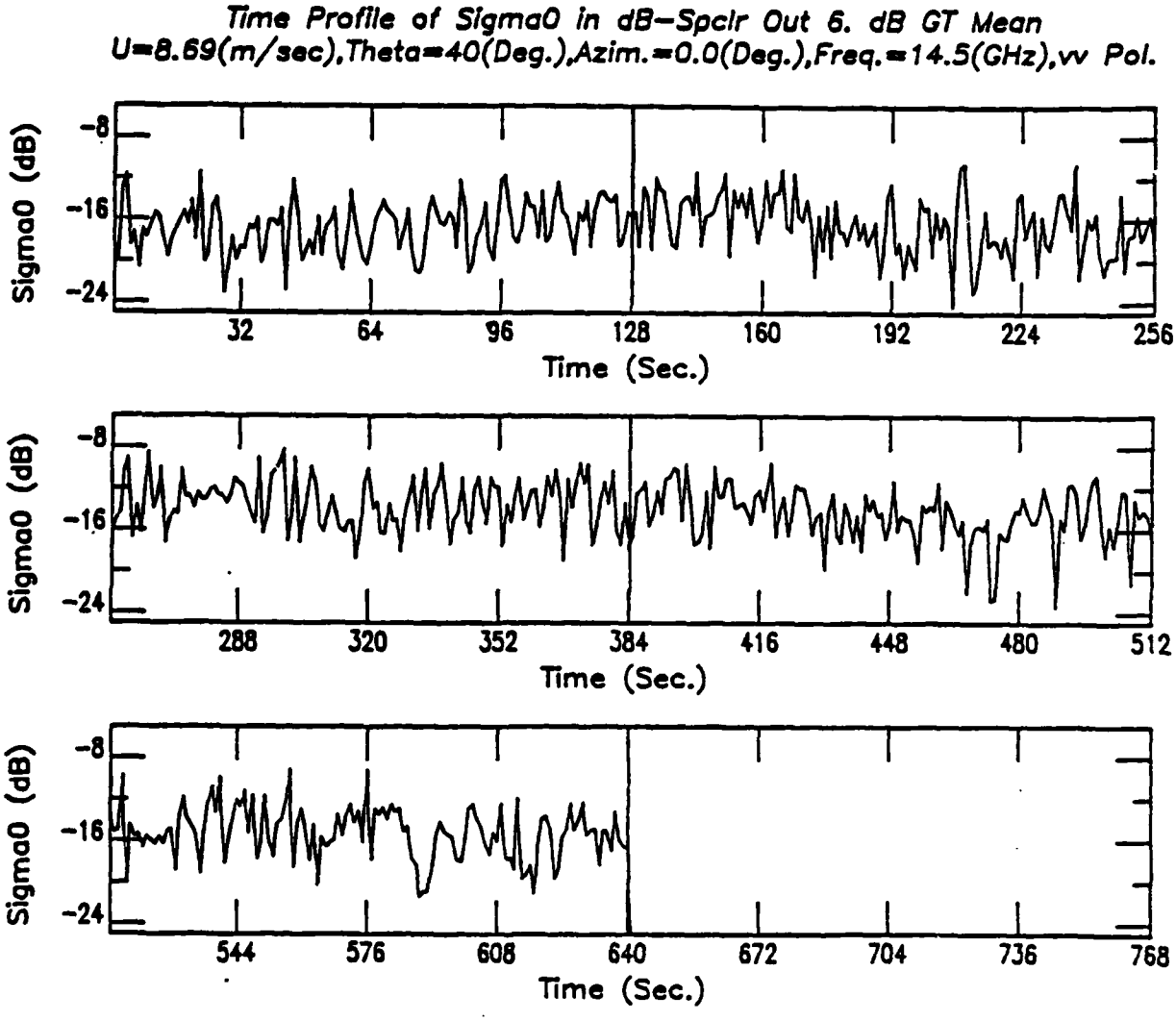

Figure 8.6b
Sample of σ^{o} (dB) replacing the specular events by 7 point average of an adjacent sample. Each 128-sec record is from a different time.

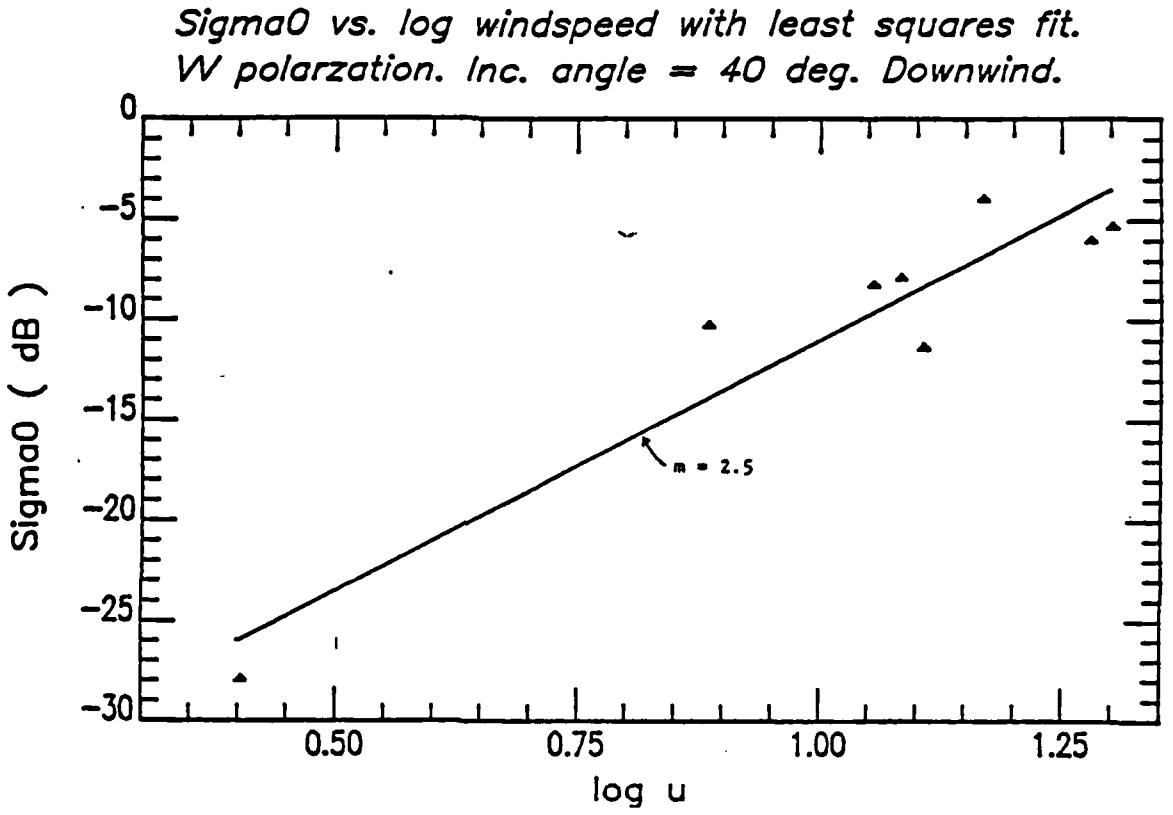

Figure 8.7
Sample preliminary estimate of wind speed response of σ^0 from 3 days of data

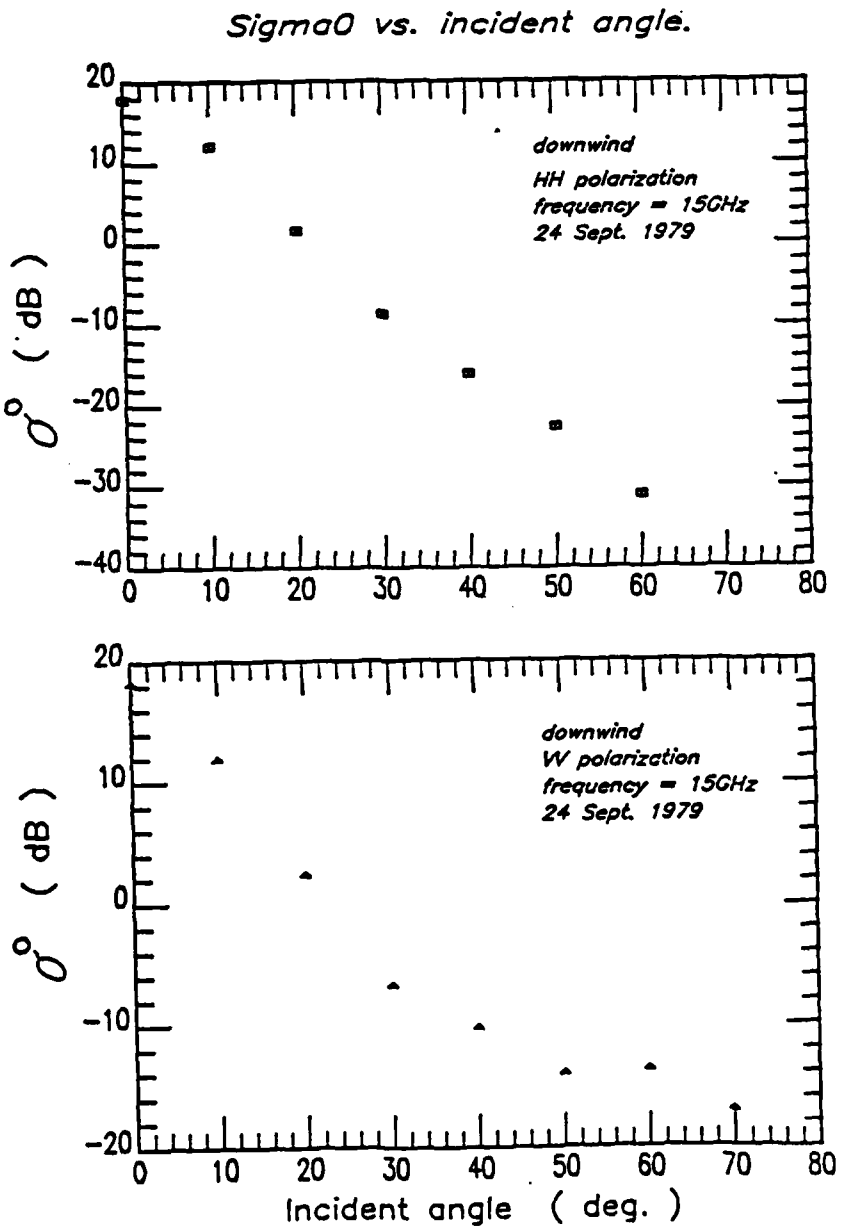

Figure 8.8
A sample preliminary estimate of σ^0 vs angle of incidence based on 10 GHz calibration used at 15 GHz.

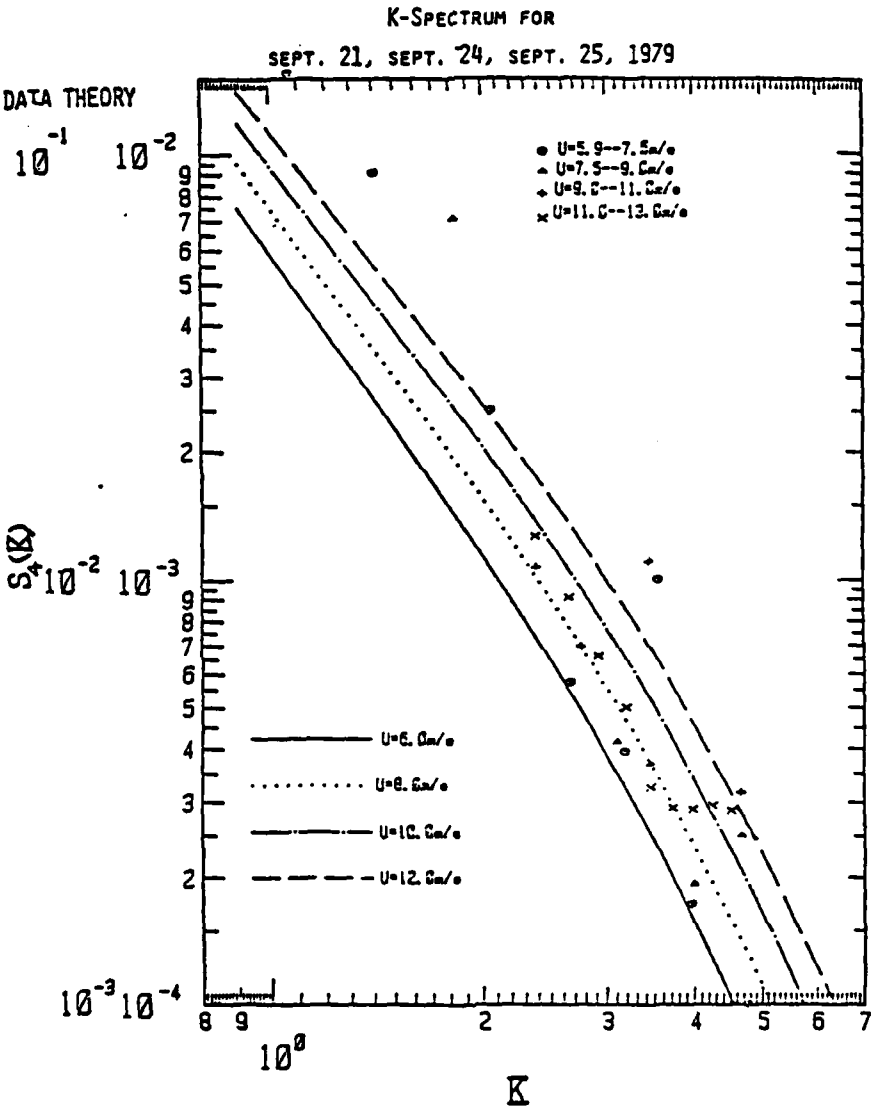

Figure 8.9
Sample preliminary estimate of measured Mitsuyasu-Honda range of wave spectrum. Some of scatter may result from use of 10 GHz reference calibration for both 10 GHz and 15 GHz data.

modulation index μ or $\Delta\sigma$ (Section 4.4.2) can show the modulation effect and tilting effect on total scattering coefficient. Having the cross-correlation between the $\mu(t)$ and slope one can estimate the phase relation of the peak of the modulation with respect to peak of the slope. The phase relation of the peak of the modulation with respect to crest of the wave can be found by the same means.

The ensemble-average RMS value of modulation index has been calculated both for HH- and VV-polarization. The average RMS modulation index is 0.876 with standard deviation of 0.34 for HH-case and is 0.673 with standard deviation of 0.044 for VV-case.

Figures 8.10a and 8.11 illustrate the autocorrelation of wave height and slope. The wave height autocorrelations show that the wave height is a quasi-periodic type of function with a period between 5.5 to 6.5 seconds, which corresponds to a dominant wave with frequency of about 0.15 - 0.17 Hz. The slope autocorrelation function shows that the slope is the same type of the quasi-periodic function, but with shorter periods, about 3.5 seconds, which corresponds tc a dominant frequency of 0.29 Hz. The higher dominant frequency in slope is expected because the slope spectrum components are calculated by multiplication of wave-height spectrum components with the square of corresponding angular frequency, ω_i, divided by g, the gravitational acceleration. This would definitely shift the spectrum peak to the higher frequency. Figure 8.10b shows the cross-correlation of slope and wave height and cross-correlation of theoretical scattering coefficient and slope. As is shown, the slope leads the wave height by about 1.0 second. The cross-correlation of theoretical scattering coefficient and slope has a maximum at zero lag, as it should.

AVE. OF 10 RUNS Sept. 21st/70 - (FILT. .35 Hz)

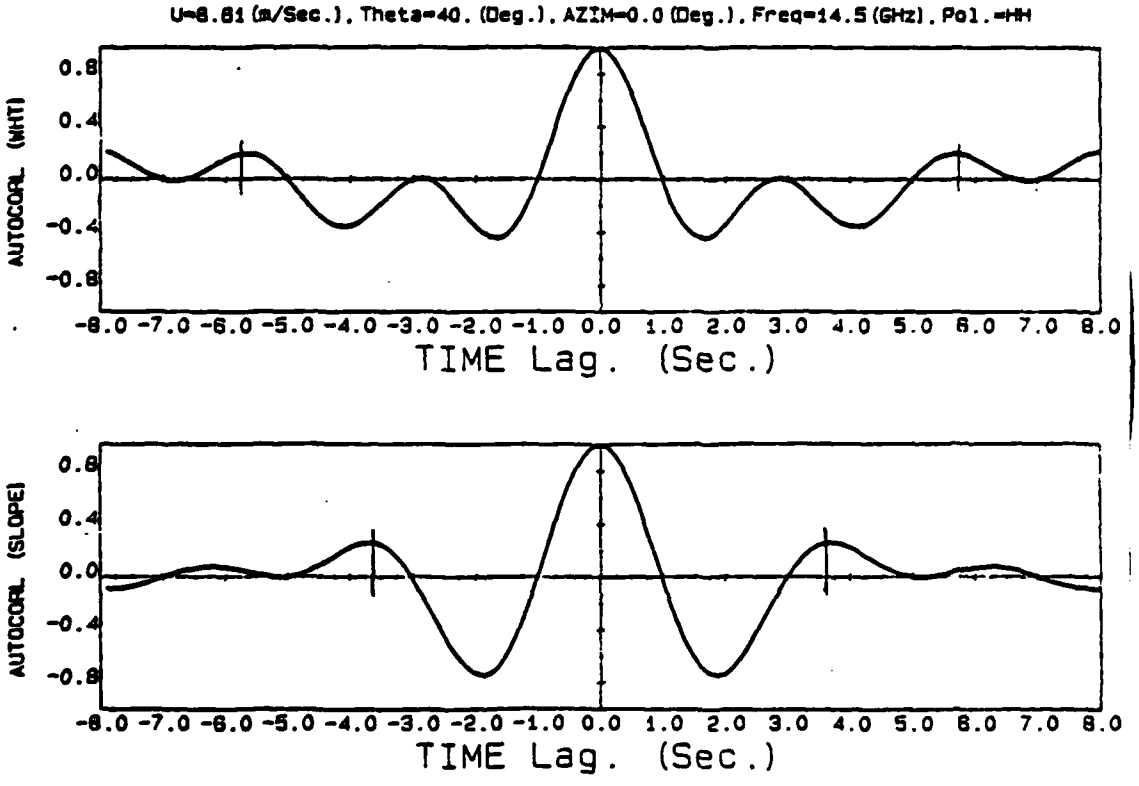

Figure 8.10a
Temporal autocorrelation of wave-height. Dominant period is 5.8 sec.
Temporal autocorrelation of slope. Dominant period is 3.5 sec.

Ave. of 10 Runs Sept.21st/70 (SPCLR OUT 6. dB GT MEAN) - (FILT .35 Hz)

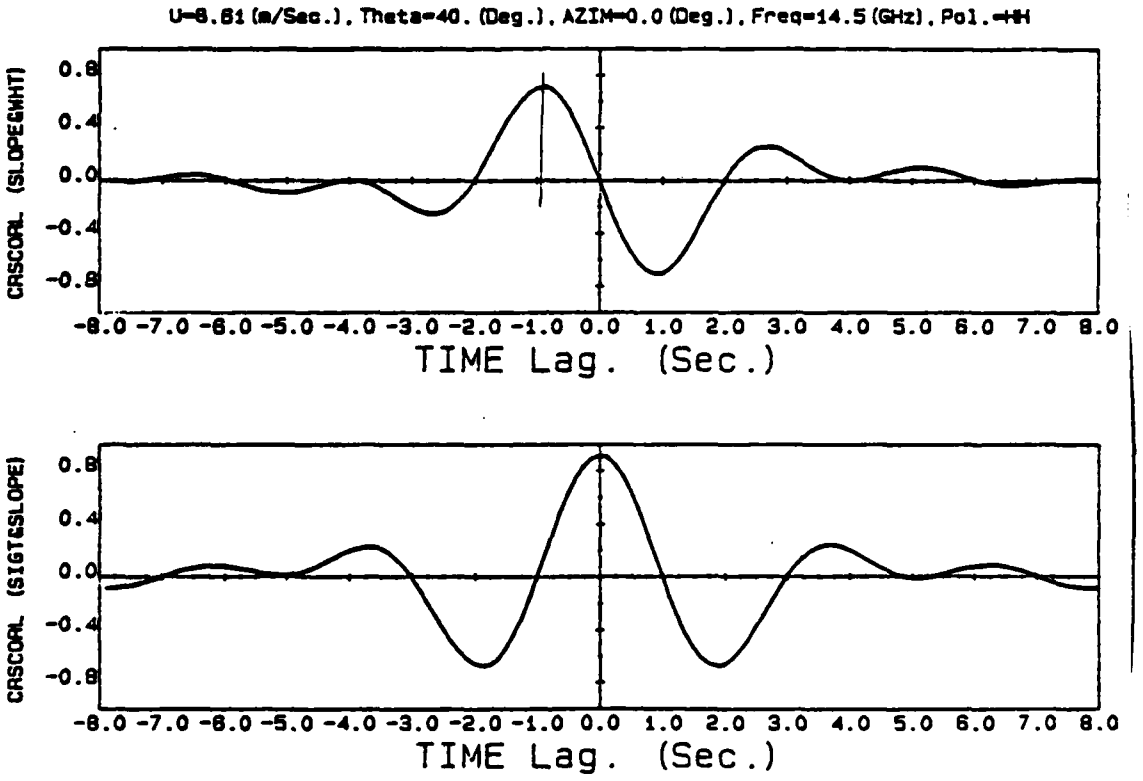

Figure 8.10b
Cross-correlation of slope and wave-height. Slope leads the wave-height by about 1.0 sec. Cross-correlation of theoretical σ^o and slope. Maximum peak at zero lag.

Ave of 5 Runs Sept. 21st/79 - (FILT .35 Hz)

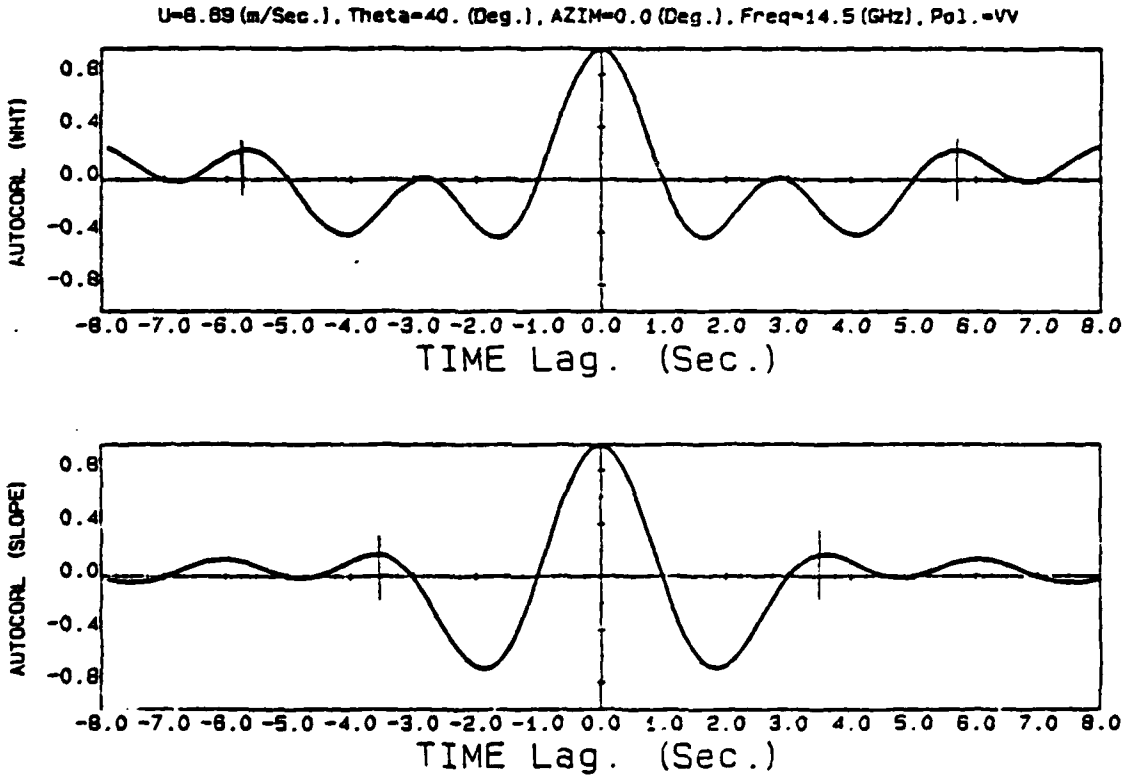

Figure 8.11
Autocorrelation of wave-height. Dominant period is about 5.8 sec.
Autocorrelation of slope. Dominant period is about 3.5 sec.

Figures 8.12 and 8.13 illustrate the cross-correlations of the scattering coefficient and the wave height and also the scattering coefficient and the slope, for both HH- and VV-polarization cases. The values of cross-correlation are not large, since the graphs are the result of averaging ten runs for HH-cases and five runs for VV-cases. Even though much larger correlations have been observed for single cases at different lags, the most significant result is that consistent values were observed for the two polarizations, based on observations at different times. The scattering coefficient leads the slope by about 0.75 seconds or about 1/8 of the dominant large-scale wave period (45°) or 1/4.7 of the dominant slope period, 77°. The scattering coefficient leads the wave height even more, about 1.7 seconds or about 104° ahead of the crest of the dominant wave. Another peak, smaller than the dominant one, can be observed for both cross-correlation functions. The phase difference between the two peaks is about a full period of the dominant slope quasi- periodic component, 3.5 seconds. This obviously shows that the scattering coefficient is dominated by the slope effect, which one would expect from the theory (Section 4.3.1). Note that the cross-correlation function of theoretical scattering coefficient and slope peaks to maximum at zero lag (Figure 8.10b), since maximum theoretical scattering coefficient occurs at maximum slope. We believe the 'unexpected' shift of the cross-correlation of scattering coefficient and slope, 1/8 of the dominant large-scale period, is due to the fact that the capillary waves are not uniformly distributed over the large-scale wave.

The modulation index $\mu(t)$ is called $\Delta\sigma$ in the figures. For both HH and VV cases, Figures 8.14 and 8.15 show that $\Delta\sigma$ leads the

Ave. of 10 Runs Sept.21st/79 (SPCLR OUT 6. dB GT MEAN) - (FILT .35 Hz)

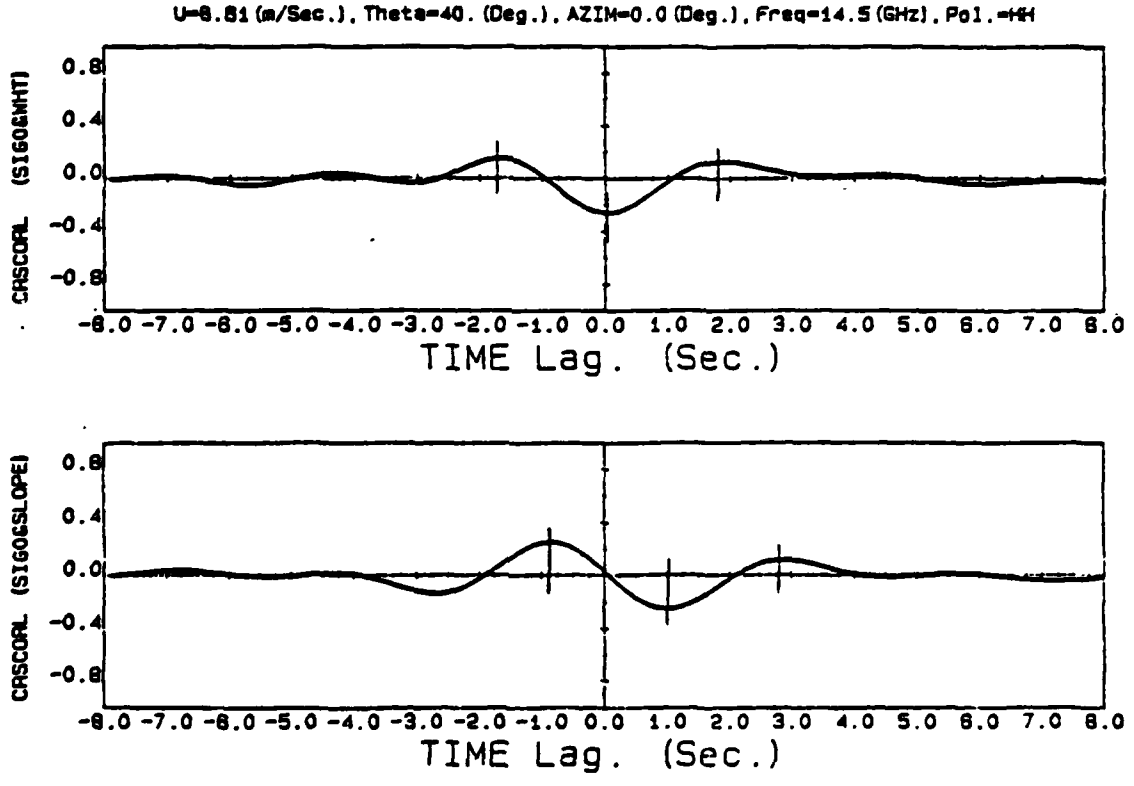

Figure 8.12
Cross-correlation of σ^0 and wave-height. σ^0 leads the wave-height by about 1.7 sec (104°). Cross-correlation of σ^0 and slope. σ^0 leads the slope by about 0.75 sec (90°).

Ave. of 5 Runs Sept.21st/79 (SPCLR OUT 6. dB GT MEAN) - (FILT .35 Hz)

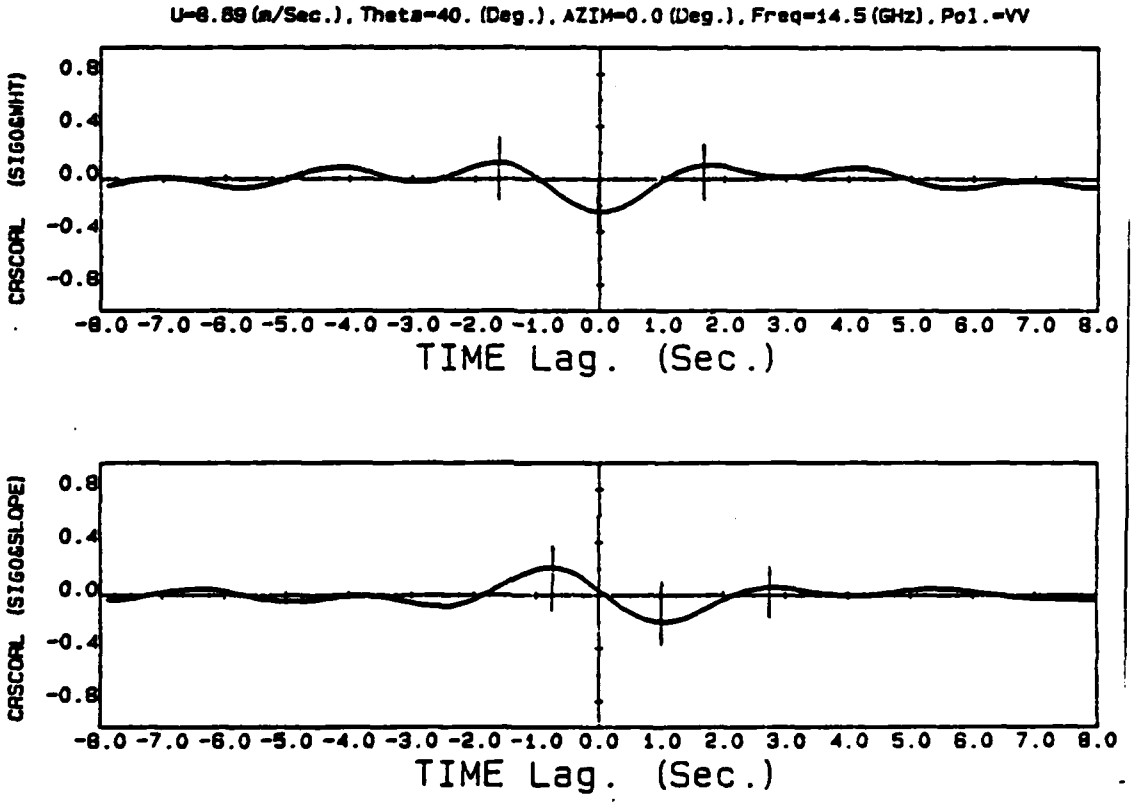

Figure 8.13
Cross-correlation of σ^o and wave-height. σ^o leads the wave-height by about 1.7 sec (104°). Cross-correlation of σ^o and slope. σ^o leads the slope by about 0.75 sec (90°).

slope by about 1.6 seconds or about 1/3.6 of the dominant period of the large-scale wave (about 1/2.19 of the dominant period of the slope (about 165°)). The cross- correlation of $\Delta\sigma$ and wave height, Figures 8.14 and 8.15, shows that $\Delta\sigma$ leads the wave height by about 2.5 seconds which is about 1/2.35 of dominant period of the large-scale wave or about 153 degrees ahead of the crest of the wave. Note that the cross-correlation of the $\Delta\sigma$ and wave height for HH is stronger than for VV, but the locations of the peaks are reasonably consistent.

Since the spatial cross-correlation functions should be studied for an estimation of the spatial distribution of the capillary waves over the large-scale waves, a set of spatial profiles has been determined using the method described in Chapter 7. Figure 8.16 shows the profiles of the wave height for a sample record in the temporal and spatial domains and Figure 8.17 shows the comparable slope profiles. These spatial slope profiles were used to compute a theoretical scattering coefficient profile in the spatial domain as shown in Figure 8.18. The relationship between the scattering coefficient and the wave height is very nonlinear. Consequently, the assumptions of Chapter 7 regarding transformation from temporal to spatial domain probably are not sufficiently good to justify a direct transformation of the scattering coefficient to the spatial domain. Accordingly, a transformation has been made of the values of $\Delta\sigma$. For relatively small values of $\Delta\sigma$ the relation should be sufficiently close to linear that the transformation has a reasonable chance of success. A sample is shown in Figure 8.19. For larger values of $\Delta\sigma$ the values presented in the spatial domain probably are not very accurate. A simple set of spatial autocorrelations is presented in Figure 8.20 for

Ave. of 10 Runs Sept.21st/79 (SPCLR OUT 6. dB GT MEAN) - (FILT .35 Hz)

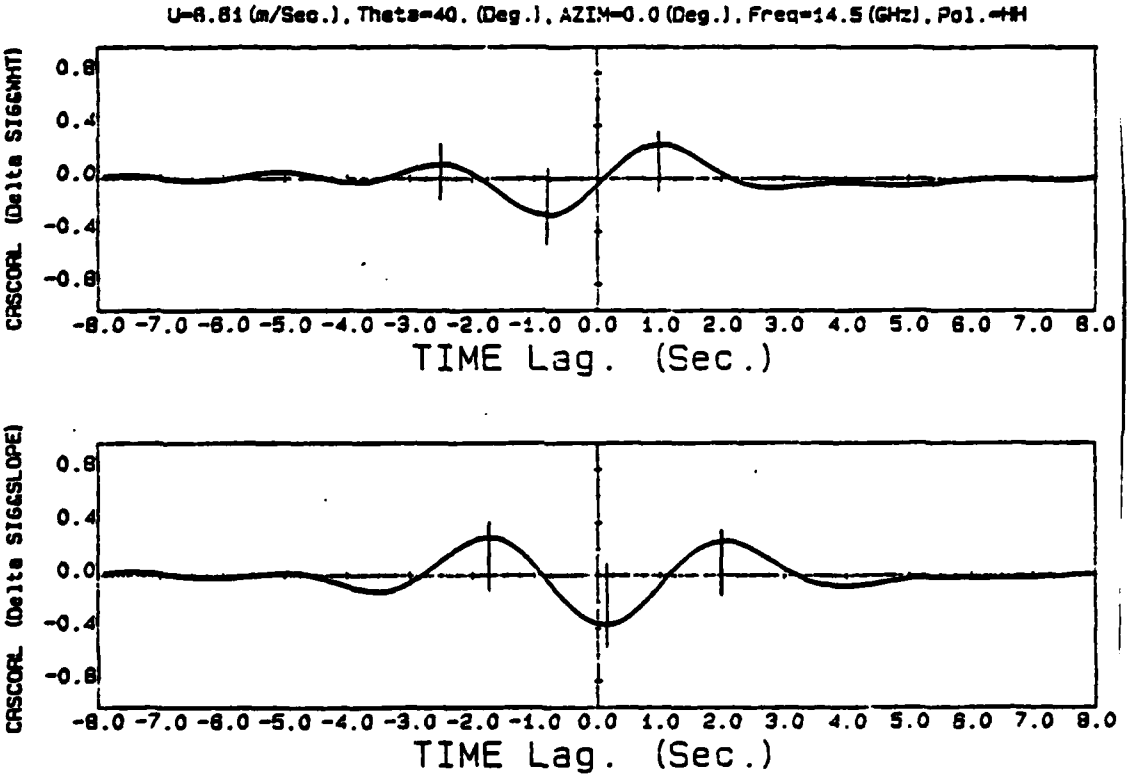

Figure 8.14
Cross-correlation of $\Delta\sigma$ and wave-height. $\Delta\sigma$ leads the wave-height by about 2.5 sec (153°). Cross-correlation of $\Delta\sigma$ and slope. $\Delta\sigma$ leads the slope by about 1.6 sec (165°).

Ave. of 5 Runs Sept. 21st/79 (SPCLR OUT 6. dB GT MEAN) - (FILT .35 Hz)

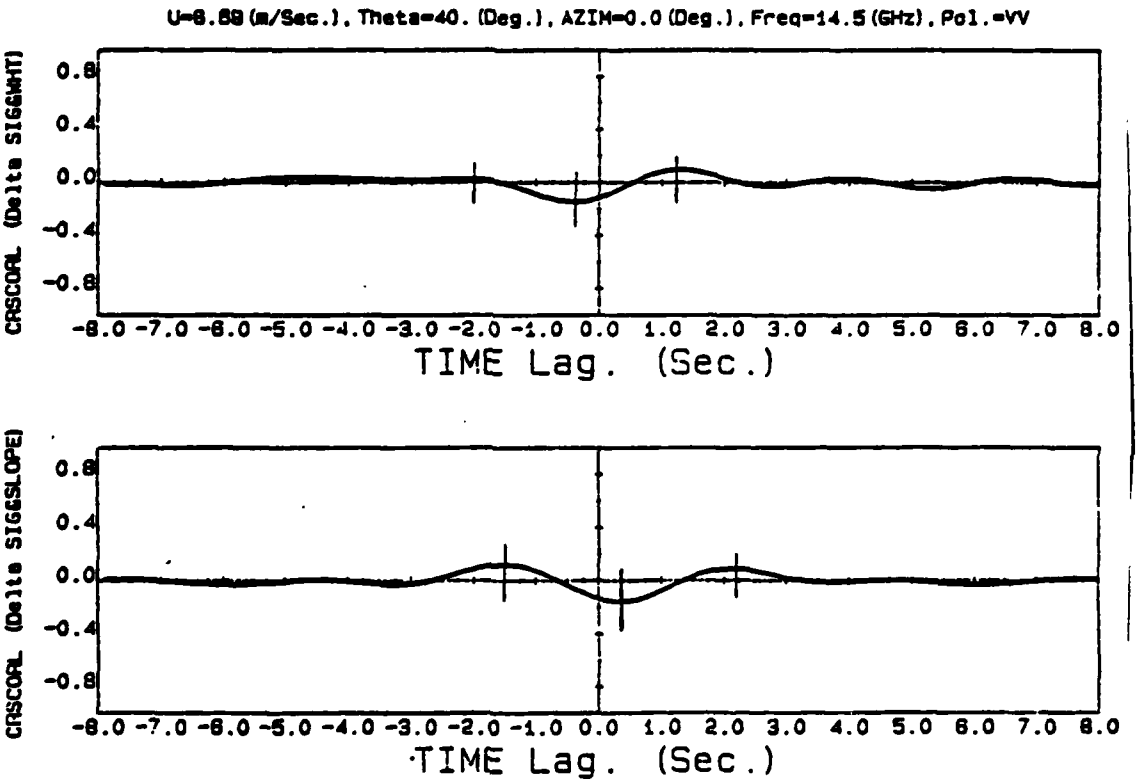

Figure 8.15
Cross-correlation of $\Delta\sigma$ and wave-height. $\Delta\sigma$ leads the wave-height by about 2.5 sec (153°). Cross-correlation of $\Delta\sigma$ and slope. $\Delta\sigma$ leads the slope by about 1.6 sec (165°).

wave height and slope. It seems the dominant spatial wave length is about 70 m and the dominant slope wave length is about 42 m. Figure 8.21 shows the spatial cross-correlations between $\Delta\sigma^{\circ}$ and wave height and slope for the same data set.

Spatial analysis has just started and requires considerably more study before conclusions can be drawn. Hence, the above presentations of results must be considered as very preliminary.

The final quantity of interest is the modulation transfer function, MTF (Section 6.5). Figures 8.22 and 8.23 illustrate the MTF for HH and VV polarization cases. Both the Alpers form R(f) and the NRL form m(f) are shown. Below 0.35 Hz the MTFs have more or less the same characteristics. R(f) has a minimum at about 0.1 Hz, and m(f) decreases monotonically. More smoothing and more sample averaging needs to be done for more stable, smooth characteristics. R(f) above 0.35 Hz has more noiselike characteristcs because the wave-height power spectrum, which is in the denominator of the MTF expression, would not have proper information beyond 0.35 Hz (Section 5.3). For both VV and HH polarization cases shown in Figures 8.24 and 8.25, the power spectra have similar characteristics, except for some peaks at 0.22 Hz and 0.35 Hz for VV cases. Note that for VV only 5 sample records were averaged whereas for HH 10 samples have been averaged. Hence, one would expect more smooth and stable characteristics in power spectra and MTF for HH case. The wave height power spectra of both cases have been plotted in Figures 8.26 and 8.27. Both have a single peak around 0.15 Hz.

The average coherence for function for radar power return spectra and wave height spectra have been found both for HH and VV polarization and plotted in Figures 8.28 and 8.29. The average value of coherence

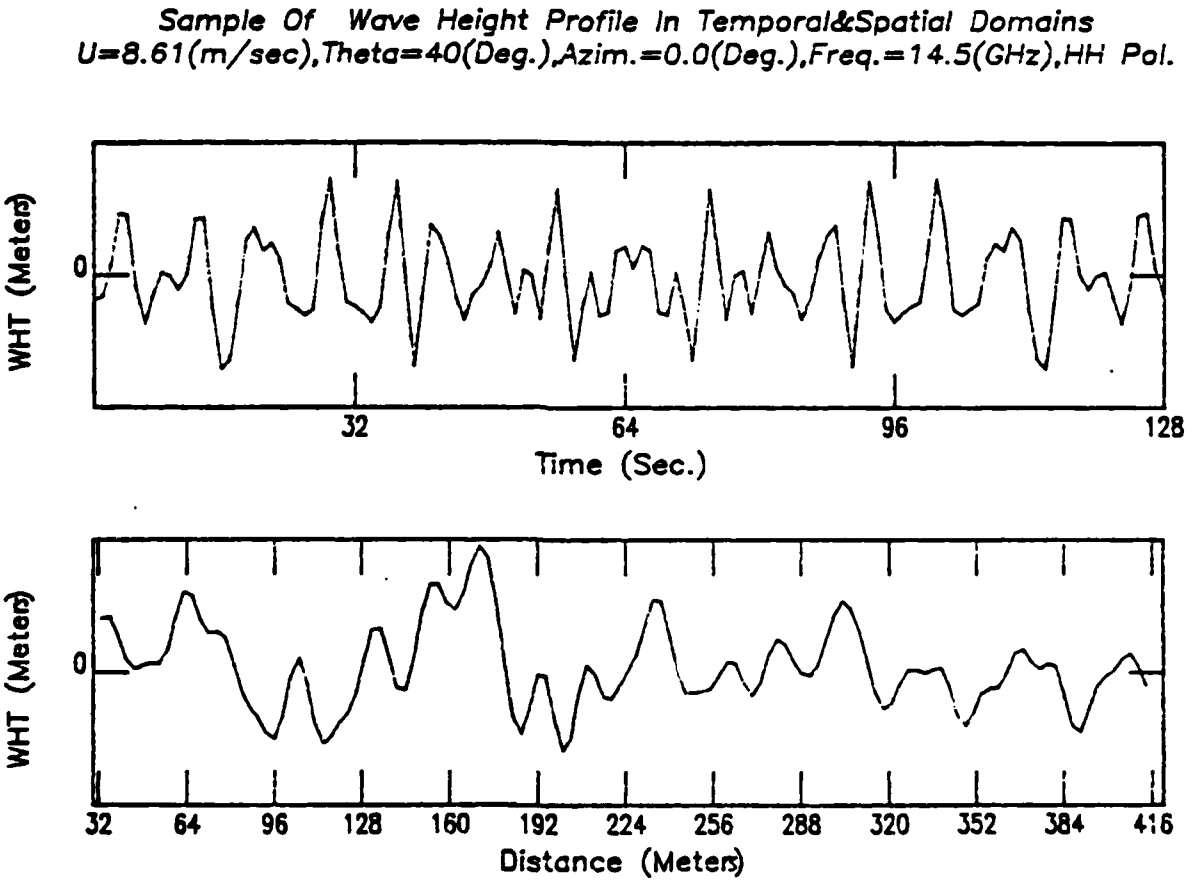

Figure 8.16
Sample of wave-height profiles in temporal and spatial domains

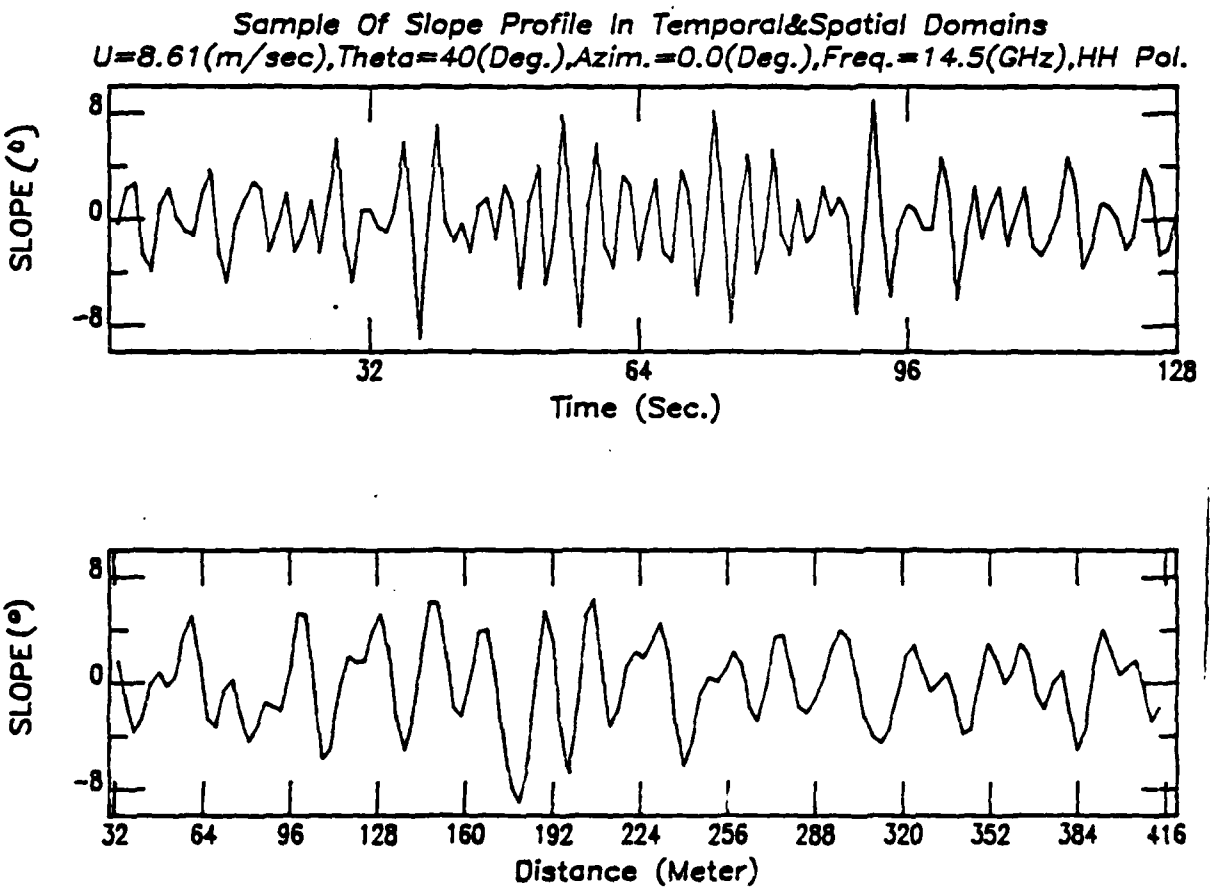

Figure 8.17
Sample of slope profile in temporal and spatial domains

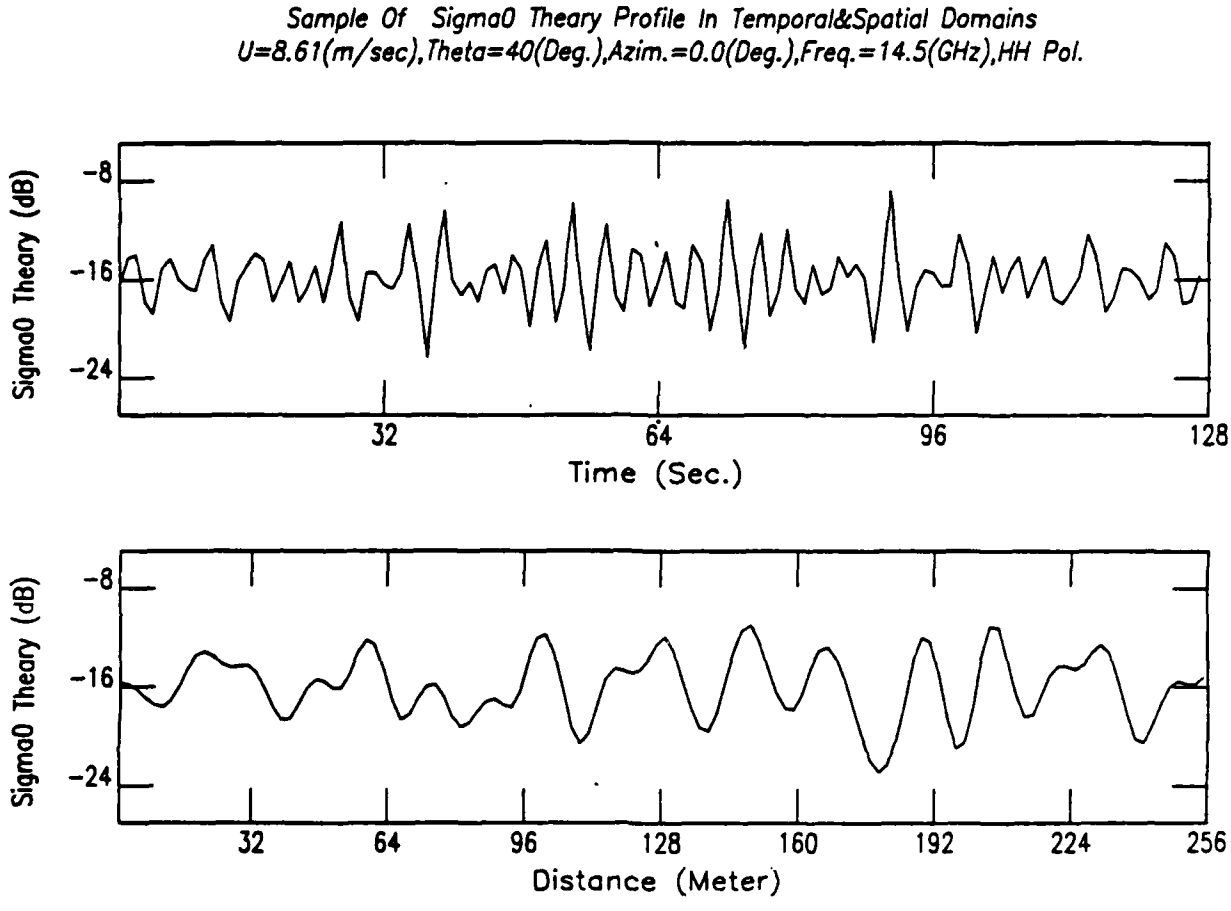

Figure 8.18
Sample of σ^{o} theory profile in temporal and spatial domains

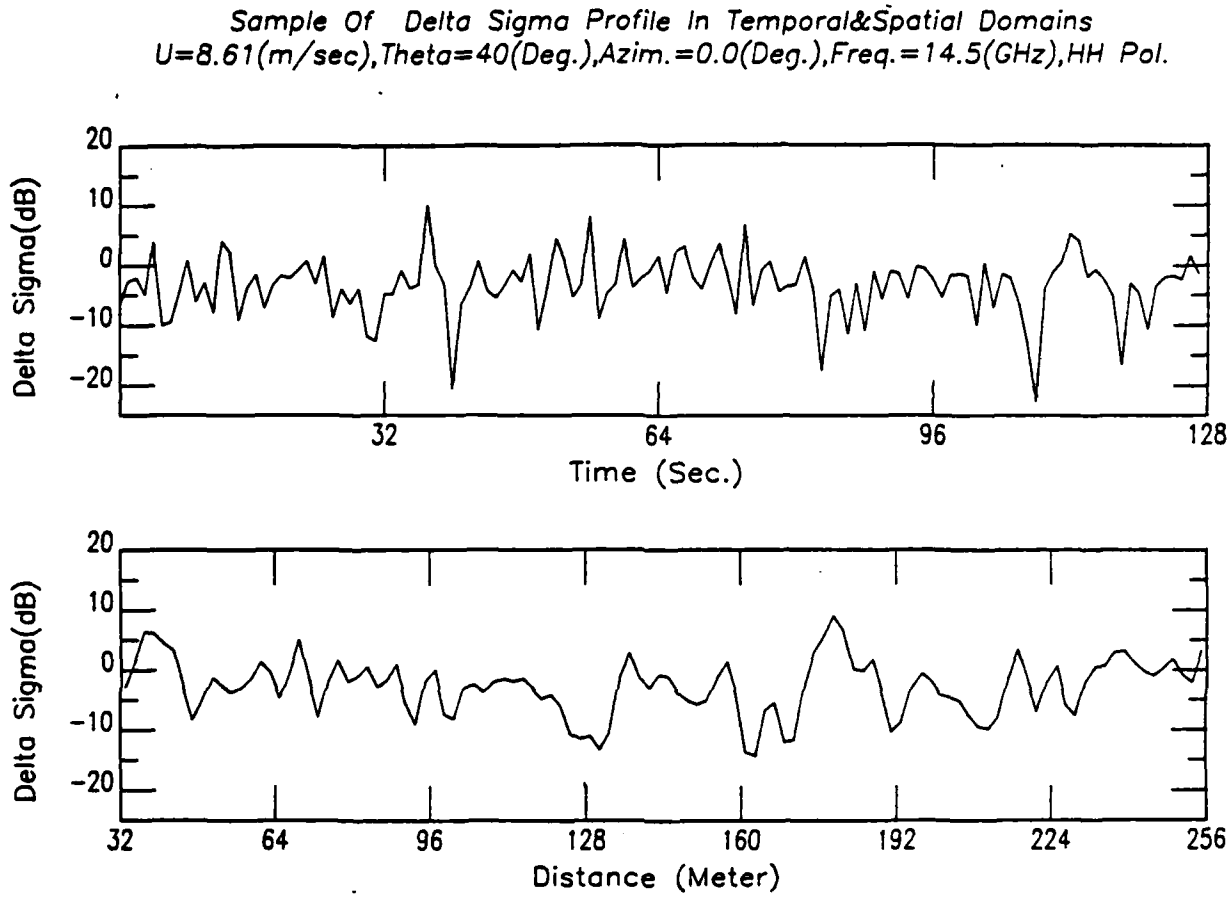

Figure 8.19
Sample of Δσ profile in temporal and spatial domains

Ave. of 10 Runs Sept. 21st/79 - (FILT .35 Hz)

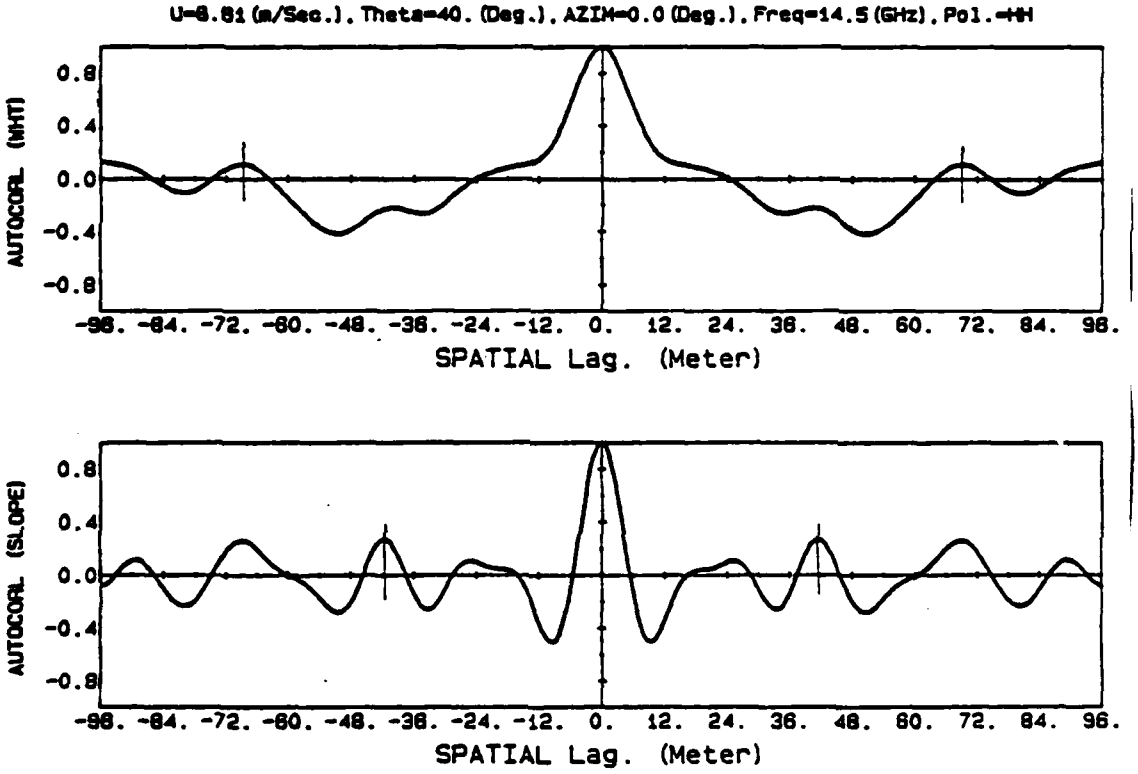

Figure 8.20
Spatial autocorrelation of wave-height. The dominant period is about 72 meters.
Spatial autocorrelation of slope. The dominant period is about 42 meters.

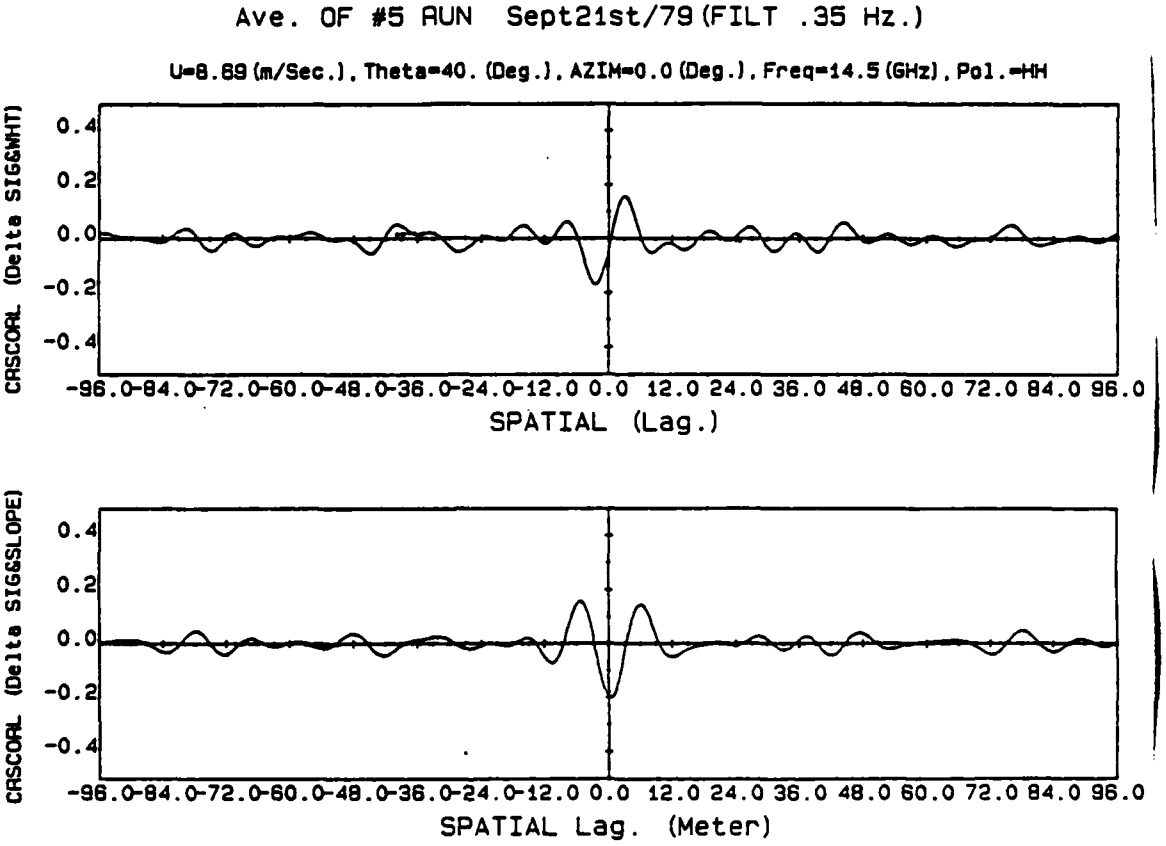

Figure 8.21
Cross-correlation between $\Delta\sigma$ and wave height and slope.

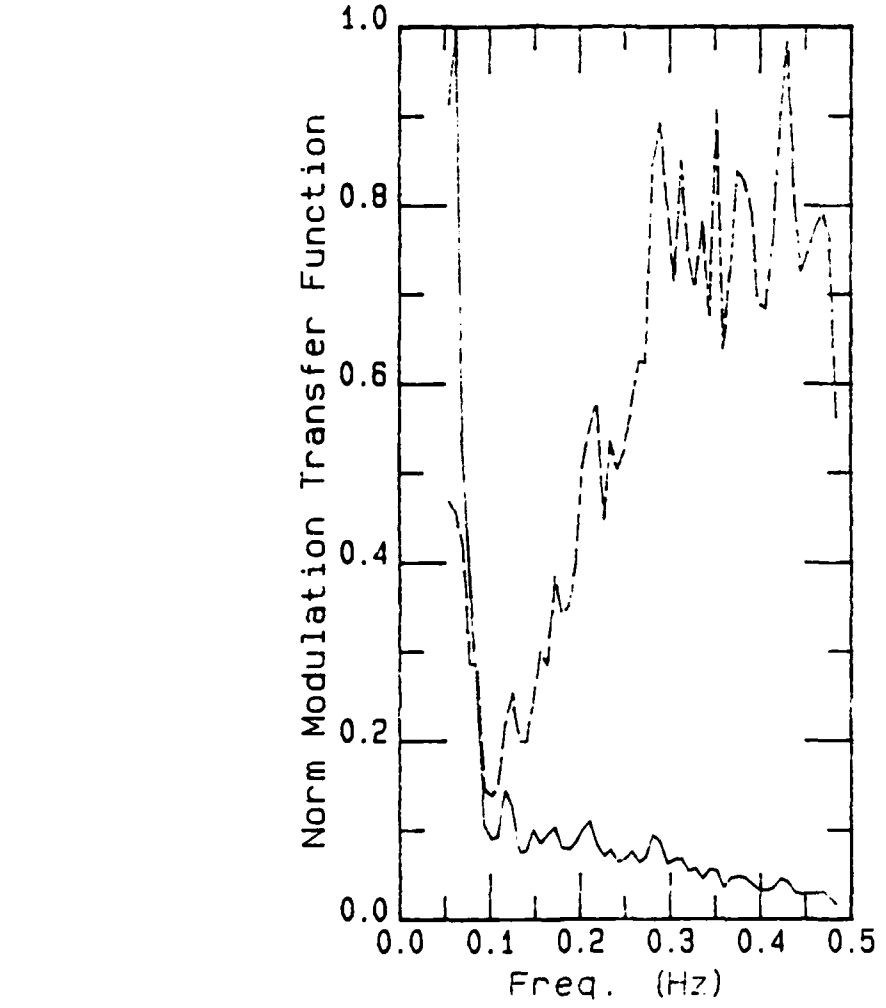

Figure 8.22
Normalized modulation transfer functions R(f) (dash line)
and m(f) (solid line).

Sept. 21st, 79, Ave. Of 5, 128pts. Subruns & 7pt. Moving Ave.
U=8.69 (m/sec), Theta=40 (Deg.), Azim.=0.0 (Deg.), Freq=14.5 (GHz), vv Pol.
Spclr Out 6. dB GT. Mean

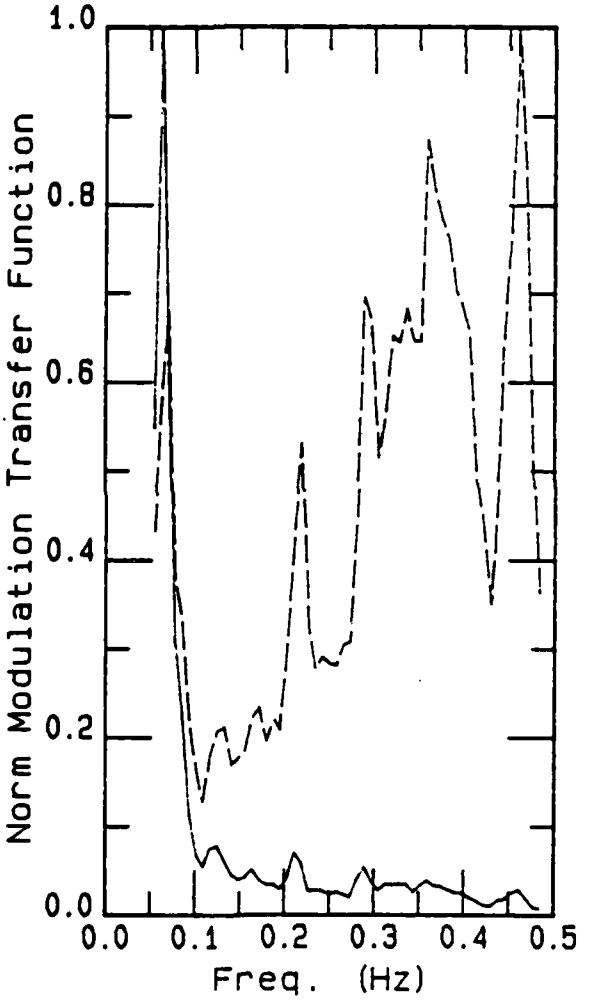

Figure 8.23
Normalized modulation transfer functions R(f) (dash line) and m(f) (solid line). Note it is not as smooth and stable as the HH MTF.

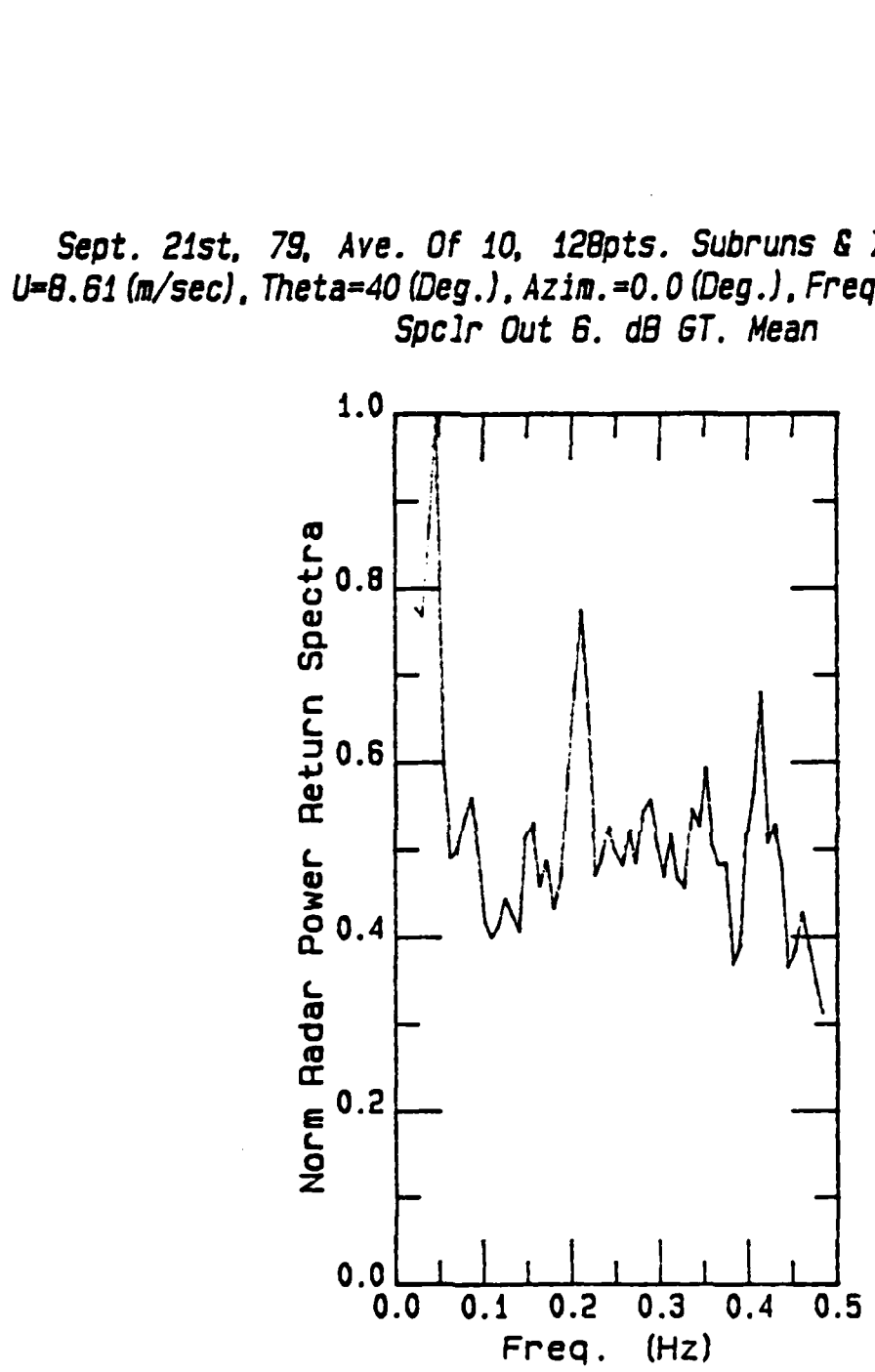

Figure 8.24
Normalized power return power spectra.

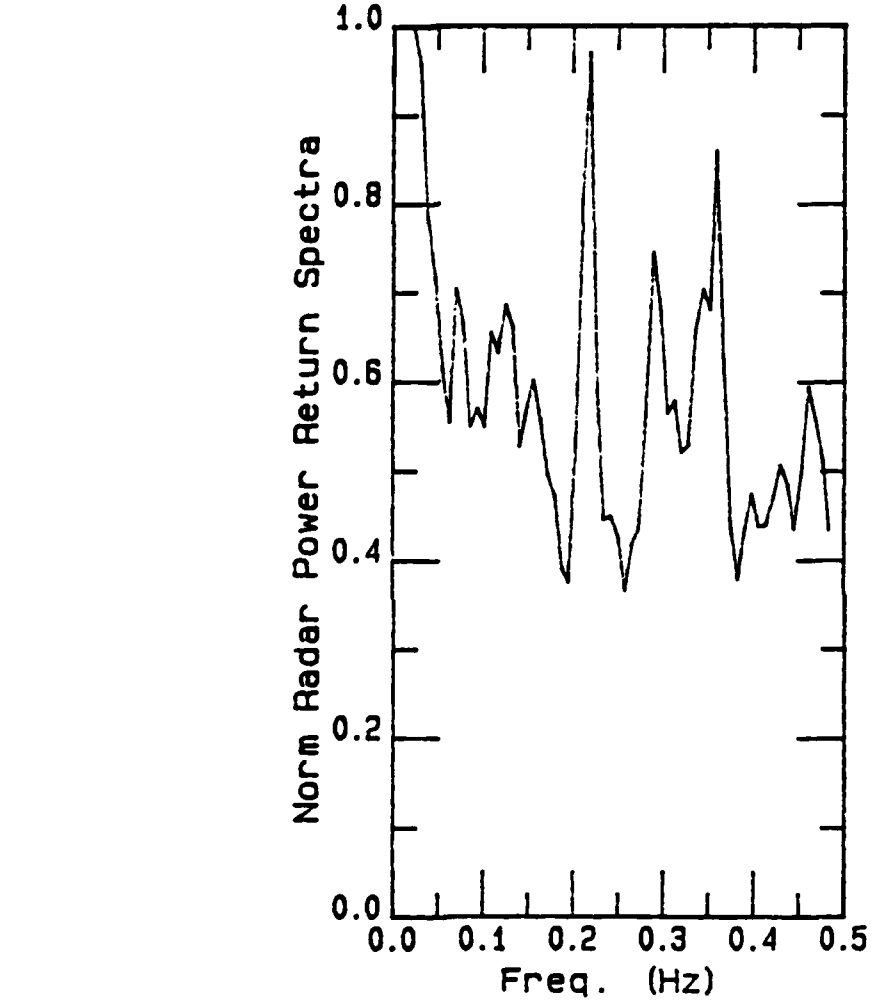

Figure 8.25
Normalized radar power return spectra.

Sept. 21st, 79, Ave. Of 10, 128pts. Subruns & 7pt. Moving Ave.
U=8.61 (m/sec), Theta=40 (Deg.), Azim.=0.0 (Deg.), Freq=14.5 (GHz), HH Pol

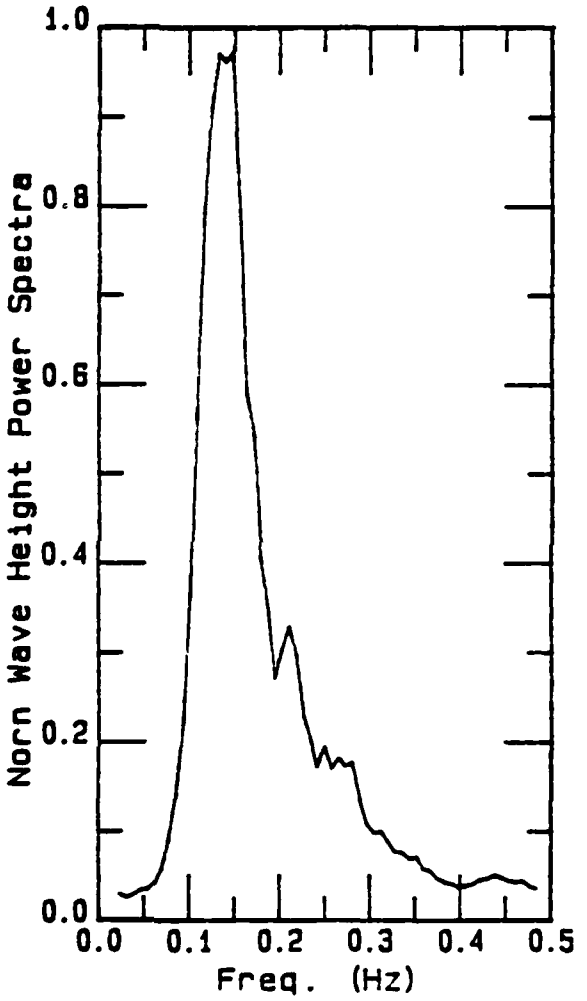

Figure 8.26
Normalized wave-height power spectra;
single peak about 0.15 Hz.

Sept. 21st, 79, Ave. Of 5, 128pts. Subruns & 7pt. Moving Ave.
U=8.69 (m/sec), Theta=40 (Deg.), Azim.=0.0 (Deg.), Freq=14.5 (GHz), vv Pol

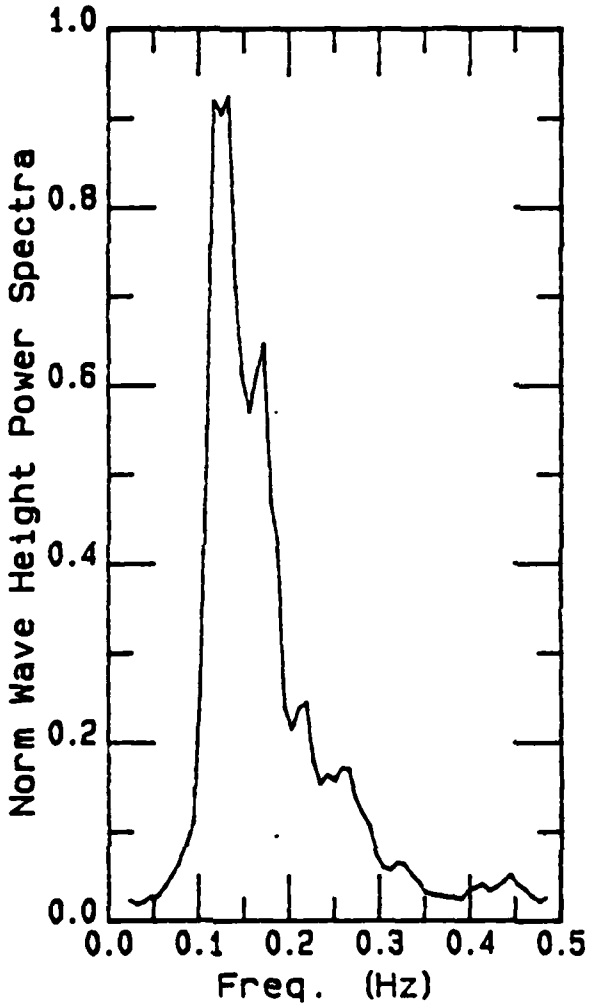

Figure 8.27
Normalized wave-height power spectra;
single peak about 0.14 Hz.

over the frequency for HH is 0.321 with standard deviation of 0.013 and for VV is 0.72 with standard deviaton 0.02. The coherence functions show more dependence between radar power return spectra and wave height for VV than for HH. Further study is needed to explain the difference. Plant [1980] stated that a useful, though arbitrary, convention in analyzing the MTF is to use only data for which the coherence is greater than 0.3. One result of a low value of coherence function is that the corresponding values of MTF have large variances.

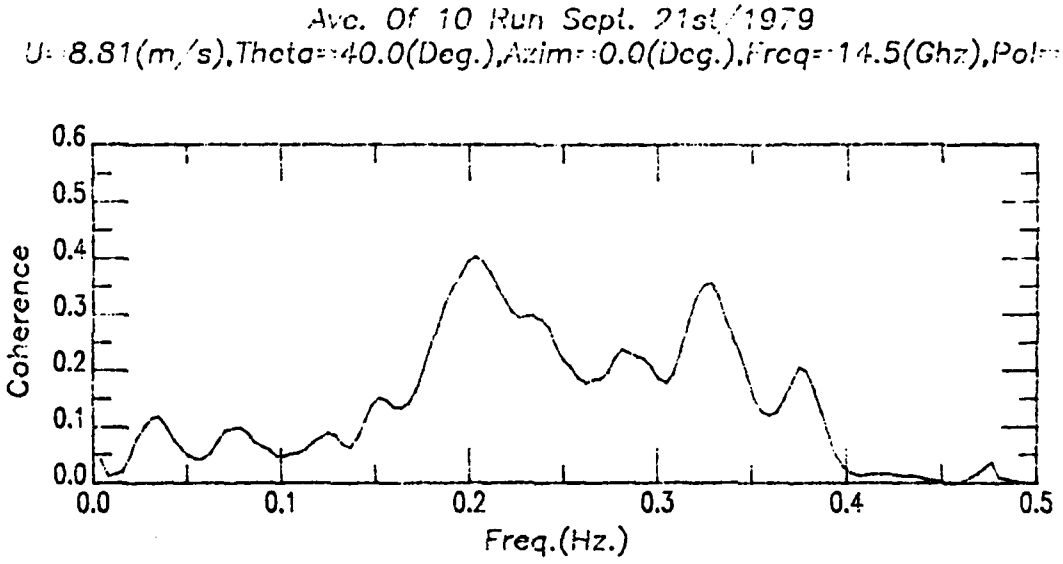

Figure 8.28
Coherence function for horizontal polarization

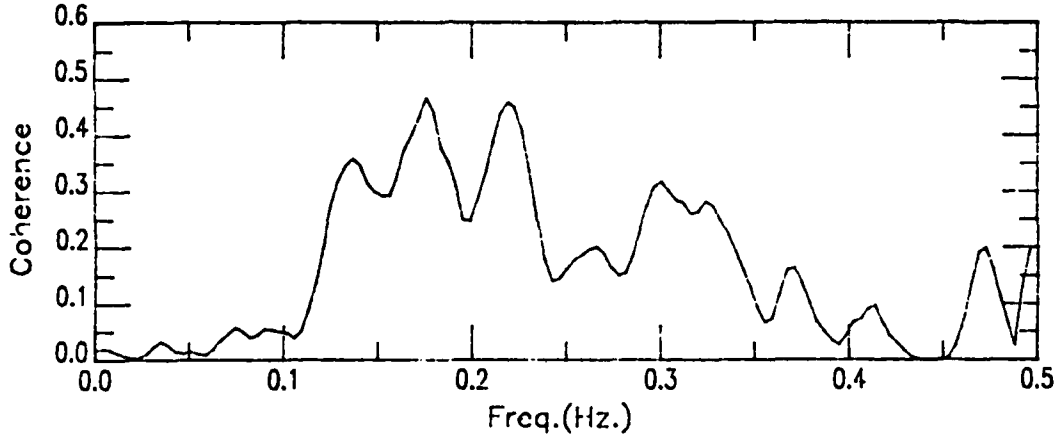

Figure 8.29
Coherence function for vertical polarization

9.0 DISCUSSION AND CONCLUSIONS

9.1 General Discussion

Methods have been developed for analysis of the University of Kansas measurements of radar cross-section and wave height as a function of time that were made as part of Project MARSEN from the Noordwijk platform in the North Sea off the Dutch coast during September through November 1979. The radar spectrometer was unique in two ways:

1. It could operate over a band of frequencies from 8 to 18 GHz, whereas most previous measurements have been made at single frequencies or groups of widely separated spot frequencies.
2. The range-tracker in the system permitted determination of the instantaneous wave height at the centroid of the radar footprint, whereas previous measurements have depended upon wave gauges located some distance from the radar footprint or upon integration of the velocity obtained by Doppler-frequency measurement to obtain the instantaneous wave height.

The first capability permits observations over a range of Bragg-resonant ocean wave numbers (K) not previously studied. The second permits development of cross-correlations between radar cross-section and wave height not previously possible.

The overall experiment provides information that permits determination of the apparent wave spectrum S(K) in the capillary region, as well as empirical observations of the radar scattering coefficient over a wide range of controlled conditions. These studies are the subject of other reports in this series. This report concentrates on the methodology and preliminary results of the study of

modulation of the radar cross-section, and consequently of the Bragg-resonant capillary-wave components, associated with the structure of the underlying larger waves.

Because of the large number of parameters that could be varied during the experiment (frequency, polarization, angle of incidence, look direction relative to the wind), the individual observation runs were relatively short. This means that the statistics of this experiment are somewhat less stable than those for experiments where fewer parameters had to be varied. Typical data runs varied from 3 to 7 minutes. However, on many days observations with the same radar parameters were repeated often enough to improve the stability of the statistical results. Because of the relatively short duration of the individual runs, simplification of data processing (involving numerous FFT operations) was achieved by standardizing on 128-second sequences. For the case analyzed as an example in this report (21 September 1979, 40° angle of incidence) this meant that averages could be obtained for 5 vertically polarized (VV) and 10 horizontally polarized (HH) 128-second samples.

Algorithms were developed to compute the modulation transfer functions (MTFs) used by other investigators, so that comparisons are facilitated. Because the instantaneous wave heights were measured, it is possible to calculate the instantaneous slopes for the underlying larger waves, on the assumption that these waves are long-crested. One can then calculate the scattering coefficient variations that would be observed if there were no modulation of the capillary waves by using the capillary wave spectrum S(K) in the theoretical expression for scattering—and the S(K) used can be that derived from the experiments

themselves. The difference of the observed radar scattering coefficient and the one that would be observed without modulation is therefore a measure of the modulation, here called the modulation index.

This instantaneous modulation index is then, in our analysis, cross-correlated with the instantaneous record of wave height and that of wave slope to obtain new measures of the variation of the modulation over the underlying larger waves (previously only frequency-domain measures have been used). Furthermore, the RMS value of this index represents a new measure of the size of the modulation of the capillary waves. Preliminary interpretations for the correlation with wave height have been made here for the sample case studied. The interpretation of the correlation with wave slope remains to be developed.

In the course of the analysis it became obvious that ''specular events'' or ''sea spikes'' were present in most of the measurements. A technique was developed for removing these from the data used in analysis of the modulation phenomenon, but a study of these anomalies themselves will be important as the data analysis proceeds.

The observations used in this preliminary study were for the radar looking in the upwind direction. The same methods can be used for the downwind direction. For the crosswind direction the analysis can be simplified, since the long-crested assumption (and the available point measurement of wave height) precludes assuming any slopes relative to the radar look direction. Crosswind data analyses will be presented in future reports in the series.

An algorithm has been developed to convert the time histories of

the waves into spatial descriptions of appropriate parts of the wave trains. This technique can be used readily with the wave-height and wave-slope records, but its use with the radar cross-section has more doubtful validity. The wave height can be described by a series with terms of the form $\exp(i(\omega t + Kx))$, but the radar signal is nonlinearly related to this series. Further study is required to determine whether the difference between the observed radar signal and that due to uniformly distributed capillary waves is sufficiently small that a linear approximation can be made that would validate the spatial Fourier-like series for this quantity.

The remainder of the discussion in this section relates to the preliminary results obtained by analysis of the sample data set for 21 September at 40° angle of incidence.

9.2 Discussion of Results for Sample Data Set

The preliminary analysis of the Noordwijk 1979 data has shown that the measured scattering coefficient leads the wave height by about 1.8 sec. The full period of the dominant wave is about 5.8 sec so 1.8 sec corresponds to about 104°. The measured scattering coefficient leads the maximum slope by 1.0 sec. Note that the full period of the dominant slope component is about 3.5 sec, so 1.0 sec corresponds to 103° for both HH- and VV-polarizations.

These phase differences, especially the phase difference of the scattering coefficient with respect to slope, brought up the idea of modulation index, $\mu(t)$ or $\Delta\sigma$, the ratio of total scattering coefficient (based on the instantaneous footprint of the radar antenna beam) to the theoretical scattering coefficient that would be found if

capillary wave amplitude were uniform over the large-scale waves. The theoretical value is also based on $S_4(K)$, where K is the instantaneous Bragg-resonant wave number. The RMS value of modulation index is 0.876 with a standard deviation of 0.349 for HH-polarization and 0.623 with standard deviation of 0.044 for VV-polarization.

The apparent phase relations between the modulation and the dominant wave and slope components are illustrated in Figure 9.1. An apparent discrepancy exists between the relations with the dominant ''slope wave'' and the dominant ''waveheight wave'' because of the higher frequency of the dominant slope (associated with the larger influence of the high-frequency components of the wave on the slope than on the height). Interpretation of this point remains to be established.

Figure 9.1a shows that the largest modulation appears 62° back from the crest of the wave, on the upwind side, but a relatively strong modulation peak appears to be 153° ahead of the crest. These do not appear to be artifacts of the data handling procedure, so one must assume that they are real, pending analysis of other data sets.

Figure 9.1b is a similar illustration indicating the location of the modulation peaks relative to the dominant slope component. These appear to be symmetrical and near the point of minimum slope. This is consistent with the location of the maximum modulation on the back face of the dominant wave, but since the dominant wave and slope have different periods, one must use caution in this interpretation.

As indicated, the interpretation of the locations of the modulation peaks is confused because one cannot simply use the ideas that come from a very-narrow-band process. Furthermore, the 1-second

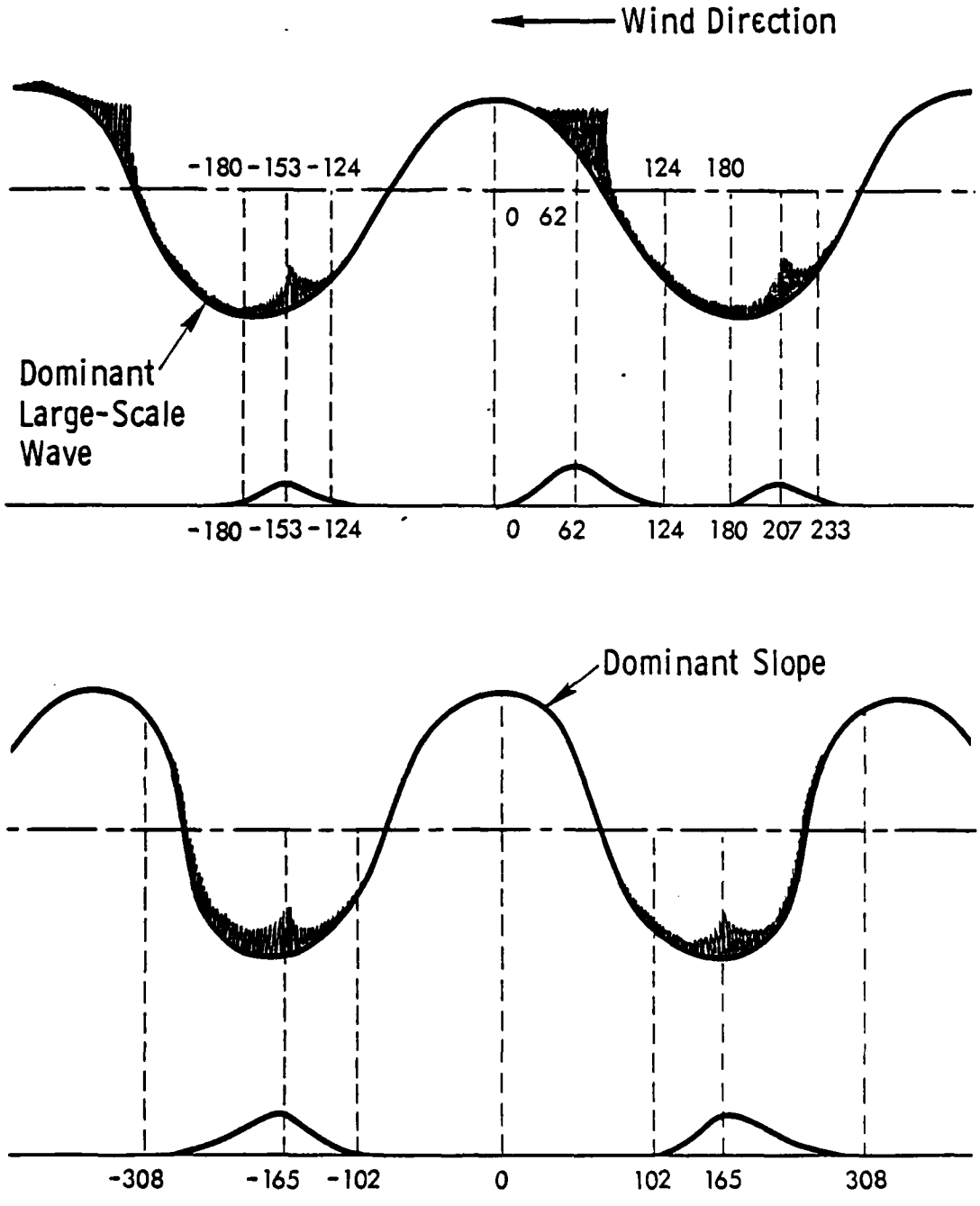

Figure 9.1
Graphic illustration of the nature of the results of the correlation study. The locations of the maximum correlations between apparent capillary amplitude (from $\Delta\sigma$) and wave height on the dominant component are shown in (a) and the locations relative to the dominant slope component are shown in (b). The apparent locations of maximum capillary-wave amplitude are sketched on large sinusoids representing dominant large-wave components. The sketches below show more quantitatively the apparent distribution of capillary amplitudes, but these sketches should not be considered accurate as to amplitude --they are intended only to illustrate the nature of the waves.

sampling interval used to measure the wave height may have been too great to give a good estimate of the slope spectrum, i.e., the latter may be corrupted by aliasing since its components are multiplied by 2, thereby enhancing the effect of the higher-frequency components of the measured spectrum that are more subject to corruption by aliasng. Clearly more study is needed.

The study of modulation in the spatial domain has just started, and more attention to the basic assumptions underlying it should be given before quantitative results are presented in the spatial domain.

9.3 Discussion

9.3.1 The Validity of the Analysis

The validity of this analysis is directly related to the goodness of the theoretical scattering coefficient estimation. Two different problems arise in estimating the theoretical scattering coefficient: first, the validity of the estimate of the K-spectrum of the capillary wave region $S_4(K)$, and second the effect the computer calibration factor which differs from run to run (Section 6.2) has on the true value of the theoretical scattering coefficient. The $S_4(K)$ which has been used in preliminary analysis was based on an average of three days of data in the windspeed range of 8.0 - 10.0 m/sec. The average calibration factor (ratio of the mean of the measured scattering coefficient to the mean of the theoretical scattering coefficient) is 17.5 with standard deviation of 4.8 for HH-polarization and 3.04 with standard deviation of 0.66 for VV-polarization.

9.3.2 Further Study Needed

The preliminary results have shown that the idea of modulation index can describe the phenomenon of capillary modulation over the large-scale wave. For further analysis a more accurate model of the K-spectrum $S_4(K)$ is needed. Note that in preliminary analysis, each set of theoretical scattering coefficient profile has been normalized to the ratio of the average of measured scattering coefficient to the average of theoretical scattering coefficient. This should be checked to make sure that this is the best approach for further analysis.

The next phase of the analysis is to test the idea of modulation index for different conditions (wind speed and pointing angle) to find out how the modulation index varies as a function of different parameters. The third phase of the analysis is to see if the modulation index can be expressed as a 'simple' function. At the end, one not only can estimate the amount of modulation and the location of the peaks of the modulation with respect to the slope, but also can give a idea about the 'dominant' shape of this modulation as a function of wind speed.

Comparison with cross-wind observations should be especially interesting. The slope, under the long-crested-wave assumption is always zero at crosswind. Viewing the capillary wave components normal to the predominant waves may also provide useful insights into the capillary distribution process.

APPENDIX A

Calculation of the Goodness of Estimation Based on 90 Percent of Confidence Interval

The cross-correlation of two proper finite functions, x(t),y(t), can be represented as

$$C(\tau) = \sum_m (ac + bd)\cos(\omega_m \tau) + (bc - ad)\sin(\omega_n \tau) \quad \text{(A.1a)}$$

$$= \sum_m p_m^2 \cos\left(\frac{2\pi n}{N}\tau\right) + q_m^2 \sin\left(\frac{2\pi n}{N}\tau\right) \quad \text{(A.1b)}$$

where a,b c,d are Fourier components of two functions:

$$X(t) = \sum_m a_n \cos\left(\frac{2\pi n}{N} t\right) + b_n \sin\left(\frac{2\pi n}{N} t\right) \quad \text{(A.2)}$$

$$y(t) = \sum_m c_n \cos\left(\frac{2\pi n}{N} t\right) + d_n \sin\left(\frac{2\pi n}{N} t\right) \quad \text{(A.3)}$$

The Fourier coefficients are unique for each set of records.

The quantities p_m^2 and q_n^2 have a probability density functions given approximately by [Donelan and Pierson, 1981]

$$f(p_m^2)\,dp_m^2 = \exp\left(-\frac{p_m^2}{S_n}\right) d\left(\frac{p_m^2}{S_n}\right) \quad \text{(A.4)}$$

$$S_n = S\left(\frac{N}{n}\right) = \int_{\frac{n}{N} - \frac{1}{2N}}^{\frac{n}{N} + \frac{1}{2N}} S(f)\,df \quad \text{(A.5)}$$

where $S(f)$ is the 'true', but unknown, cross-spectrum of the random

process which is assumed to be approximately a stationary Gaussian process.

Equation (A.4) is a chi-square distribution with two degrees of freedom with an unknown parameter, .

Given just one set of time profiles the values of p_m^2 must be smoothed over frequency as in

$$p_m^2 = \frac{1}{2R+1} \sum_{m-R}^{m+K} p_s^2 \qquad \text{(A.6a)}$$

or more generally

$$\overline{p_n^2} = \sum_{n-R}^{n+R} \delta_s p_s^2 \qquad \text{(A.6b)}$$

where

$$\Sigma \delta_s = 1 \qquad \text{(A.7)}$$

so as to obtain a smoother function for the cross-spectrum estimate by means of the assumption, which may not always be correct, that the true spectrum is slowly varying. If the cross-spectrum is slowly varying, then the values of $\overline{p_n^2}$ will be approximately distributed according to a chi square distribution with 2(2R+1) degrees of freedom. Successive estimates will not be independent. Those elemental frequency bands that are 2R+1 bands apart will be independent. With five pooled

samples and a triangular moving window, the value of $\overline{p_n^2}$ could be shown as

$$\overline{p_n^2} = \frac{1}{3}\left\{\frac{1}{3}\left(p_{n-2}^2 + p_{n+2}^2\right) + p_n^2 + \frac{2}{3}\left(p_{n-1}^2 + p_{n+1}^2\right)\right. \qquad \text{(A.8)}$$

If one gets an average of 10 individual sample records of $\overline{p_n^2}$ then equation (A.5) can be estimated by 100 degrees of freedom.

For a chi-square distribution with 2 degrees of freedom, it can be shown that

$$P\left(0.103 < 2\,\frac{\overline{p_n^2}}{S_n} < 5.99\right) = 0.90 \qquad \text{(A.9)}$$

and since the value of $\overline{p_n^2}$ is known from the FFT, it follows that

$$P\left(0.334 < \frac{S_n}{p_n^2} < 19.42\right) = 0.90 \qquad \text{(A.10a)}$$

$$P\left(0.334\,p_n^2 < S_n < 19.42\,p_n^2\right) = 0.90 \qquad \text{(A.10b)}$$

Given just one value of p_n^2, the value of the cross-spectrum is not known to within a factor of 58 at the 90 percent confidence level. For the 5 point, triangle moving average, 10 different sample

records, the estimate of $\bar{p}_n^{-2}$ has 100 degrees of freedom so that

$$P\left(77.93 < \frac{100\bar{p}_n^{-2}}{S_n} < 124.34\right) = 0.90 \quad \text{(A.11a)}$$

so that

$$P\left(\frac{100}{124.34} < \frac{S_n}{\bar{p}_n^{-2}} < \frac{100}{77.93}\right) = 0.90 \quad \text{(A.11b)}$$

$$P\left(0.804\,\bar{p}_n^{-2} < S_n < 1.283\,\bar{p}_n^{-2}\right) = 0.90 \quad \text{(A.12)}$$

The true cross-spectrum is known to within about $\pm$ 23.9 percent or a range of 47.9 percent at 90 percent confidence level.

APPENDIX B

Theoretical Development of 'Events' Effect (based on Moore, 1981)

For the theoretical development a simplified model involving a uniform capillary-wave distribution is assumed (Section 5.4). It further is assumed that randomly located specular points occur. The waves are assumed to be one-dimensional traveling in the direction of the wind.

The Bragg-scatter component is made up of a coherent sum of the voltages associated with scatter from each individual capillary wavelet. The voltage received from an individual capillary wavelet is V_c. The voltage associated with the scatter from an individual specular point is V_p. The total number of capillary wavelets in a footprint is n_c and the total number of specular points is n_p.

Assume a resolution cell with length L and width W. The radar is at a height h and has both vertical and horizontal beamwidths .

The transverse dimension of the footprint is

$$W = \beta R \tag{B.1}$$

and the longitudinal dimension is

$$L = \frac{\beta R}{\cos\theta} = \frac{\beta h}{\cos^2\theta} \tag{B.2}$$

since

$$h = R\cos\theta \tag{B.3}$$

Consequently the footprint area is

$$A = \frac{\beta^2 h^2}{\cos^3 \theta} \tag{B.4}$$

The total voltage received from the capillary waves is proportional to the number of them because of the coherent additions, that is,

$$V_{rc} = n_c V_c \tag{B.5}$$

Consequently, the square of the received voltage is

$$V_{rc}^2 = n_c^2 V_c \tag{B.6}$$

Note that the scattering coefficient is an ensemble average that is proportional to V_{rc}^2. Consequently the scattering coefficient is given by

$$\sigma_{rc}^2 = \mathcal{M} \langle V_{rc}^2 \rangle / A = \mathcal{M} n_c^2 \langle V_c^2 \rangle / A \tag{B.7}$$

Where $\mathcal{M}$ is a constant including the various radar parameters and the other quantities have been designated above.

Since the 'events' occur at random, the voltage due to them do not add coherently. Rather, the power must be added. Thus, the mean-square received voltage for the events is given by

$$\langle V_{rp}^2 \rangle = n_p \langle V_p^2 \rangle \tag{B.8}$$

where n_p is the mean number of events per footprint. This may be less than 1 since many footprints must be averaged to obtain the ensemble average of (B.8). Using this expression we may determine a scattering coefficient for the events:

$$\sigma^{\circ}_{rp} = \frac{M\langle V^2_{rp}\rangle}{A} = \frac{M n_p}{A}\langle V^2_p\rangle \qquad \text{(B.9)}$$

The total scattering coefficient is the sum of those due to the capillary waves from (B.7) and those due to the events from (B.8). Thus

$$\sigma^{\circ} = \sigma^{\circ}_{rc} + \sigma^{\circ}_{rp} = \frac{M}{A}\left(n_c^2\langle V_c^2\rangle + n_p\langle V_p^2\rangle\right) \qquad \text{(B.10)}$$

For a given length L of the illuminated area, one may obtain n_c and n_p. n_c is simply the length divided by the Bragg-resonant wavelength on the surface.

$$n_c = \frac{L \sin\theta}{\lambda/2} \qquad \text{(B.11)}$$

n_p is the ratio of the length L of the footprint to the mean spacing s_p between events

$$n_p = \frac{L}{s_p} \qquad \text{(B.12)}$$

Substituting these values into (B.8) gives

$$\frac{\sigma^{\circ} A}{N} = \frac{4L^2}{\lambda^2}\sin\theta\,\langle V_c^2\rangle + \frac{L}{s_p}\langle V_p^2\rangle \qquad \text{(B.13)}$$

which may be rewritten in terms of the capillary wave scattering coefficient and a correction term as

$$\sigma^\circ = \frac{4(\langle v_c^2\rangle M L^2 \sin^2\theta}{\lambda^2 A}\left(1+\frac{\langle v_p^2\rangle \lambda^2}{4\langle v_c^2\rangle S_p L \sin^2\theta}\right) \quad \text{(B.14a)}$$

or

$$\sigma^\circ = \sigma^\circ_{rc}\left(1+\frac{\langle v_p^2\rangle}{\langle v_c^2\rangle S_p}\frac{\lambda^2}{4h\beta}\cot^2\theta\right) \quad \text{(B.14b)}$$

The first factor in the second term is an unknown quantity because we do not know the ratio of the mean power returned for an event to the mean power returned from an individual component of the Bragg scattering capillary waves. The quantity S_p is also an unknown at the present time, although it may be possible to find a value for S_p. At present, however, these unknown quantities are simply combined into a single unknown factor Q. The second factor in the second term involves parameters of the system, and is readily determined. The third factor depends, of course, on the angle of incidence. Thus, we may write this equation as

$$\sigma^\circ = \sigma^\circ_{rc}\left(1+Q\left(\frac{\lambda^2}{4h\beta}\right)\cot^2\theta\right) \quad \text{(B.15)}$$

Although the value of Q is unknown, we can compare results for tower and aircraft. Examples are shown in the tables. Table B.1 gives the variation of the ratio of the scattering coefficient including the

effect of the events to that ignoring the events and including only capillary-wave Bragg scatter for the tower experiment. Values of Q of 100 to 50,000 are presented. If Q is only 100 the events have little effect on the scattering. However, a value of Q of 10,000 gives a difference of over 10 dB with and without the events at 20 degrees, falling off to a negligible value at 80_0.

Table B.2 gives a comparable set of calculations for an aircraft at 3000 m altitude except that the minimum value of Q is 1000 and computations are carried out up to $Q = 5 \times 10_{-6}$. If one assumes that Q is somewhere between 10,000 and 20,000, in accord with the observation that tower experiments give 20 degree measurements between 11.7 and 14.5 dB higher than aircraft experiments, we can check Tables B.1 and B.2 to see if this is really the case. For Q = 10,000 at 20 degrees with the aircraft the difference is only .23 dB between considering and ignoring the events. Yet, this was the case where there was more than a 10 dB difference at two heights. For Q = 20,000 the effect of the events is still less than 0.5 dB for the aircraft, yet it is more than 13 dB for the tower.

Thus, one can use this to explain the difference between tower and aircraft measurements on the assumption that Q is between 10,000 and 20,000 for the condition of measurement.

Q \ θ°	20 dB	30 dB	40 dB	50 dB	60 dB	70 dB	80 dB
100	0.56	0.23	0.11	0.06	0.03	0.01	0.002
1000	3.77	1.90	1.01	0.53	0.26	0.10	0.02
10,000	11.71	8.13	5.57	3.60	2.07	0.94	0.24
20,000	14.58	10.79	7.93	5.54	3.47	1.72	0.47
30,000	16.29	12.43	9.45	6.88	4.52	2.38	0.69
50,000	18.46	14.55	11.47	8.72	6.08	3.45	1.09

TABLE B.1
The variation of the ratio of the scattering coefficient including the effect of the events to that ignoring the events and including only capillary-wave Bragg-scatter for tower experiment

Q \ θ°	20 dB	30 dB	40 dB	50 dB	60 dB	70 dB	80 dB
1000	0.02	0.01	0.004	0.002	0.001	0.0004	0.0061
5000	0.12	0.05	0.02	0.01	0.01	0.002	0.0005
10,000	0.23	0.09	0.04	0.02	0.01	0.004	0.001
20,000	0.46	0.19	0.09	0.04	0.02	0.01	0.002
5×10^5	5.76	3.22	1.82	1.0	0.50	0.21	0.05
5×10^6	14.58	10.79	7.93	5.54	3.47	1.72	0.47

TABLE B.2:
A comparable set of calculations of the ratio of the scattering coefficient including the effect of the events to ignoring the events and including only capillary-wave Bragg-scatter for an aircraft at 3000 m altitude

APPENDIX C

Computer Programs

The main goal of these computations is to calculate the theoretical value of ° based on instantaneous slope, determine the spatial data profile from the time-data profile and ultimately calculate the proper cross-correlations both in the time and spatial domains.

The processing routine consists of a main program (*EEN353*), two main sub-routines (CCA3G3 and HH03L3) and a large block of calculation routines. Figure C.1 shows the block diagram of the processing routine.

(a) EEN353 reads the first set of raw data and feeds it through HH03L3, which controls and provides the inputs to the calculation routines. Calculated values will be located in the buffer of EEN353. When the first set of calculations is complete, the second and third will be fed through HH03L3. Calculated results will be averaged by means of CCA3G3 routine. Note that in cross-correlation calculations the results will be smoothed and averaged in the frequency domain and then will be transformed to the time domain (Figure C.2).

(b) Low-pass filtering: FLTRR: This block low-pass filters the wave height time profile by means of an FFT routine. It transforms the h(0,t) from the time domain to the frequency domain, chops all frequency components which are greater than .35 Hz, and transforms the chopped spectrum to the time domain (Figure C.3).

(c) Slope calculation SSLLPP: This block takes the filtered wave height and computes the spatial derivatives by means of an FFT routine

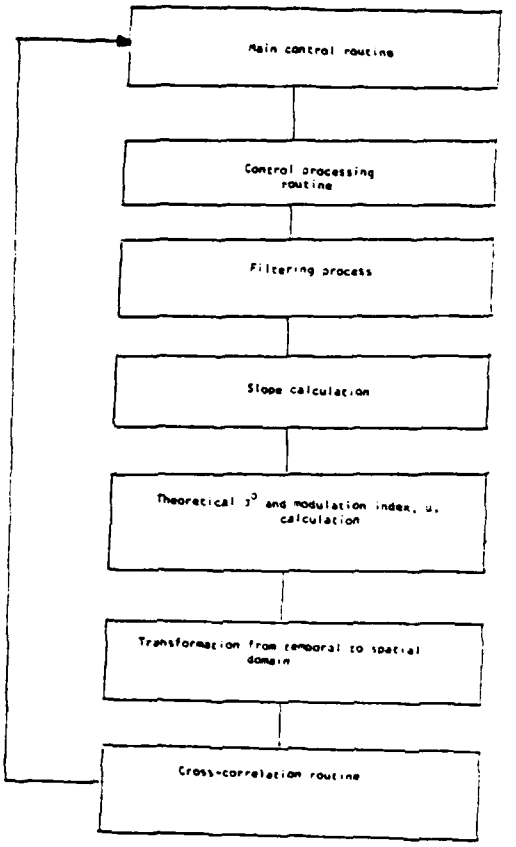

Figure C.1
Overall block diagram of processing

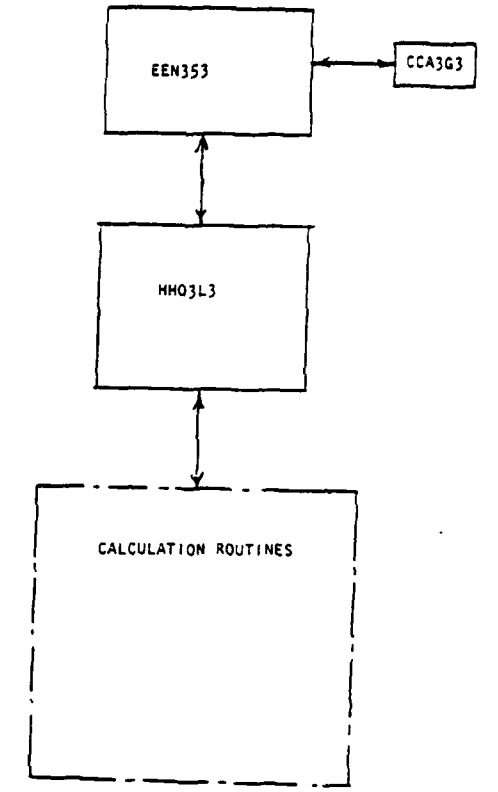

Figure C.2
Block diagram of control processing routine.
EEN353 is main controller; HH03L3 is the controller of the calculation routines; CCA3G3 transforms the averaged cross-spectra to cross-correlation.

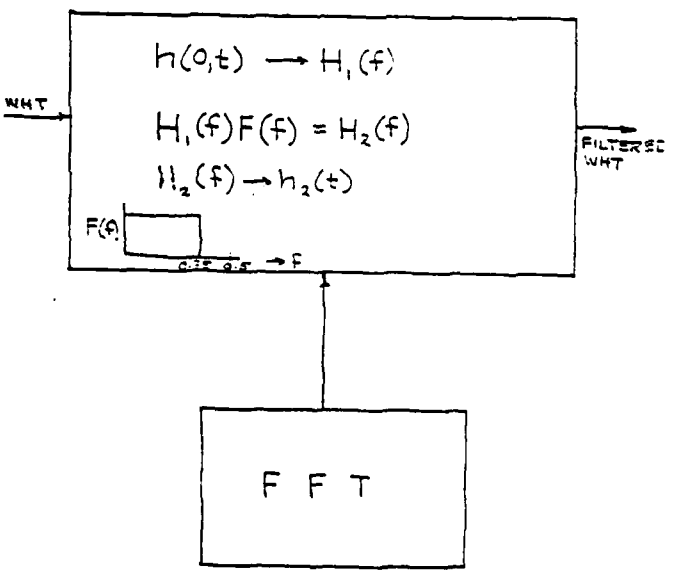

Figure C.3
Block diagram of lowpass filtering process (FLTRR)

(Figure C.4). Note that

$$h(x,t) = Re \sum_i b_i e^{j(\omega_i t + \omega_i^2 x/g)} \quad (C.1)$$

$$\frac{\partial h(x,t)}{\partial x} = Re \sum_i j b_i \frac{\omega_i^2}{g} e^{j(\omega_i t + \frac{\omega_i^2}{g} x)} \quad (C.2)$$

$$\frac{\partial h(0,t)}{\partial x} = Re \sum_i j b_i \frac{\omega_i^2}{g} e^{j(\omega_i t)} \quad (C.3)$$

$$\alpha = \tan^{-1}\left(\frac{\partial h(0,t)}{\partial x}\right) \quad (C.4)$$

(d) Theoretical σ° Calculation: This block consists of three different routines, DIECO, DDSTPP, and PWRSK. DIECO is a standard routine which calculates the sea-water dielectric constant, $\epsilon = \epsilon' - j\epsilon''$, and R_p, T_p, Fresnel reflection and transmission coefficients from θ, (antenna pointing angle), α, (sea slope), f, (frequency), p (polarization HH or VV), s_x (salinity) and T (water temperature) (Figure C.5).

PWRSK is a routine which calculates the value of S(K), based on $\bar{u}$, (average windspeed), f, (frequency) and θ', (local angle of incidence).

DDSTPP is a routine which computes the theoretical scattering coefficient based on Chan and Fung's model [1977]

$$\sigma^\circ_{theory}(t) = 8 k^4 |\alpha_{pp}|^2 S(k) \quad (C.5)$$

and also $\Delta\sigma$, $\frac{\sigma^\circ_{total}}{\sigma^\circ_{theory}}$ (measured σ° over theoretical σ°). Finally,

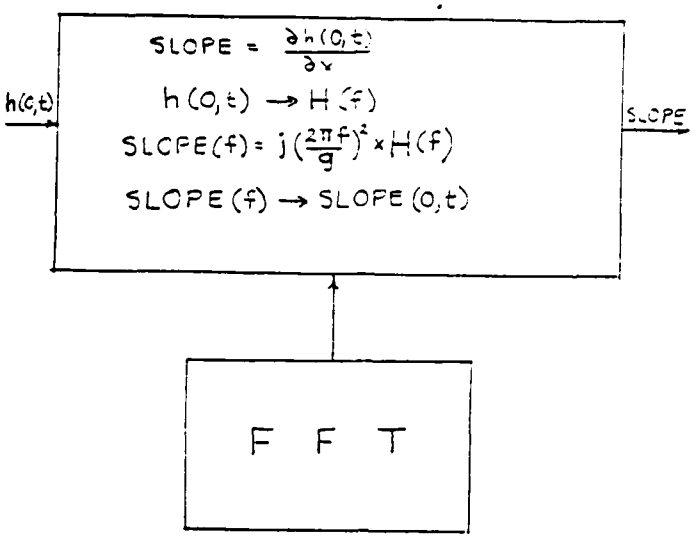

Figure C.4
Block diagram of slope calculation routine
from filtered wave height (SSLLPP)

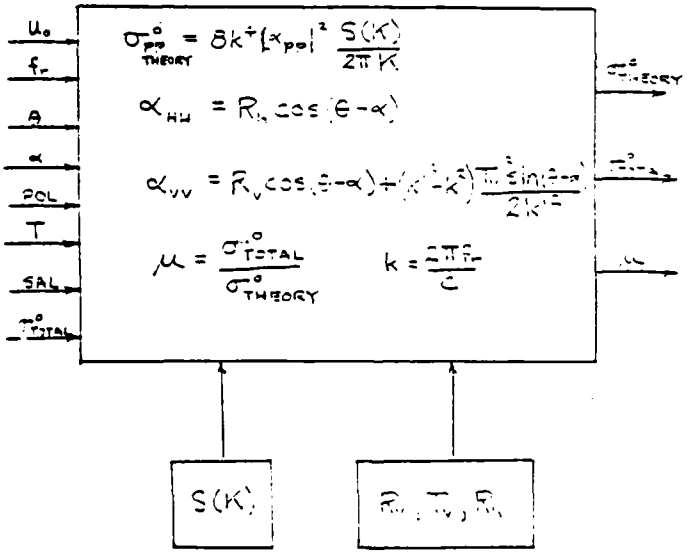

Figure C.5
Block diagram of theoretical σ^0 and modulation index, μ
calculation (DDSTPP)

it calculates the RMS modulation 'index' based upon:

$$\sigma^{\circ}_{total} = (1+\mu(t))\,\sigma_{Theory} \tag{C.6}$$

$$\mu(t) = \frac{\sigma^{\circ}_{total}}{\sigma^{\circ}_{Theory}} - 1 \tag{C.7}$$

$$RMS(\mu) = \left[\sum_{n} \mu_n^2(t)/N\right]^{1/2} \tag{C.8}$$

where N is number of samples per set.

(e) Spatial Transformation routine: This block consists of two routines, FRCFGN and XXFFCC. FRCFGN generates the proper Fourier coefficients and makes a table which can be used by XXFFCC.

XXFFCC transforms the time profile data set to a spatial profile (Figure C.6).

$$\eta(0,t) = Re \sum_{i} c_i e^{j(\omega_i t)} \tag{C.9}$$

$$\eta(x,0) = Re \sum_{i} c_i e^{j\left(\frac{\omega_i^2}{g} x\right)} \tag{C.10}$$

Note that if the transformation is not made this block can be ignored.

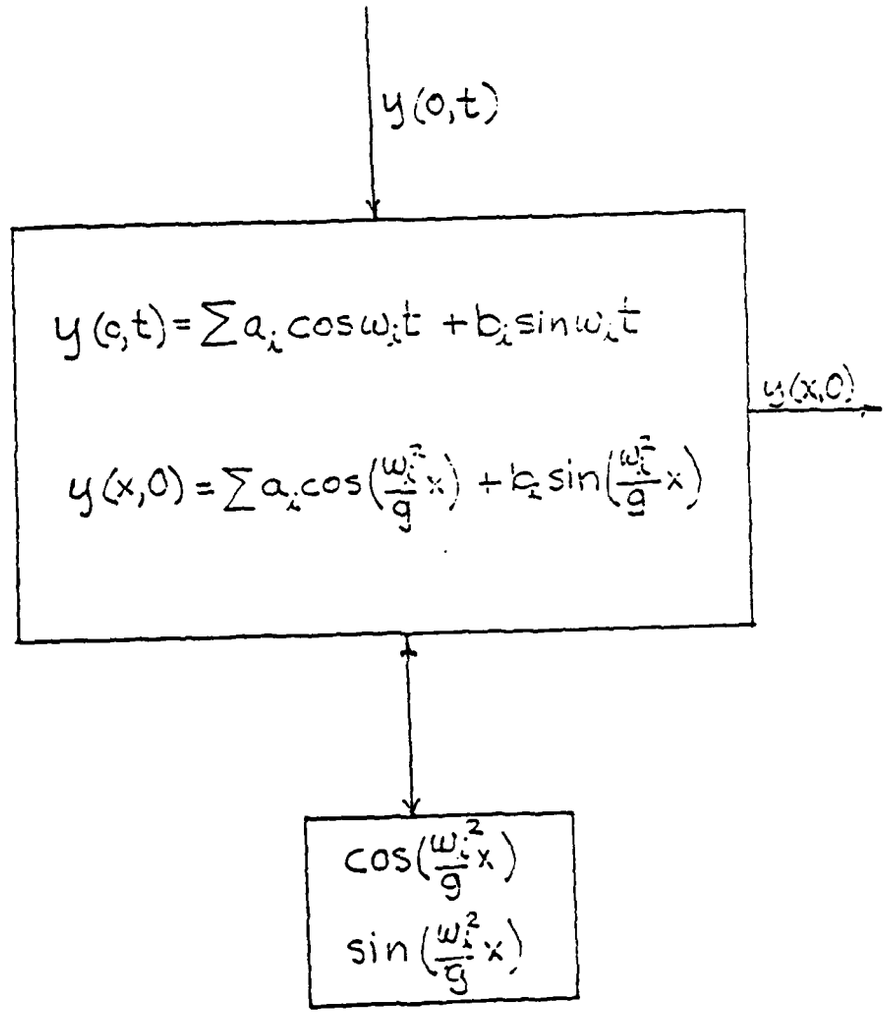

Figure C.6
Block diagram of temporal to spatial domain transformation (XXFFCC)

(f) Cross-Correlation routine: This block consists of four routines: MMOOTT, ZZGGNN, CCS323, and CCL3T3.

MMOOTT subtracts the mean from the sample set (Figure C.7).

$$\bar{p} = \frac{\Sigma p}{N} \tag{C.11}$$

$$p' = p - \bar{p} \tag{C.12}$$

ZZGGNN adds a string of zeroes at the end of each file. This provides an interpolation process when the FFT routine is used for cross-correlation calculation.

CCS3L3 and CCL3T3 process and calculate the cross-spectra by means of FFT. The result of averaged n_1 samples of cross-spectra are saved in EEN353.

(g) The final cross-correlation functions are provided when CCA3G3 smooths the provided values of cross-spectra by means of a five-point moving average and transforms it to the time or spatial domain. The smoothing process, five-point moving average improves the estimation of the 'true' value of cross-spectra. (Appendix B)

Miscellaneus Programs:

(1) Spclout:

This program calculates the upper limit of the maximum value of scattering coefficient which can occur. It calculates the mean of scattering coefficient and adds about 6.0dB to the mean and compares this value to all the sample points of measured scattering coefficient.

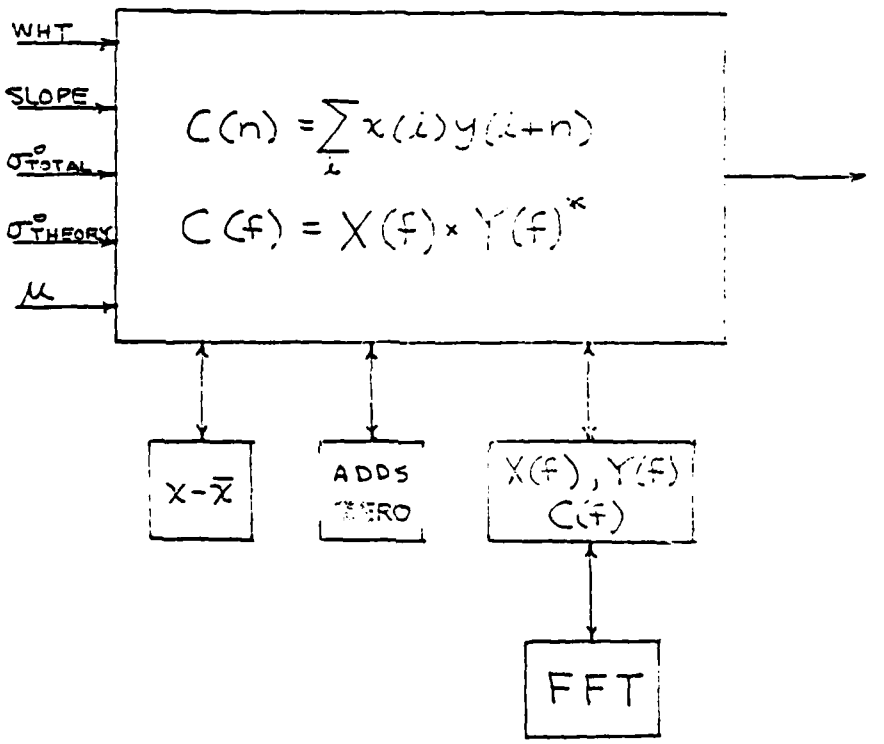

Figure C.7
Block diagram of cross-correlation calculation routine (CCS3L3). Note that the final transform, from frequency to time domain will be completed by means of CCA3G3.

If the value is greater than this 'threshold', a specular event (Section 5.4) will be replaced by a weighted average of its 5 adjacent points. Note that for 90 percent of the time the scattering coefficient over a range from 5.8 dB above the mean envelope level to 11.9 dB below the mean.

(2) MDTRNC

This program calculates MTF, Section 3.0. It simply calculates the smoothed, averaged cross-spectra of wave height and power return over the smoothed averaged power-spectra of wave height and mean of power return. For obtaining the 'stable' and smooth modulation transfer function, the result will be smoothed by means of seven point moving average.

$$R(f) = \frac{\langle P(f)\, H^{*}(f) \rangle}{\langle \bar{P}\, |H(f)|^{2} \rangle} \qquad \text{(C.13)}$$

(3) Coherence:

This program calculates the coherence function for power return and wave height. It simply finds the average cross-spectrum of wave height and power over the square root average of wave height power spectrum and square root of average power return power spectrum.

$$C^{2}(f) = \frac{\left\{ E\left[P(f)\, H^{*}(f) \right] \right\}^{2}}{E\left[|P(f)|^{2} \right] E\left[|H(f)|^{2} \right]} \qquad \text{(C.14)}$$

(4) FOURT

This is an FFT standard Fast Fourier Transform routine. It

takes a data set and will transform it from time to frequency or from frequency to time domain. The direction of the transformation depends on how the variables have been set.

$$Y(m) = \sum_{n} y(n) e^{-j\frac{2\pi}{N}nm} \qquad (C.15)$$

$$y(n) = \sum_{m} Y(m) e^{j\frac{2\pi}{N}nm} \qquad (C.16)$$

Call.FOURT (DATA, Num,a,b,c,d)

where:

Data is the name of the array

Num is the number of Data elements

a,b if a=1, b=-1. The Data will be transformed from time to frequency domain.

a,b if a=1, b=1. The Data will be transformed from frequency to time domain.

c=0 if imaginary part of Data is zero.

c=1 if imaginary part of Data is not zero.

d=0 if No. of element is the power of 2.

d=1 is no. of element is not the power of 2.

PROGRAM LISTS

```
*L EEN353

0010   PARAMETER ENS=10,V=[illegible],S1=128,W1=2048,U1=256,W1=64
0011C            NOTE THAT W IS 2*S , G IS S/2.
0013C   PARAMETER FC1=30,FC2=12,FC3=13C,FC4=10,FC5=.1,FC6=14
0014C PARAMETER FC7=06,FC8=09,FC9=16
0015C  PARAMETER FRQ=10.,POL=1.,THETA=90.,UO=21.84
0016C   PARAMETER FRQ=3.,POL=1.,THETA=90.,UO=2.44
0020  PARAMETER FRQ=14.5,POL =1.,THETA=40.,UO=8.61
0021C     <IF POL=1. POLARIZATION=HH,IF POL=2. POLARIZATION=VV.
0022C  PARAMETER [illegible]
0023  PARAMETER MTL=8
0024 REAL AVE1(V),AVE2(V) ,AVE3(V),AVE4(V),AVE5(V),AVE6(V),AVE7(V)
0025 REAL AVE8(V),AVE9(V),AVE10(V),AVE11(V)
0025 REAL UR(V),LL(V)
0026 REAL TATA(S.),XATA(S1),FINT(2,61),ICOS(61,S1),ISIN(61,S1),FCOS(61,S.),
0027FSIN(61,S1)
0027  REAL DATA(2,W1),EATA(2,W1),FILT(2,S1),CATA(W1),RATA(S1)
0028  REAL SLOP(2,S1),FREQ(S1),ALPHA(S1),JUNK(2,S1)
0029  REAL CRSTSL(W1),CRSOSW(W1),CRSTSW(W1),CRSOSL(W1),CRSSSW(W1),CROSS(W1)
0030  REAL CRSDSL(W1),CRSLSW(W1),CRSWW(W1),CRSSS(W1),CRSHH(W1)
0031 REAL SATA(2,W1),ZATA(2,W1),BATA(W1),DUM(W1)
0032  INTEGER GDS,PUM1,UUZ
0033 REAL MOP
0034 GDS=W1/(S1*2)
0035 PUM1=GDS*MTL
0036 PRINT,"PUM1=",PUM1
0037  UUZ=2*PUM1
0038 MOP=1./FLOAT(ENS)
0039 SLP=0.0
0039 HGT=0.0
0039 SGT=0.0
0039 S60=0.0
0039 TMOD=0.0
0040 DO 17  K=1,W1
0041  CRSTSL(K)=0.0
0042  CRSOSW(K)=0.0
0043  CRSTSW(K)=0.0
0044  CRSOSL(K)=0.0
0045  CRSSSW(K)=0.0
0046  CRSDSL(K)=0.0
0047  CRSLSW(K)=0.0
0048  CRSWW(K)=0.0
0049  CRSSS(K)=0.0
0050  CRSHH(K)=0.0
0051 17 CONTINUE
0051   DO 13 K=1,ENS
0052 PRINT,"NO.=",K
0053 REWIND 30
0054 DO 89 N=1,S1
0055  READ(30,150)J,AA,BB,CC
0056  WRITE(30,450)J,AA,BB,CC
0057 89 CONTINUE
0058 REWIND 30
0059  CALL DUMM(S1,W1,U1,W1,PUM1,
0060&MOP,AATA,FINT,ICOS,ISIN,FCOS,FSIN,
0070&DATA,EATA,FILT,CATA,RATA,
0080&SLOP,FREQ,ALPHA,JUNK,
0090&CRSTSL,CRSOSW,CRSTSW,CRSOSL,CRSDSL,CROSS,
0090&CRSDSL,CRSLSW,CRSWW,CRSSS,CRSHH,
0094&SATA,ZATA,BATA,DUM,
0100&HGT,SLP,S60,SGT,TMOD)
0110C
0115 REWIND 06
0116 REWIND 07
0117 REWIND 10
0122 REWIND 17
0123 DO 332 M=1,S1
0124 READ(7,450)J,BB
0125 WRITE(6,*)M,J,BB,PUM1,UU
0126 33C CONTINUE
0127 REWIND 17
0129 10 CONTINUE
0130  PRINT,"ISUEEEEEEEE"
0131  CALL CRSLTW(PUM1,PUM1,CRSWW,...,...,...,DATA,...,...,...
```

EEN353 (cont'd.)

```
0258  GO TO 445
0262  CALL CRSLTN(DATA,EATA,CRSmm,ZATA,SATA,GATA,DUM,U1,U1)
0263  CALL CRSLTN(DATA,EATA,CRSTSL,ZATA,SATA,GATA,DUM,U1,U1)
0264  CALL CRSLTN(DATA,EATA,CRSSS,ZATA,SATA,GATA,DUM,U1,U1)
0265  CALL CRSLTN(DATA,EATA,CRSLSU,ZATA,SATA,GATA,DUM,U1,U1)
0266  CALL CRSLTN(DATA,EATA,CRSOSU,ZATA,SATA,GATA,DUM,U1,U1)
0267  CALL CRSLTN(DATA,EATA,CRSTSU,ZATA,SATA,GATA,DUM,U1,U1)
0268  CALL CRSLTN(DATA,EATA,CRSOSL,ZATA,SATA,GATA,DUM,U1,U1)
0269  CALL CRSLTN(DATA,EATA,CRSDSU,ZATA,SATA,GATA,DUM,U1,U1)
0270  CALL CRSLTN(DATA,EATA,CRSDSL,ZATA,SATA,GATA,DUM,U1,U1)
0280 445 CONTINUE
0290 REWIND 08
0300 REWIND 09
0316 REWIND 16
0315 REWIND17
0316 PRINT,H6T,SLP,SG0,SGT,
0317 DO 15 K=((U1/2)-PUM1+2),((U1/2)+PUM1+1)
0318  J=K-(U1/2)-1
0320  BB=FLOAT(J)/8.
0322C  BB=FLOAT(J)+3./8.
0324  URITE(09,100)BB,CRSDSU(K)/(SQRT(TMOD)*SQRT(HGT)),CRSOSL(K)/(SQRT(SG0)
03254SQR1(SLP)),CASLSL(K)/(SQRT(TMOD)*SQRT(SLP))
0326  WRITE(08,100)BB,CASLSU(K)/(SQR1.SLP)*SQRT(H6T)),CASOSU(K)/(SQRT(SG0)
03274SQRT(H6T)),CRSTSL(K)/(SQRT(SGT)*SQRT(SLP))
0328  URITE(16,100)BB,CASSU(K)/AU1,CASSS(K)/SLP,CASmm(K)/TMOD
0370C
0380 15 CONTINUE
0382 DO 336 K=1,ST
0384 URITE(17,450)K-1,AVE11(K)
0386 336 CONTINUE
0390 450 FORMAT(V)
0395 100 FORMAT(V)
0400 STOP
0410 END
```

```
L MH03L3

0001   SUBROUTINE DDON(S,U,V,Q,POM,
0002&TATA,XATA,FINT,ZCOS,ZSIN,FCOS,FSIN,
0003&DATA,EATA,FILT,CATA,BATA,
0004&SLOP,FREQ,ALPHA,JUNK,
0005&CRSTSL,CRSDSU,CRSTSU,CRSDSL,CRSDSU,CROSS,
0006&CRSDSL,CRSLSU,CRSUU,CRSSS,CRSMM,
0007&SATA,ZATA,BATA,DUM,
0008&HGT,SLP,S60,S6T,TMOD)
0010C    INTEGER S=128,U=2048,V=256,Q=64
0011C             ONOTE THAT U IS 2*S , Q IS S/2>
0013    PARAMETER FC1=30,FC2=12,FC3=13,FC4=10,FC5=11,FC6=14
0014 PARAMETER FC7=08,FC8=09,FC9=16
0015C  PARAMETER FRQ=13.,POL=1.,THETA=50.,U0=21.64
0016C   PARAMETER FRQ=15.,POL=1.,THETA=40.,U0=20.44
0020  PARAMETER FRQ=14.5,POL =1.,THETA=40.,U0=8.51
0021C     <IF POL=1. POLARIZATION=HH, IF POL=2. POLARIZATION=VV>
0022  PARAMETER LF=0.0,HF=.35
0023 INTEGER S,U,V,Q,POM,S2,U2,V2,Q2,POM2
0024 REAL TATA(S),XATA(S),FINT(2,Q),ZCOS(Q,S),ZSIN(Q,S),FCOS(Q,S),FSIN(Q,S)
0027  REAL DATA(2,U),EATA(2,U),FILT(2,S),CATA(U),BATA(S)
0028  REAL SLOP(2,S),FREQ(S),ALPHA(S),JUNK(2,S)
0029  REAL CRSTSL(U),CRSDSU(U),CRSTSU(U),CRSDSL(U),CRSDSU(U),CROSS(U)
0030  REAL CRSDSL(U),CRSLSU(U),CRSUU(U),CRSSS(U),CRSMM(U)
0031 REAL SATA(2,U),ZATA(2,U),DATA(U),DUM(U)
0032 S2=S
0033 U2=U
0034 V2=V
0035 Q2=Q
0036 POM2=POM
0037 PRINT,"POM=",POM2
0036  REWIND FC1
0036  REWIND FC2
0036  REWIND FC3
0036  REWIND FC4
0036  REWIND FC5
0036  REWIND FC6
0038C   GO TO 997
0039     CALL FILTER(FC1,FC2,S2,LF,HF,BATA,FILT,CATA)
0040     CALL SLOPE(FC2,FC3,S2,SLOP,FREQ,ALPHA,JUNK)
0045    CALL DISTRM(FC1,FC3,FC4,FC5,FC6,S2,FRQ,POL,THETA,U0,DATA,EATA)
0047 GO TO 997
0049  CALL XFUNC(FC2,S2,Q2,TATA,XATA,ZCOS,ZSIN,FCOS,FSIN,FINT)
0050C
0052  CALL XFUNC(FC3,S2,Q2,TATA,XATA,ZCOS,ZSIN,FCOS,FSIN,FINT)
0053  CALL XFUNC(FC4,S2,Q2,TATA,XATA,ZCOS,ZSIN,FCOS,FSIN,FINT)
0054  CALL XFUNC(FC5,S2,Q2,TATA,XATA,ZCOS,ZSIN,FCOS,FSIN,FINT)
0055  CALL XFUNC(FC6,S2,Q2,TATA,XATA,ZCOS,ZSIN,FCOS,FSIN,FINT)
0057    997 CONTINUE
0058     CALL AMOUT(FC2,S2,BATA)
0059     CALL AMOUT(FC3,S2,BATA)
0060     CALL AMOUT(FC4,S2,BATA)
0070     CALL AMOUT(FC5,S2,BATA)
0080     CALL AMOUT(FC6,S2,BATA)
0090     CALL ZRGEN(FC2,2*S2,CATA)
0092     CALL ZRGEN(FC3,2*S2,CATA)
0094     CALL ZRGEN(FC4,2*S2,CATA)
0096     CALL ZRGEN(FC5,2*S2,CATA)
0098     CALL ZRGEN(FC6,2*S2,CATA)
0099C GO TO 998
0099C PRINT,"POM2",POM2
0100     CALL CRSSLL(FC2,FC3,FC4,FC5,FC6,FC7,FC8,FC9,U2,V2,DATA,EATA,CRSTSL
01058,CRSDSU,CRSTSU,CRSDSL,CRSDSU,CRSUSL,CROSS,CRSLSU,CRSUU,CRSSS,CRSMM,ZATA,
01078&SATA,DUM,BATA,POM2,
01088&HGT,SLP,S60,S6T,TMOD)
0109 998 CONTINUE
0110C     STOP
0115 RETURN
0120     END
*
```

```
- FLTRR

0005   SUBROUTINE   FILTER(FC1,FC2,S,LF,HF,DATA,FILT,CATA)
0007   INTEGER FC1,FC2,S
0008   REAL LF,HF
0010C   PARAMETER  S=128
0020   REAL DATA(2,S),FILT(2,S)
0025  REAL CATA(S)
0030  REAL SUM,SUN
0040C
0050C
0060C
0070   REAL NUN
0075   NUN=S
0077 PRINT,"NUM=",NUM
0081 FREQ=.35
0082  LUM=INT(FREQ*NUM)
0083 PRINT,LUM
0085   NUN=1./FLOAT(NUM)
0087   SUM=0.0
0090   DO 10 K=1,NUM
0100   READ(30,100)J,UNT,PUT,SIGO
0110   DATA(1,K)=UNT
0115  CATA(K)=UNT
0120   DATA(2,K)=0.0
0125   FILT(1,K)=0.0
0126   FILT(2,K)=0.0
0127   SUM=SUM+DATA(1,K)
0130 10 CONTINUE
0135   AVE=SUM/NUM
0136   PRINT,"SUM",SUM
0137   PRINT,"UNT",AVE
0138   CALL FOURT(DATA,NUM,1,-1,0,0)
0140  DO 11 K=1,(NUM/2)
0142 if (k.gt.lum) go to 666
0144  FILT(1,K+1)=1.
0146  FILT(2,K+1)=1.
0148  FILT(1,NUM-K+1)=FILT(1,K+1)
0150  FILT(2,NUM-K+1)=-FILT(2,K+1)
0152  11 CONTINUE
0153 666 CONTINUE
0154  FILT(1,1)=1.
0156 FILT(2,1)=0.0
0158  FILT(1,NUM/2)=0.0
0160  FILT(2,NUM/2)=0.0
0200   DO 12 K=1,NUM
0210   DATA(1,K)=DATA(1,K)*FILT(1,K)*NUN
0220   DATA(2,K)=DATA(2,K)*FILT(2,K)*NUN
0222   filt(1,k)=nun*filt(1,k)
0224   filt(2,k)=nun*filt(2,k)
0228C   WRITE(14,100)K,DATA(1,K),DATA(2,K)
0229C write(14,100)k-1,filt(1,k),filt(2,k)
0230 12 CONTINUE
0240C
0250C
0260   CALL FOURT(DATA,NUM,1,1,1,0)
0265    CALL FOURT(FILT,NUM,1,1,1,0)
0270C
0280   SUN=0.0
0290   DO 14 K=1,NUN
0295   SUN=SUN+DATA(1,K)
0300   WRITE(12,1000)K,DATA(1,K)
0302C  write(11,100)k-1,FILT(1,k),FILT(2,k)
0305C   WRITE(13,100)K,CATA(K),DATA(1,K),DATA(2,K),FILT(K)
0310 14 CONTINUE
0315  PRINT,"SUN",SUN
0320    PRINT,"UNTFILT",SUN/NUM
0330 1000 FORMAT(V)
0335  100 FORMAT(V)
0337  RETURN
0340C   STOP
0350   END
```

```
L SSLLPP


0005 SUBROUTINE SLOPE(FC2,FC3,S,SLOP,FREQ,ALPHA,JUNK)
0010  INTEGER S,FC2,FC3
0023C DIMENSION FILT(S)
0030  REAL SLOP(2,S),FREQ(S),JUNK(2,S),ALPHA(S)
0050 INTEGER NUM
055 REAL NUM
0060 NUM=S
065 NUM=1./FLOAT(NUM)
0070 PI=3.141519
0100 SUM=0.0
0105 F0=.35
0107 REWIND 12
0110   DO 59 K=1,NUM
0125   READ(12,100)J,AVHT
0130 SLOP(1,K)=AVHT
0140 SLOP(2,K)=0.0
0150 SUM=SUM+AVHT
0160 59 CONTINUE
0170 AVHT=SUM/NUM
0180 PRINT,AVHT
0185 PRINT,"SUM",SUM
0190C
0200 CALL FOURT(SLOP,NUM,1,-1,0,0)
0205 PRINT,"O.K.!!!!!!!"
0210C
0220 DO 101 I=1,NUM
0240 FREQ(I)=FLOAT(I-1)/FLOAT(NUM)
0250 101 CONTINUE
0251C
0252C
0253C DO 112 K=1,NUM/2
0254C FILT(K)=1./(1+(FREQ(K)/F0)**16)
0255C FILT(K)=1.
0256C SLOP(1,K)=FILT(K)*SLOP(1,K)
0258C SLOP(1,NUM-K+1)=SLOP(1,NUM-K+1)*FILT(K)
02e0C SLOP(2,NUM-K+1)=SLOP(2,NUM-K+1)*FILT(K)
02e2C SLOP(2,K)=FILT(K)*SLOP(2,K)
0264C 112 CONTINUE
0265 JUNK(1,1)=0.0
0266 JUNK(2,1)=0.0
0268C
0270 DO 102 K=1,NUM/2
0280 Z=(2.*PI*FREQ(K+1)*2.*PI*FREQ(K+1))/(9.81)
0285 IF(FREQ(K+1) .GE. 5.) Z=0.0
0290 JUNK(1,K+1)=-Z*NUM*SLOP(2,K+1)
0300 JUNK(2,K+1)=Z*NUM*SLOP(1,K+1)
0310 JUNK(1,NUM-K+1)=JUNK(1,K+1)
0320 JUNK(2,NUM-K+1)=-JUNK(2,K+1)
0331 102 CONTINUE
0332 DO 30 K=1,NUM
0334 SLOP(1,K)=NUM*SLOP(1,K)
0336 SLOP(2,K)=NUM*SLOP(2,K)
0338 30 CONTINUE
0340 JUNK(2,(NUM/2)+1)=0.0
0343 DO 107 K=1,NUM
0347C WRITE(15,400)FREQ(K),SLOP(1,K),SLOP(2,K),Z(K),JUNK(1,K),JUNK(2,K)
0349 107 CONTINUE
03e0C
0370 CALL FOURT(SLOP,NUM,1,1,1,0)
0380C
0390 CALL FOURT(JUNK,NUM,1,1,1,0)
04000
0410 DO 103 I=1,NUM
0420 ALPHA(I)=ATAN(JUNK(1,I))
0430 ALPHA(I)=180./PI*ALPHA(I)
0440 103 CONTINUE
0450 DO 104 K=1,NUM
0460C WRITE(08,200)K-1,SLOP(1,K),JUNK(1,K),ALPHA(K),FREQ(K
0464  WRITE(13,300)K,ALPHA(K)
0470 104 CONTINUE
0475 100 FORMAT(I)
0480 900 FORMAT(I4,4X,F9.3,4X,F9.3
0485 400 FORMAT(F9.3,4X,F9.3,4X,F9.3,4X,F9.3,4X,F9.3,4X,F9.3
0490 200 FORMAT(I4,4X,F9.3,4X,F9.3,4X,F9.3,4X,F9.3,4X,F9.3
 410 300 FORMAT(
 420 500 F
 430 600
 440 700
 450
```

```
C  DUSTHM

0005 SUBROUTINE DUSTFM(FC1,FC2,FC4,FC5,FC6,S,FRM,FUL,THETM,UU,WMIM,GAMM)
0007 INTEGER FC1,FC2,FC4,FC5,FC6,S
0009 REAL FRQ,FUL,THETA,UU
0010 COMPLEX DIECO,AV,RR
0020   REAL  RI(2),EMISS(2)
0030 REAL DATA(2,5),ENTA(2,5)
0035 REAL SS(1,1)
0037 REAL LAMDA
0040  T=286.
0045  SML=55.
00500  FREQ=10.
00550  THETA=40.
00600  UU=5.76
00650 UU=8.6
00700 UU=8.10
0075C  UU=11.77
00800 LAMDA=2.3076923
0081 LAMDA=30./FRM
0082 PRINT,FRM,LAMDA,THETA,FUL,UU
0083 PI=4.*ATAN(1.)
0085 NUM=S
0087 ZEG=0.0
0088  SUM=0.0
0090 REWIND 13
0095 REWIND 30
0080      DO 10 K=1,NUM
0090  READ(13,100)WW,ALPHA
0110   READ(30,600)U,WMI,FWI,SIGO
0120  BETA=THETA-ALPHA
0122 GAMA=BETA
0123  ALPHA=ALPHA*PI/180.
0125 BETA=PI*BETA/180.
01260 PRINT,BETA
0127 X=4.*PI*SIN(BETA)/(LAMDA)
0130  AA=ALOG10(1./(2.*PI)**(2*PI/(LAMDA)**3))
0160   CALL EMISCN(T,SAL,FRQ,GAMA,DIECO,RH,RV,RI,EMISS)
01700
0180  FERS=((CABS(RH))**(CABS(RH))
01850 PRINT,FERS
0190 BB=ALOG10(FERS)
0192 BB=BB+ALOG10((COS(BETA))**4)
01930 PRINT,BB
0195   CALL SR(UU,X,SS)
0202 CC=SS
02050  PRINT,CC,X,UU
0210 DD=ALOG10(1./SIN(BETA))
0220 EE=AA+BB+CC+DD
00223 DATA(1,K)=10.**EE
0225C WRITE(19,100)K-1,AA,BB,CC,DD,EE,FERS,DATA(1,K)
0235 IF(ALPHA.LT.0.0)  ENTA(1,K)=SIGO*COS(ALPHA)
0237 IF(ALPHA.GT.0.0)  ENTA(1,K)=SIGO/COS(ALPHA)
0240 ZEG=ZEG+DATA(1,K)
0250 SUM=SUM+ENTA(1,K)
02550 WRITE(17,100)K-1,10.*ALOG10(SIGO)
0260   WRITE(16,700)K-1,THETA,ALPHA*180./PI,GAMA,AA,BB,X,CC,DD,DATA(1,K),DIECO
0260 10 CONTINUE
0270 ZEG=ZEG/FLOAT(NUM)
0280 SUM=SUM/FLOAT(NUM)
0290 RATIO=SUM/ZEG
0292 PRINT,'RATIO=',RATIO,SUM,ZEG
02930 RATIO=1.
0294 REWIND 17
0296 SUM=0.0
```

DDSTHH (cont'd.)

```
0297 DO 13 K=1,NUM
0300 DMTA(I,K)=RATIO*DATA(I,K)
0301C DATA(I,K)=10.*ALOG10(DATA(I,K)
0302C EATA(I,K)=10.*ALOG10(EATA(I,K)
0305  UU=ABS((EATA(I,K)/DATA(I,K))-1.)
0306 SUM=SUM+UU*UU
0307C UU=EATA(I,K)-DATA(I,K)
0308  WRITE(10,100)K-1,EATA(I,K)
0309  WRITE(11,100)K-1,DATA(I,K)
0310  WRITE(14,100)K-1,UU
0315 WRITE(17,100)K-1,UU
0320 13 CONTINUE
0325 RMS=SQRT(SUM /NUM)
0327 PRINT,'RMS OF H(t)=',RMS
0330  200 FORMAT(V)
0335 300 FORMAT(V)
0337 100 FORMAT(V)
0340 400 FORMAT(V)
0342 700 FORMAT(V)
0345C 700 FORMAT(I3,3X,F7.4,3X,F7.4,3X,F7.4,3X,F7.4,3X,F7.4,3X,F7.4,3X,F7.4,3X,F7.4,3X,F7.4,3X,F9.5,3X,F7.4,1X,F11.4)
0345  700 FORMAT(I3,3X,9(F7.4,3X),F9.5,3X,F7.4,1X,F11.4)
0350  RETURN
0360    END
```

```
C DDSTOV

0005 SUBROUTINE DISTRN(FC1,FC3,FC4,FC5,FC6,S,FRQ,POL,THETm,UU,DATA,EMISS)
0007 INTEGER FC1,FC3,FC4,FC5,FC6,S
0009 REAL FRQ,POL,THETm,UU
0010 COMPLEX DIECO,...,RH,RR,RV
0020   REAL  R2(2),EMISS(2)
0030 REAL DATA(1,S),EMTA(1,S)
0035 REAL SS,A,UU
0037 REAL LAMDA
0040  T=286.
0043  SAL=35.
0050C  FREQ=10.
0055C  THETm=40.
0056C  UC=5.75
0057C JO=8.9
0058C UU=8.25
0059C  UC=21.77
0060C LAMDA=2.3078923
0061 LAMDA=30./FRQ
0062 PRINT,FRQ,LAMDA,THETA,POL,UU
0063 PI=4.*ATAN(1.)
0065 NUM=S
0067 ZEG=0.0
0068  SUM=0.0
0070 REWIND 13
0075 REWIND 30
0080     DO 10 K=1,NUM
0090  READ(13,100)UU,ALPHA
0110   READ(30,600)J,WHT,PUT,SIGO
0120  BETA=THETA-ALPHA
0122 GAMA=BETA
0123  ALPHA=ALPHA*PI/180.
0125 BETA=PI*BETA/180.
0126C PRINT,BETA
0127 A=4.*PI*SIN(BETA)/(LAMDA)
0130  AA=ALOG10((2./PI)*((2*PI/LAMDA)**3))
0140C  AA=AA+ALOG10(COS(BETA)**4)
0160   CALL EMISUN(T,SAL,FRQ,GAMA,DIECO,RH,RV,R2,EMISS)
0170C
0196  GV=RV*(((COS(BETA))**2)+.5*((1.+RV)**2)*(1.-(1./DIECO))*(SIN(BETA))**2)
0198 FERS=(CABS(GV))**(CABS(GV))
0199  BB=ALOG10(FERS)
0200   CALL SR(UU,A,SS)
0202 CC=SS
0205C  PRINT,CC,A,UU
0210 DD=ALOG10(1./SIN(BETA))
0220 EE=AA+BB+CC+DD
00223 DATA(1,K)=10.**EE
0225C WRITE(19,100)K-1,AA,BB,CC,DD,EE,FERS,DATA(1,K)
0235 IF(ALPHA.LT.0.0)  EMTA(1,K)=SIGO+COS(ALPHA)
0237 IF(ALPHA.GT.0.0)  EMTA(1,K)=SIGO/COS(ALPHA)
0240 ZEG=ZEG+DATA(1,K)
0250 SUM=SUM+EMTA(1,K)
0255C WRITE(17,100)K-1,10.*ALOG10(SIGO)
0257   WRITE(18,700)K-1,THETA,ALPHA*180./PI,GAMA,AA,BB,RV,1,CC,DD,DATA(1,K),DIECO
0260 10 CONTINUE
0270 ZEG=ZEG/FLOAT(NUM)
0280 SUM=SUM/FLOAT(NUM)
0290 RATIO=SUM/ZEG
0292 PRINT, RATIO=',RATIO,SUM,ZEG
0293C RATIO=1.
0294 REWIND 17
0295 SUM=0.0
```

DDSTVV (cont'd.)

```
0297 DO 13 K=1,NUM
0300 DATA(1,K)=RATIO*DATA(1,K)
0301C DATA(1,K)=10.*ALOG10(DATA(1,K)
0302C EATA(1,K)=10.*ALOG10(EATA(1,K)
0303  UU=ABS((EATA(1,K)/DATA(1,K))-1.)
306  SUM=SUM+UU*UU
0307C UU=EATA(1,K)-DATA(1,K)
0308  WRITE(10,100)K-1,EATA(1,K)
0309  WRITE(11,100)K-1,DATA(1,K)
0310  WRITE(14,100)K-1,UU
0313 WRITE(17,100)K-1,UU
0320 13 CONTINUE
0325  RMS=SQRT(SUM/NUM)
0326  PRINT,"RMS OF H(L)=",RMS
0330  200 FORMAT(V)
0335 600 FORMAT(V)
0337 100 FORMAT(V)
0340 400 FORMAT(V)
0342 700 FORMAT(V)
0345 900 FORMAT(I3,3X,F7.4,3X,F7.4,3X,F7.4,3X,F7.4,3X,F7.4,3X,F7.4,3X,F7.4,3X,F7.4,3X,F7.4,3X,F7.3,3X,F7.4,1X,F7.4)
0350  RETURN
```

```
L DIECO

9480        SUBROUTINE EMISSN(TEMP,SAL,FREQ,THETA,  DIECO,RH,RV,
9490       &        R2,EMISS)
9500*
9510*       PURPOSE
9520*
9530*        1. THE EMISSN ROUTINE CALCULATES THE DIELECTRIC
9540*           CONSTANT OF SEA WATER AT ANY FREQUENCY IN
9550*           THE MICROWAVE BAND USING THE DEBYE EXPRESSION
9560*           (DEBYE,P., 'POLAR MOLECULES', J.CHEM. PHYS.,
9570*           VOL. 9, 1941).  THE COEFFICIENTS OF THIS
9580*           EXPRESSION ARE FROM THE MOST RECENT EMPIRICAL
9590*           MODELING (MY BUDDIES) L. KLEIN AND C. SWIFT
9600*           (KLEIN,L.A, C.T. SWIFT,  AN IMPROVED
9610*           MODEL FOR THE DIELECTRIC CONSTANT OF SEA
9620*           WATER AT MICROWAVE FREQUENCIES', IEEE
9630*           TRANS. ANTENNAS AND PROPAGAT., VOL. AP-25(1),1971).
9640*
9650*        2. THE FRESNEL REFLECTION COEFFICIENTS ARE
9660*           CALCULATED USING METHOD BY STRATTON
9670*           (STRATTON,J.A, ELECTROMAGNETIC THEORY,
9680*           MC GRAW-HILL BOOK CO., 1941)
9690*
9700*        3. THE POWER REFLECTION COEFFICIENTS AND
9710*           EMISSIVITY ARE DETERMINED(MANUAL OF REMOTE
9720*           SENSING, AMER. SOC. OF PHOTOGRAMMETRY, CHAPTER 9).
9730*
9740*       INPUT ARGUMENTS
9750*
9760*           TEMP          *       SEA SURFACE TEMPERATURE, KELVIN.
9770*           SAL           *       SALINITY, O/OO.
9780*           FREQ          *       FREQUENCY,GHZ.
9790*           THETA         *       NORMAL INCIDENCE ANGLE, DEGREES.
9800*
9810*       OUTPUT ARGUMENTS
9820*
9830*           DIECO         *       DIELECTRIC CONSTANT (COMPLEX).
9840*           RH,RV         *       FRESNEL REFLECTION COEFFICENTS,
9850*                         *       H- AND V- POLARIZATIONS.
9860*           R2            *       POWER REFLECTION COEFFICENT,
9870*                         *       1 = H-POL, 2 = V-POL.
9880*           EMISS         *       EMISSIVITY, = 1,H-POL.
9890*                         *                   = 2, V-POL.
9900*
9910*
9920*       CALCULATION OF DIELECTRIC CONSTANT
9930*
9940        DIMENSION R2(2),EMISS(2)
9950*
9960*                     COMPLEX VARIABLES
9970*
9980        COMPLEX DIECO,RV, RH
9990*                     COMPLEX DUMMY VARIABLES
10000*
10010       COMPLEX DUMMY1,DUMMY2,TEP1,TEP2,COST,SQ
10020*
10030*                      DEFINE DIELCTRIC CONSTANT AT INFINITE FREQUENCY,EFIN.
10040*                      AND PERMITIVITY OF FREE SPACE,E0.
10050*
10060       DATA EFIN,E0/4.9, 8.854E-12/
10070*
10080       DATA PI/3.14159/
10090*
```

DIECO (cont'd.)

```
10090*
10100*                        INITIALIZE CERTAIN VARIABLES
10110*
10120        T = TEMP - 273.16
10130       DELTA = 25.0 - T
10140        W = 2. * PI * FREQ * 1.0 E09
10150*
10160*                        EXPRESSION FOR IONIC CONDUCTIVITY OF SEA WATER,COND
10170*
10180        S = SAL * (0.182521 - 1.46192E-3*SAL + 2.09324E-5*SAL**2
10190       &        -1.28205E-7*SAL**3)
10200        B = 2.033E-2 + 1.266E-4*DELTA + 2.464E-6*DELTA**2
10210       &        -SAL * (1.849E-5 - 2.551E-7*DELTA + 2.551E-8*DELTA**2)
10220        COND = S *EXP(-DELTA*B)
10230*
10240*                        EXPRESSION FOR THE STATIC DIELECTRIC CONSTANT,ES.
10250*
10260        F = 87.134 - 1.949E-1*T - 1.276E-2*T**2
10270       &        +2.491E-4*T**3
10280        A = 1.0 +1.613E-5*SAL*T - 3.656E-3*SAL
10290       &        +3.21E-5*SAL**2 - 4.232E-7*SAL**3
10300        ES = F * A
10310*
10320*                        RELAXATION TIME, TAU
10330*
10340        TT = 1.768E-11 - 6.086E-13*T + 1.104E-14*T**2
10350       &        -8.111E-17*T**3
10360        BT = 1. + 2.282E-5*SAL*T - 7.638E-4*SAL
10370       &        -7.760E-6*SAL**2 + 1.105E-8*SAL**3
10380        TAU = TT / BT
10390*
10400*                        SOLVE DEBYE EXPRESSION FOR DIELECTRIC CONSTANT,DIECO.
10410*
10420        DUMMY1 = CMPLX(1.0, W*TAU)
10430        DUMMY2 = CMPLX(0.0,COND/(W*E0))
10440*
10450        TEP1 = CMPLX(EFIN,0.0)
10460        TEP2 = CMPLX(ES-EFIN, 0.0)
10470*
10480        DIECO = TEP1 + TEP2/DUMMY1 - DUMMY2
10490*
10500*                        CALCULATION OF FRESNEL REFLECTION COEFFICIENT,RH&RV
10510*
10520        COST = CMPLX( COS(THETA/57.296), 0.0)
10530        SQ = CSQRT(DIECO - CMPLX(SIN(THETA/57.296)**2, 0.0) )
10540        RH = (COST - SQ) / (COST + SQ)
10550        RV = (DIECO * COST - SQ) / (DIECO * COST + SQ)
10560*
10570*                        CALCULATE POWER REFLECTION COEFFICIENTS,R2(1=H,2=V)
10580*                        AND EMISSIVITY, EMISS(1=H,2=V).
10590*
10600        R2(1) = RH * CONJG(RH)
10610        R2(2) = RV * CONJG(RV)
10620        DO 10 I=1,2
10630        EMISS(I) = 1. - R2(I)
10640 10     CONTINUE
10650*
10660        RETURN
10670        END
```

L XXFFCC

```
 SUBROUTINE XFUNC(FC,S,Q,TATA,XATA,ZCOS,ZSIN,FCOS,FSIN,FINT)
 INTEGER S,Q,FC
C PARAMETER S=128,Q=64
  REAL TATA(S),XATA(S),ZCOS(Q,S),ZSIN(Q,S),FINT(2,Q)
  REAL FCOS(Q,S),FSIN(Q,S)
  REAL MUN
  PI=4.*ATAN(1.)
  G=9.81
  A0=0.0
   NUM=S
  MUN=1./FLOAT(NUM)
 W=2.*PI*MUN
 PRINT,W
 PRINT,NUM,FC,S,Q
 REWIND FC
   DO 12 K=1,NUM
C   AA=COS(W*1.*K)
C   AA=SIN(2.*PI*.17*K)+COS(2.2*K)+SIN(2.6*K)
  READ(FC,1000)VV,AA
   TATA(K)=AA
c PRINT,J
   A0=A0+TATA(K)*MUN
  XATA(K)=0.0
 12 CONTINUE
  D0 15 K=1,NUM/2
   FINT(1,K)=0.0
   FINT(2,K)=0.0
 15 CONTINUE
  REWIND 19
C print,"00000009090"
     D0 10 K=1,NUM/2
C   V=W*K*K/G
C   V=FLOAT(K)
         DO 20 J=1,NUM
C   U=FLOAT(J)
C   U=1.5*J
C      FCOS(K,J)=COS(W*V*U)
C      FSIN(K,J)=SIN(W*V*U)
C      ZCOS(K,J)=COS(W*K*J)
C     ZSIN(K,J)=SIN(W*K*J)
    READ(19,1000)AA,BB,CC,DD
    FCOS(K,J)=AA
    FSIN(K,J)=BB
    ZCOS(K,J)=CC
    ZSIN(K,J)=DD
C WRITE(06,1000)K,J
    20 CONTINUE
 10  CONTINUE
C print,"999989898989"
    DO 30 K=1,NUM/2
C
      DO 40 J=1,NUM
     FINT(1,K)=FINT(1,K)+MUN*TATA(J)*ZCOS(K,J)
    FINT(2,K)=FINT(2,K)+MUN*TATA(J)*ZSIN(K,J)
     40 CONTINUE
C   WRITE(16,200)K,FINT(1,K),FINT(2,K)
 30 CONTINUE
C
   DO 50 L=1,NUM
C
       DO 60 J=1,(NUM-2)/2
      XATA(L)=XATA(L)+2.*FINT(1,J)*FCOS(J,L)+2.*FINT(2,J)*FSIN(J,L)
C PRINT,CATA(L)
C   print,fcos(j,l),fsin(j,l)
  60 CONTINUE
C PRINT,"!!!!!!!!!!!!!!!!!!!...OK"
C PRINT,CATA(L)
  XATA(L)=XATA(L)+A0
 XATA(L)=XATA(L)+FINT(1,(NUM/2))*FCOS((NUM/2),L)
 XATA(L)=XATA(L)+FINT(2,(NUM/2))*FSIN((NUM/2),L)
C
   50 CONTINUE
C
```

XXFFCC (cont'd.)

```
0696
695   PRINT,"AO=",AO
0697 REWIND FC
0700   DO 70 L=1,NUM
0701C   U=4.+16.*L/FLOAT(NUM)
0702   U=30.+3.*L
0703C  READ(12,100)J,X,Z,GG,HH,UU,RR
0704C   READ(09,1000)U,Y
0705C   Y=SIN(4.*PI*PI*.17*.17*U/6)+COS(4.84*U/6)+SIN(6.76*U/6)
0706C   Y=COS(1.44*L)
0707C    Y=COS(U*U*L)
0708C   Y=DATA(L)
0709C    DIF=Y-XATA(L)
0710C  WRITE(15,100)U,DATA(L),Y,XATA(L),DIF,FINT(1,L),FINT(2,L)
0715C   WRITE(17,300)L,DATA(L),Y,CATA(L),GG,DIF,HH,ABS(CATA(L)-GG)
0717   WRITE(FC,1000)U,XATA(L)
0718  IF(FC.EQ.14)   WRITE(18,1000)U,XATA(L)
0720 70 CONTINUE
0725 100 FORMAT(F7.3,4X,F9.5,4X,F9.5,4X,F9.5,4X,F9.5,4X,F9.5,8X,F9.7,4X,F9.7)
0728 300 FORMAT(I3,4X,F9.5,4X,F9.5,4X,F9.5,4X,F9.5,4X,F9.5,4X,F9.5,4X,F9.5,4X,F9.5)
0727 200 FORMAT(I3,4X,F9.5,4X,F9.5)
0729 1000 FORMAT(V)
0730   RETURN
0735C STOP
0740  END
*
```

```
L PWRSK

0010 SUBROUTINE SK(UO,X,SS)
0020 REAL SS,UO,X
0030     IF((8.LE.UO).AND.(UO.LE.10.)) SS=-4.6115*ALOG10(X)+ALOG10(.1782)
0040     IF((18.LE.UO).AND.(UO.LE.22.)) SS=-2.0904*ALOG10(X)+ALOG10(.0460)
0050C
0060C
0070C
0080C
0090C
0100    RETURN
0110    END
```

```
 L FRCFGN

0290    PARAMETER S=128,B=64
0300 REAL ZCOS(B,S),ZSIN(B,S),FCOS(B,S),FSIN(B,S)
0320  REAL NUM
0330 PI=4.*ATAN(1.)
0335  G=9.81
0340    NUM=S
0350  NUM=1./FLOAT(NUM)
0355 W=2.*PI*NUM
0356 PRINT,W
0410      DO 10 K=1,NUM/2
0415   V=W*K*K/G
0417C    V=FLOAT(K)
0420         DO 20 J=1,NUM
0427C    U=FLOAT(J)
0428  U=30.*3.*J
0430       FCOS(K,J)=COS(U*V*J)
0440       FSIN(K,J)=SIN(U*V*U)
0444       ZCOS(K,J)=COS(U*K*J)
0446       ZSIN(K,J)=SIN(U*K*J)
0447    WRITE(19,1000)FCOS(K,J),FSIN(K,J),ZCOS(K,J),ZSIN(K,J)
0450    20 CONTINUE
0460 10  CONTINUE
0490 1000 FORMAT(4)
500  STOP
0510  END
```

```
L MMOOTT
0005 SUBROUTINE MMOUT(FC7,S,RATA)
0010 INTEGER FC7,S
0011 REAL J,RATA(S)
0012 num=s
0015 SUM=0.0
0018 REWIND FC7
0020 de 10 k=1,num
0030 READ(FC7,100)J,BB
0040   SUM=SUM+BB
0075 10 CONTINUE
0077 v=sum/float(sum)
0078 PRINT,"MEAN=",V
0079 REWIND FC7
0080 100 FORMAT(V)
0082 DO 12 K=1,NUM
0084 READ(FC7,100)J,BB
0086 RATA(K)=BB-V
0088 12 CONTINUE
0089 REWIND FC7
0090 DO 16 K=1,NUM
0092 WRITE(FC7,100)K-1,RATA(K)
0094 16 CONTINUE
0096 RETURN
0100 END
```

```
L ZZGGNN
0010 SUBROUTINE ZRGEN(FC8,S,CATA)
0020 INTEGER FC8,S
0025 REAL CATA(S)
0027 NUM=S
0030 de 10 k=1,NUM
0040 CATA(K)=0.0
0050 10 CONTINUE
0055 REWIND FC8
0060 DO 12 K=1,NUM/2
0070 READ(FC8,100)J,BB
0080 CATA(K)=BB
0090 12 CONTINUE
0092C
0093 REWIND FC8
0095 DO 14 K=1,NUM
0100 WRITE(FC8,100)K-1,CATA(K)
0105 14 CONTINUE
0110 100 format(v)
0120 RETURN
0130 end
```

```
*L CCS3L3


10 SUBROUTINE CRSSLL(FC2,FC3,FC4,FC5,FC6,FC7,FC8,FC9,S,U,DATA,EATA,CRSTSL
20&,CRSOSU,CRSTSU,CRSOSL,CRSOSU,CRSBSL,CROSS,CRSLSU,CRSUU,CRSSS,CRSMM,ZATA,
30&SATA,DUM,QATA,LON,
31&NGT,SLP,SGO,SGT,TMOD)
32C PRINT,"LON",LON
40  INTEGER FC2,FC3,FC4,FC5,FC6,FC7,FC8,FC9,S,U
50   REAL DATA(2,S),EATA(2,S)
60  INTEGER DUM,LON,LAM
70  REAL CRSTSL(U),CRSOSU(U),CRSTSU(U),CRSOSL(U),CRSBSU(U),CRSBSL(U)
80  REAL CROSS(U),CRSLSU(U),CRSUU(U),CRSSS(U),CRSMM(U)
90  REAL ZATA(2,S),SATA(2,U),QATA(U),DUM(U)
100   LAM=LON
110 REWIND FC2
120 REWIND FC3
130 REWIND FC4
140 REWIND FC5
150 REWIND FC6
163    NUM=S
170    QUM=U
180 PRINT,"LON=",LON,"NUM=",NUM,"QUM=",QUM
190   DO 34 K=1,NUM
200   READ(12,100)J,WHT
210    DATA(1,K)=WHT
220    EATA(1,K)=WHT
230   DATA(2,K)=0.0
240   EATA(2,K)=0.0
242   NGT=NGT+WHT*WHT
245 34 CONTINUE
250C 34 WRITE(18,100)DATA(1,K),EATA(1,K)
260 REWIND 12
270 CALL COROL(DATA,EATA,CROSS,ZATA,SATA,QATA,DUM,NUM,QUM)
280 DO 35 K=1,QUM
290   CRSUU(K)=CRSUU(K)+CROSS(K)
300 35 CONTINUE
0302 DO 334 K=1,NUM
0304 READ(14,100)J,DIFF
0306 DATA(1,K)=DIFF
0307 EATA(1,K)=DIFF
0308 DATA(2,K)=0.0
0309 EATA(2,K)=0.0
0310 TMOD=TMOD+DIFF*DIFF
0311 334  CONTINUE
0312 REWIND 14
0313   CALL COROL(DATA,EATA,CROSS,ZATA,SATA,QATA,DUM,NUM,QUM)
0315 DO    335 K=1,QUM
0316 CRSMM(K)=CRSMM(K)+CROSS(K)
0317 335 CONTINUE
0319 REWIND 11
320 DO 10 K=1,NUM
330    READ(11,100)J,SIGT
340    READ(13,100)J,SLOP
350    DATA(1,K)=SIGT
360    EATA(1,K)=SLOP
370    DATA(2,K)=0.0
380    EATA(2,K)=0.0
0384   SGT=SGT+SIGT*SIGT
0388   SLP=SLP+SLOP*SLOP
390   10 CONTINUE
400   CALL COROL(DATA,EATA,CROSS,ZATA,SATA,QATA,DUM,NUM,QUM)
410   DO 13 K=1,QUM
440 13 CRSTSL(K)=CRSTSL(K)+CROSS(K)
0445 REWIND 11
450 REWIND 13
460 DO 29 K=1,NUM
470 READ(13,100)J,SLOP
480 DATA(1,K)=SLOP
490 EATA(1,K)=SLOP
500 DATA(2,K)=0.0
510 EATA(2,K)=0.0
520 29 CONTINUE
530   CALL COROL(DATA,EATA,CROSS,ZATA,SATA,QATA,DUM,NUM,QUM)
```

CCS3L3 (cont'd.)

```
540   DO 49 K=1,QUM
550 49 CRSSS(K)=CRSSS(K)+CROSS(K)
560 REWIND 13
570C
580   DO 88 K=1,NUM
590   READ(13,100)J,SLOP
600    READ(12,100)J,UNT
610    DATA(1,K)=SLOP
620    EATA(1,K)=UNT
630    DATA(2,K)=0.0
640    EATA(2,K)=0.0
650 88 CONTINUE
660    CALL COROL(DATA,EATA,CROSS,ZATA,SATA,QATA,NUM,NUM,QUM)
670    DO 99 K=1,QUM
680 99 CRSLSU(K)=CRSLSU(K)+CROSS(K)
690 REWIND 10
700 REWIND 12
710 DO 14 K=1,NUM
720 READ(10,100)J,SIGO
730 READ(12,100)J,UNT
740 DATA(1,K)=SIGO
750    EATA(1,K)=UNT
760    DATA(2,K)=0.0
770    EATA(2,K)=0.0
0775    SGO=SGO+SIGO*SIGO
780 14 CONTINUE
790C
800    CALL COROL(DATA,EATA,CROSS,ZATA,SATA,QATA,NUM,NUM,QUM)
810C
820     DO 15 K=1,QUM
830 15 CRSOSU(K)=CRSOSU(K)+CROSS(K)
840C
850 REWIND 11
860 REWIND 12
870C
880 DO 16 K=1,NUM
890 READ(11,100)J,SIGT
900    READ(12,100)J,UNT
910     DATA(1,K)=SIGT
920    EATA(1,K)=UNT
930    EATA(2,K)=0.0
940     DATA(2,K)=0.0
950 16 CONTINUE
960C
970     CALL COROL(DATA,EATA,CROSS,ZATA,SATA,QATA,NUM,NUM,QUM)
980C
990 DO 17 K=1,QUM
1000 17 CRSTSU(K)=CRSTSU(K)+CROSS(K)
1010C
1020REWIND 11
1030 REWIND 12
1040 REWIND 10
1050 REWIND 13
1060 DO 18 K=1,NUM
1070READ(10,100)J,SIGO
1080 READ(13,100)J,SLOP
1090    DATA(1,K)=SIGO
1100    EATA(1,K)=SLOP
1110    DATA(2,K)=0.0
1120    EATA(2,K)=0.0
1130 18 CONTINUE
1140C
1150      CALL COROL(DATA,EATA,CROSS,ZATA,SATA,QATA,NUM,NUM,QUM)
1160C
```

CCS3L3 (cont'd.)

```
540   DO 49 K=1,SUM
550 49 CRSSS(K)=CRSSS(K)+CROSS(K)
560 REWIND 13
570C
580   DO 88 K=1,NUM
590   READ(13,100)J,SLOP
600   READ(12,100)J,UNT
610   DATA(1,K)=SLOP
620   EATA(1,K)=UNT
630   DATA(2,K)=0.0
640   EATA(2,K)=0.0
650 88 CONTINUE
660   CALL COROL(DATA,EATA,CROSS,ZATA,SATA,QATA,NUM,NUM,SUM)
670   DO 99 K=1,SUM
680 99 CRSLSW(K)=CRSLSW(K)+CROSS(K)
690 REWIND 10
700 REWIND 12
710 DO 14 K=1,NUM
720 READ(10,100)J,SIGO
730 READ(12,100)J,UNT
740 DATA(1,K)=SIGO
750   EATA(1,K)=UNT
760   DATA(2,K)=0.0
770   EATA(2,K)=0.0
0775   SG0=SG0+SIG0*SIGO
780 14 CONTINUE
790C
800   CALL COROL(DATA,EATA,CROSS,ZATA,SATA,QATA,NUM,NUM,SUM)
810C
820    DO 15 K=1,SUM
830 15 CRSOSW(K)=CRSOSW(K)+CROSS(K)
840C
850 REWIND 11
860 REWIND 12
870C
880 DO 16 K=1,NUM
890 READ(11,100)J,SIGT
900   READ(12,100)J,UNT
910    DATA(1,K)=SIGT
920   EATA(1,K)=UNT
930   EATA(2,K)=0.0
940    DATA(2,K)=0.0
950 16 CONTINUE
960C
970    CALL COROL(DATA,EATA,CROSS,ZATA,SATA,QATA,SUM,NUM,SUM)
980C
990 DO 17 K=1,SUM
1000 17 CRSTSW(K)=CRSTSW(K)+CROSS(K)
1010C
1020REWIND 11
1030 REWIND 12
1040 REWIND 10
1050 REWIND 13
1060 DO 18 K=1,NUM
1070READ(10,100)J,SIGO
1080 READ(13,100)J,SLOP
1090   DATA(1,K)=SIGO
1100   EATA(1,K)=SLOP
1110   DATA(2,K)=0.0
1120   EATA(2,K)=0.0
1130 18 CONTINUE
1140C
1150     CALL COROL(DATA,EATA,CROSS,ZATA,SATA,QATA,SUM,NUM,SUM)
1160C
```

```
L COL3T3


10  SUBROUTINE COROL(DATA,EATA,CROSS,ZATA,SATA,QATA,DUM,NUM,QUM)
30 INTEGER QUM,NUM
33 LUM=NUM
35 JUM=QUM
40  REAL NUM
45   REAL SATA(2,QUM)
50  REAL ZATA(2,NUM),DATA(2,NUM),EATA(2,NUM),CROSS(QUM)
60  REAL QATA(QUM),DUM(QUM)
70  NUM=1./FLOAT(NUM)
80  DO 12      K=1,QUM
82  SATA(1,K)=0.0
84  SATA(2,K)=0.0
90 12 CONTINUE
100C
102 DO 880 K=1,NUM
104C WRITE(19,1900)DATA(1,K),DATA(2,K),EATA(1,K),EATA(2,K)
106 880 CONTINUE
110   CALL FOURT(DATA,LUM,1,-1,0,0)
120   CALL FOURT(EATA,LUM,1,-1,0,0)
130C
140 DO 10 K=1,NUM
150  ZATA(1,K)=(DATA(1,K)*EATA(1,K)+DATA(2,K)*EATA(2,K))/LUM
160   ZATA(2,K)=(DATA(2,K)*EATA(1,K)-DATA(1,K)*EATA(2,K))/LUM
170 10 CONTINUE
180  DO 112 K=1,NUM
184  CROSS(K)=ZATA(1,K)
188  CROSS(NUM+K)=ZATA(2,K)
200 112 CONTINUE
210 RETURN
220 END
```

```
L CCA3G:

10  SUBROUTINE CRSLIN(DATA,EATA,CROSS,ZATA,SATA,QATA,QUM,NUM,QUM)
30 INTEGER QUM,NUM
33 LUM=NUM
35 JUM=QUM
40  REAL MUN
45   REAL SATA(2,QUM)
50  REAL ZATA(2,NUM),DATA(2,NUM),EATA(2,NUM),CROSS(QUM)
60  REAL QATA(QUM),DUM(QUM)
63C PRINT,"NUM=",NUM
70  MUN=1./FLOAT(NUM)
75  P=.33333333
80  DO 12     K=1,QUM
82  SATA(1,K)=0.0
84  SATA(2,K)=0.0
90 12 CONTINUE
92 DO 10 K=1,NUM
94  ZATA(1,K)=CROSS(K)
96  ZATA(2,K)=CROSS(NUM+K)
98 10 CONTINUE
100 DO 23 K=3,(NUM/2)-2
102  ZATA(1,K)=P*(P*(ZATA(1,K-2)+ZATA(1,K+2))+ZATA(1,K)+2.*P*(ZATA(1,K-1)
103&+ZATA(1,K+1)))
104  ZATA(2,K)=P*(P*(ZATA(2,K-2)+ZATA(2,K+2))+ZATA(2,K)+2.*P*(ZATA(2,K-1)
105&+ZATA(2,K+1)))
107 23 CONTINUE
109  ZATA(1,1)=.5*(ZATA(1,1)+P*ZATA(1,3)+2.*P*ZATA(1,2))
110  ZATA(2,1)=.5*(ZATA(2,1)+P*ZATA(2,3)+2.*P*ZATA(2,2))
111  ZATA(1,2)=(3./8.)*(P*ZATA(1,4)+ZATA(1,2)+2.*P*(ZATA(1,1)+ZATA(1,3)))
112  ZATA(2,2)=(3./8.)*(P*ZATA(2,4)+ZATA(2,2)+2.*P*(ZATA(2,1)+ZATA(2,3)))
114  ZATA(1,(NUM/2))=.5*(ZATA(1,(NUM/2))+P*ZATA(1,(NUM/2)-2)+2.*P*ZATA(
115&1,(NUM/2)-1))
117  ZATA(2,(NUM/2))=.5*(ZATA(2,(NUM/2))+P*ZATA(2,(NUM/2)-2)+2.*P*ZATA(
118&2,(NUM/2)-1))
120 ZATA(1,(NUM/2)-1)=(3./8.)*(ZATA(1,(NUM/2)-1)+P*ZATA(1,(NUM/2)-3)+2.*P*(ZATA
122&(1,(NUM/2)-2)+ZATA(1,(NUM/2))))
124 ZATA(2,(NUM/2)-1)=(3./8.)*(ZATA(2,(NUM/2)-1)+P*ZATA(2,(NUM/2)-3)+2.*P*(ZATA
126&(2,(NUM/2)-2)+ZATA(2,(NUM/2))))
130 DO 156 K=1,NUM/2
132 ZATA(1,K+(NUM/2))=ZATA(1,K)
134 ZATA(2,K+(NUM/2))=-ZATA(2,K)
136 156 CONTINUE
172 DO 43 K=1,NUM/2
174  SATA(1,K)=ZATA(1,K)
176  SATA(1,QUM+1-K)=ZATA(1,NUM+1-K)
178  SATA(2,QUM+1-K)=ZATA(2,NUM+1-K)
180  SATA(2,K)=ZATA(2,K)
182  43 CONTINUE
240  CALL FOURT(SATA,JUM,1,1,1,0)
250 DO 15 K=1,QUM
300 15 DUM(K)=SATA(1,K)
310 100 FORMAT(V)
320 DO 16 K=1,QUM/2
330 CROSS(K)=DUM(K+(QUM/2))
340 CROSS(QUM/2+K)=DUM(K)
350 16 CONTINUE
360 RETURN
370  END
*
```

```
L SFCLOUT

0010 PARAMETER NUM=128,QQ=.16666667
0015C  PARAMETER TRSHOLD=-10.0
0020 REAL CATA(NUM),EATA(NUM),DATA(NUM),ZATA(NUM)
0025 REAL QATA(NUM)
0030 INTEGER SATA(NUM)
0032 INTEGER AA
0033 DO 78 J=1,5
0034  SUMS=0.0
0036  SUMP=0.0
0037  SUMST=0.0
0038  SUMPT=0.0
0039 SUMPT=0.0
0041 REWIND 30
0042  DO 56 L=1,NUM
0044  READ(40,100)AA,BB,CC,DD
0046  WRITE(30,100)AA,BB,CC,DD
0048 56 CONTINUE
0049 REWIND 30
0050  DO 10 K=1,NUM
0060  READ(30,100)SATA(K),CATA(K),EATA(K),DATA(K)
0070  ZATA(K)=DATA(K)
0075  QATA(K)=EATA(K)
0077  SUMS=SUMS+10.*ALOG10(DATA(K))
0080 10 CONTINUE
0090  TRSHOLD=(SUMS/FLOAT(NUM))+6.
0095  SUMS=0.0
0100  DO 20 K=1,NUM
0110  IF(10.*ALOG10(DATA(K)).LT.TRSHOLD) GO TO 20
0120 W1=0.0
0125  W2=0.0
0130 W4=0.0
0135 W5=0.0
0136 IF(K.EQ.1) GO TO 344
0140 IF(10.*ALOG10(DATA(K-1)).LT.TRSHOLD)   W2=2.*QQ
0145  IF(K.EQ.2)   GO TO 344
0150 IF(10.*ALOG10(DATA(K-2)).LT.TRSHOLD)    W1=QQ
0153  IF(K.EQ.NUM) GO TO 554
0154 344 CONTINUE
0155 IF(10.*ALOG10(DATA(K+1)).LT.TRSHOLD)    W4=2.*QQ
0163  IF(K.EQ.NUM-1) GO TO 554
0160 IF(10.*ALOG10(DATA(K+2)).LT.TRSHOLD)    W5=QQ
0165 554 CONTINUE
0170   WW=W1+W2+W4+W5
0175  IF(WW.EQ.0.0)   PRINT,K
0180   DATA(K)=(W1*DATA(K-2)+W2*DATA(K-1)+W4*DATA(K+1)+W5*DATA(K+2))/WW
0190  EATA(K)=(W1*EATA(K-2)+W2*EATA(K-1)+W4*EATA(K+1)+W5*EATA(K+2))/WW
0200IF(DATA(K).NE.ZATA(K))WRITE(31,100)K,10.*ALOG10(ZATA(K)),10.*ALOG10(DATA(K))
0203$,10.*ALOG10(QATA(K)),10.*ALOG10(EATA(K)),TRSHOLD
0210 20 CONTINUE
0212  DO 45 K=1,NUM
0214 SUMS=SUMS+ZATA(K)
0215 SUMP=SUMP+QATA(K)
0216 SUMST=SUMST+DATA(K)
0217 SUMPT=SUMPT+EATA(K)
0218 45 CONTINUE
0219 SUMS=10.*ALOG10(SUMS/FLOAT(NUM))
0221 SUMP=10.*ALOG10(SUMP/FLOAT(NUM))
0222 SUMST=10.*ALOG10(SUMST/FLOAT(NUM))
0224 SUMPT=10.*ALOG10(SUMPT/FLOAT(NUM))
0225 PRINT,"TRSHOLD",TRSHOLD,"SUMS",SUMS,"SUMP",SUMP,"SUMST",SUMST,"SUMPT",SUMPT
0230  DO 30 K=1,NUM
0240 WRITE(35,100)SATA(K),CATA(K),EATA(K),DATA(K)
0245 WRITE(34,100)K,DATA(K)
0250 30 CONTINUE
0255 WRITE(21,100)J,TRSHOLD
0260 78 CONTINUE
0260 100 FORMAT(V)
0270  STOP
0280  END
*
```

```
*L MDTRFNC


 08
0010 INTEGER D,F,RAW
0020 INTEGER NUM,AVE
0030 PARAMETER V=128,U=128
0040 PI=3.141593
0050 Q=.33333
0060 NUM=V
0070 PARAMETER S=1280
0080 REAL CRH(V),NORM(V)
0090 DIMENSION ERH(V),AVRFUN(V)
0100 DIMENSION DATA(2,V),EATA(2,V)
0110 DIMENSION BULK(2,S)
0120 DIMENSION AVCRS(2,V)
130 DIMENSION PURSPEC(V),PWS(V),GMAS(V),CROSPUR(V),FI(V)
0140 DIMENSION PUSPEC(V),RFS(V),CHRENCE(V),FREQ(V)
0150 DIMENSION GMASPEC(V),CROSPEC(2,V),RFUNC(2,V),RFSPEC(V)
0160 DIMENSION AVRFUNC(U),AVFRQ(U),AVFI(U),AVPUR(U),AVGMA(U)
0170 DIMENSION AVCSPUR(U),AVCOH(U)
0180C
0190 PRINT, NUMBER OF PROCESSED TERMS TO BE AVERAGED/(AVE=?)'
0200 READ,AVPTIN
0210 AVE=AVPTIN
0220C
0230 SUMPT=0.0
0240C
0250 DO 111 K=1,S
0260 READ(14,900)J,UHT,PUT,SIG
0270 PRTN=PUT
0290 SUMPT=SUMPT+PRTN
0270 PRTN=PUT
0300 BULK(1,K)=PRTN
0310 BULK(2,K)=UHT
0320 111 CONTINUE
0330C
0340 DO 124 J=1,NUM
0350 AVRFUN(J)=0.0
0360 AVFI(J)=0.0
0370 AVPUR(J)=0.0
0380 AVGMA(J)=0.0
0390 AVCSPUR(J)=0.0
0400 AVCRS(1,J)=0.0
0410 AVCRS(2,J)=0.0
0420 AVCOH(J)=0.0
0430 124 CONTINUE
0440C
0450 AVEPT=SUMPT/S
0460 PRINT,AVEPT
0470 DO 115 F=1,AVE
480 RAW=(F-1)*NUM
0490C
0500 DO 113 K=1,NUM
0510 DATA(1,K)=BULK(1,(RAW+K))
0520 DATA(2,K)=0.0
0530 EATA(1,K)=BULK(2,(RAW+K))
0540 EATA(2,K)=0.0
0550 113 CONTINUE
0560C
0570 CALL FOURT(DATA,NUM,1,-1,0,0)
0580 CALL FOURT(EATA,NUM,1,-1,0,0)
0590C
0600 DO 122 I=1,NUM
0610 GMASPEC(I)=(EATA(1,I)*EATA(1,I)+EATA(2,I)*EATA(2,I))/NUM
0620 PURSPEC(I)=(DATA(1,I)*DATA(1,I)+DATA(2,I)*DATA(2,I))/NUM
0630 CROSPEC(1,I)=(DATA(1,I)*EATA(1,I)+DATA(2,I)*EATA(2,I))/NUM
0640 CROSPEC(2,I)=(DATA(2,I)*EATA(1,I)-DATA(1,I)*EATA(2,I))/NUM
0650 PUSPEC(I)=PURSPEC(I)
0660 122 CONTINUE
0670C
```

MDTRFNC (cont'd.)

```
0680 DO 211 J=1,NUM
0690 K=J-1
0700 FREQ(J)=FLOAT(K)/FLOAT(NUM)
710 211 CONTINUE
0720 DO 117 D=1,NUM
730 AVCRS(1,D)=AVCRS(1,D)+CROSPEC(1,D)
740 AVCRS(2,D)=AVCRS(2,D)+CROSPEC(2,D)
0750 AVPUR(D)=AVPUR(D)+PURSPEC(D)
0760 AVGMA(D)=AVGMA(D)+GMASPEC(D)
0770 117 CONTINUE
0780 115 CONTINUE
0790  PRINT,"0000790"
0800 AVRG=0.0
0810 DO 116 I=1,NUM
0820 AVFRQ(I)=FREQ(I)
0830 AVPUR(I)=AVPUR(I)/AVE
0840 AVGMA(I)=AVGMA(I)/AVE
0850 AVCRS(1,I)=AVCRS(1,I)/AVE
0860 AVCRS(2,I)=AVCRS(2,I)/AVE
0870 RFUNC(1,I)=AVCRS(1,I)/(AVEPT*AVGMA(I))
0880 RFUNC(2,I)=AVCRS(2,I)/(AVEPT*AVGMA(I))
0890C AVPI(I)=ATAN(RFUNC(2,I)/RFUNC(1,I))
0900 AVRFUN(I)=SQRT(RFUNC(1,I)*RFUNC(1,I)+RFUNC(2,I)*RFUNC(2,I))
0910 NORM(I)=(AVEPT*AVGMA(I))
0920 CRH(I)=SQRT(AVCRS(1,I)*AVCRS(1,I)+AVCRS(2,I)*AVCRS(2,I))
0930C ERH(I)=AVRFUN(I)*9.8/((2*PI*AVFRQ(I))**2)
0940 116 CONTINUE
0950C
0960 DO 203 J=1,NUM
0970 K=J
0980 WRITE(07,550)K,AVFRQ(J),CRH(J),NORM(J),AVGMA(J),AVEPT,AVRFUN(J)
0990 203 CONTINUE
1000 DO 210 I=4,(NUM-4)
1005 AVPUR(I)=Q*(Q*AVPUR(I-2)+2*Q*AVPUR(I-1)+AVPUR(I)
1006 3*2*Q*AVPUR(I+1)+Q*AVPUR(I+2))
1010 NORM(I)=Q*(Q*NORM(I-2)+2*Q*NORM(I-1)+NORM(I)+2*Q*NORM(I+1)+Q*NORM(I+2))
1020CRH(I)=Q*(Q*CRH(I-2)+2*Q*CRH(I-1)+CRH(I)+Q*2*CRH(I+1)+Q*CRH(I+2))
1030 210 CONTINUE
1031C
1032 DO 214 I=4,(NUM-4)
1034 AVRFUN(I)=CRH(I)/NORM(I)
1036 ERH(I)=AVRFUN(I)*9.8/((2*PI*AVFRQ(I))**2)
1038 214 CONTINUE
01040  DO 445 K=3,NUM-8
01041 AVRFUN(K)=Q*(Q*(AVRFUN(K-2)+AVRFUN(K+2))+AVRFUN(K)*2.+Q*(AVRFUN
01043$(K+1)+AVRFUN(K-1)))
01045 445  CONTINUE
1046 DO 213 I=4,(NUM-4)
10500 WRITE(08,559)I,AVFRQ(I),AVRFUN(I),ERH(I),CRH(I),1000*NORM(I),100000000*AVPUR(I)
01052 WRITE(36,100)AVFRQ(I),1000.*NORM(I)
01054 WRITE(37,100)AVFRQ(I),100000000.*AVPUR(I)
1060 213 CONTINUE
1065 DO 667 K=3,(NUM-8)
1065 WRITE(10,100)AVFRQ(K),AVRFUN(K)
01067 667 CONTINUE
1070 557 FORMAT(I2,1X,F5.3,4X,F9.3,4X,F9.2)
1070 558  FORMAT(V)
10700 559 FORMAT(I3,1X,F5.3,4X,F9.3,4X,F9.2,4X,F9.2,4X,F9.3,4X,F9.2)
10800 700 FORMAT(I4,4X,F9.3,4X,F9.7)
1082 900 FORMAT(/)
1100 100 FORMAT(V)
11 0 550 FORMAT(I2,4X,F5.3,4X,F9.3,4X,F9.3,4X,F9.3,4X,F9.3,4X,F7.3)
  0 570
  0 END
```

```
L COHERENC

0005 PARAMETER V=128,U=128,S=1280
0010 INTEGER B,F,RAW
0020 INTEGER NUM,AVE
0040 PI=3.141593
0050 Q=.33333
0060 NUM=V
0065 REAL NUM
0080 REAL CRH(V),NORM(V)
0090 DIMENSION ERH(V),AVRFUN(V)
0100 DIMENSION DATA(2,V),EATA(2,V)
0110 DIMENSION BULK(2,S)
0120 DIMENSION AVCRS(2,V)
130 DIMENSION PURSPEC(V),PUS(V),GMAS(V),CROSPUR(V),FI(V)
0140 DIMENSION PUSPEC(V),RFS(V),CHRENCE(V),FREQ(V)
0150 DIMENSION GMASPEC(V),CROSPEC(2,V),RFUNC(2,V),RFSPEC(V)
0160 DIMENSION AVRFUNC(U),AVFRQ(U),AVFI(U),AVPUR(U),AVGMA(U)
0170 DIMENSION AVCSPUR(U),AVCOH(U)
0180  NUN=1./FLOAT(NUM)
0190 PRINT,'NUMBER OF PROCESSED TERMS TO BE AVERAGED/(AVE=?)'
0200 READ,AVPTIN
0210 AVE=AVPTIN
0220   EVA=1./FLOAT(AVE)
0230 SUMPT=0.0
0240C
0250 DO 111 K=1,S
0260 READ(14,200)J,UHT,PUT,SIGO
0270 PRTN=PUT
0290 SUMPT=SUMPT+PRTN
0270 PRTN=PUT
0300 BULK(1,K)=PRTN
0310 BULK(2,K)=UHT
0320 111 CONTINUE
0330C
0340 DO 124 J=1,NUM
0350 AVRFUN(J)=0.0
0360 AVFI(J)=0.0
0370 AVPUR(J)=0.0
0380 AVGMA(J)=0.0
0390 AVCSPUR(J)=0.0
0400 AVCRS(1,J)=0.0
0410 AVCRS(2,J)=0.0
0420 AVCOH(J)=0.0
0430 124 CONTINUE
0440C
0450 AVEPT=SUMPT/S
0460C PRINT,AVEPT
0470 DO 115 F=1,AVE
480 RAW=(F-1)*NUM
0490C
0500 DO 113 K=1,NUM
0510 DATA(1,K)=BULK(1,(RAW+K))
0520 DATA(2,K)=0.0
0530 EATA(1,K)=BULK(2,(RAW+K))
0540 EATA(2,K)=0.0
0550 113 CONTINUE
0560C
0570 CALL FOURT(DATA,NUM,1,-1,0,0)
0580 CALL FOURT(EATA,NUM,1,-1,0,0)
0590C
0600 DO 122 I=1,NUM/2
0610 GMASPEC(I)=(EATA(1,I)*EATA(1,I)+EATA(2,I)*EATA(2,I))/NUM
0620 PURSPEC(I)=(DATA(1,I)*DATA(1,I)+DATA(2,I)*DATA(2,I))/NUM
0630 CROSPEC(1,I)=(DATA(1,I)*EATA(1,I)+DATA(2,I)*EATA(2,I))/NUM
0640 CROSPEC(2,I)=(DATA(2,I)*EATA(1,I)-DATA(1,I)*EATA(2,I))/NUM
0650 PUSPEC(I)=PURSPEC(I)
0660 122 CONTINUE
0670C
0680 DO 211 J=1,NUM
0690 K=J-1
0700 FREQ(K)=FLOAT(K)/FLOAT(NUM)
710 211 CONTINUE
```

COHERENC (cont'd.)

```
0720 DO 117 D=1,NUM/2
0730    IX=SQRT((CROSPEC(1,D))*(CROSPEC(1,D))+(CROSPEC(2,D))*(CROSPEC(2,D)))
0735  AVCRS(1,D)=AVCRS(1,D)+EVA*XI
0736 AVPUR(D)=AVPUR(D)+EVA*(PURSPEC(D))
0737 AVGMA(D)=AVGMA(D)+EVA*(GMASPEC(D))
0770 117 CONTINUE
0775 115 CONTINUE
0777 SUM=0.0
0780 DO 346 K=1,NUM/2
0785 AVCRS(2,K)=SQRT(AVGMA(K))*SQRT(AVPUR(K))
0790  CRH(K)=AVCRS(1,K)/AVCRS(2,K)
0793  CRH(K)=CRH(K)*CRH(K)*CRH(K)
0795C PRINT,FREQ(K),CRH(K),AVCRS(1,K),AVCRS(2,K)
0800 WRITE(08,100)FREQ(K),AVPUR(K),AVGMA(K),AVCRS(2,K),CRH(K)
0805  SUM=SUM+CRH(K)
0810 346 CONTINUE
0812 AVERAGE=SUM*2.*MUN
0814 SUM=0.0
0816 DO 989 K=1,NUM/2
0818 SUM=SUM+CRH(K)*CRH(K)-AVERAGE*AVERAGE
0820 989 CONTINUE
0822 STDEV=SUM*2.*MUN
0824 PRINT,'COHERENCE MEAN=',AVERAGE,'COHERENCE STAND. DEV.=',STDEV
0825 100 FORMAT(5(1X,F12.9))
0830 200 FORMAT(9)
0838 STOP
0840 END
*
```

```
*L FFT

      SUBROUTINE FOURT(DATA,NN,NDIM,ISIGN,IFORM,WORK)
C       bounded by 3*2**(-b)*sum(factor(j)**1.5), where b is the number
C       of bits in the floating point fraction and factor(j) are the
C       prime factors of ntot.
C
C       program by norman brenner from the basic program by charles
C       rader.  ralph alter suggested the idea for the digit reversal.
C       mit lincoln laboratory, august 1967.  this is the fastest and most
C       versatile version of the fft known to the author.  shorter pro-
C       grams four1 and four2 restrict dimension lengths to powers of two.
C       see-- ieee audio transactions (june 1967), special issue on fft.
C       see math explanation in pdp-15 documentation
C
C
C       the discrete fourier transform places three restrictions upon the
C       data.
C       1.  the number of input data and the number of transform values
C       must be the same.
C       2.  both the input data and the transform values must represent
C       equispaced points in their respective domains of time and
C       frequency.  calling these spacings deltat and deltaf, it must be
C       true that deltaf=2*pi/(nn(i)*deltat).  of course, deltat need not
C       be the same for every dimension.
C       3.  conceptually at least, the input data and the transform output
C       represent single cycles of periodic functions.
C
C       example 1.  three-dimensional forward fourier transform of a
C       complex array dimensioned 32 by 25 by 13 in fortran iv.
C       dimension data(32,25,13),work(50),nn(3)
C       complex data
C       data nn/32,25,13/
C       do 1 i=1,32
C       do 1 j=1,25
C       do 1 k=1,13
C 1     data(i,j,k)=complex value
C       call fourt(data,nn,3,-1,1,work)
C
C       example 2.  one-dimensional forward transform of a real array of
C       length 64 in fortran ii.
C       dimension data(2,64)
C       do 2 i=1,64
C       data(1,i)=real part
C 2     data(2,i)=0.
C       call fourt(data,64,1,-1,0,0)
C
      dimension data(1),nn(1),ifact(32),work(1)
      common /nam/ nam
      twopi=6.283185307
      if(ndim-1)920,1,1
    1  ntot=2
      do 2 idim=1,ndim
      if(nn(idim))920,920,2
    2  ntot=ntot*nn(idim)
C
C       main loop for each dimension
C
      np1=2
      do 910 idim=1,ndim
      n=nn(idim)
      np2=np1*n
      if(n-1)930,900,5
C
C       factor n
C       decompose input into n discrete time
C       samples, n/2 odd and n/2 even.  keep decomposing until
C       n/2 contains two samples.
C
```

FFT (cont'd.)

```
2010 5    n=n
2020      ntwo=np1
2030      if=1
2040      idiv=2
2050 10     iquot=n/idiv
2060      irem=n-idiv*iquot
2070      if(iquot-idiv)50,11,11
2080 11     if(irem)20,12,20
2090 12     ntwo=ntwo+ntwo
2100      n=iquot
2110      go to 10
2120 20     idiv=3
2130 30     iquot=n/idiv
2140      irem=n-idiv*iquot
2150      if(iquot-idiv)40,31,31
2160 31     if(irem)40,32,40
2170 32     ifact(if)=idiv
2180      if=if+1
2190      n=iquot
2200      go to 30
2210 40     idiv=idiv+2
2220      go to 30
2230 50     if(irem)60,51,60
2240 51     ntwo=ntwo+ntwo
2250      go to 70
2260 60     ifact(if)=n
2270c
2280c      separate four cases--
2290c         1. complex transform or real transform for the 4th, 5th,etc.
2300c            dimensions.
2310c         2. real transform for the 2nd or 3rd dimension.  method--
2320c            transform half the data, supplying the other half by con-
2330c            jugate symmetry.
2340c         3. real transform for the 1st dimension, n odd.  method--
2350c            transform half the data at each stage, supplying the other
2360c            half by conjugate symmetry.
2370c         4. real transform for the 1st dimension, n even.  method--
2380c            transform a complex array of length n/2 whose real parts
2390c            are the even numbered real values and whose imaginary parts
2400c            are the odd numbered real values.  separate and supply
2410c            the second half by conjugate symmetry.
2420c
2430 70     non2=np1*(np2/ntwo)
2440      icase=1
2450      if(idim-4)71,90,90
2460 71     if(ifac)72,72,90
2470 72     icase=2
2480      if(idim-1)73,73,90
2490 73     icase=3
2500      if(ntwo-np1)90,90,74
2510 74     icase=4
2520      ntwo=ntwo/2
2530      n=n/2
2540      np2=np2/2
2550      ntot=ntot/2
2560      i=3
2570      do 80 j=2,ntot
2580      data(j)=data(i)
2590 80     i=i+2
2600      if=np1
2610      if(icase-2)100,95,100
2620 95     i1rng=np0*(1+nprev/2)
2630c
2640c      shuffle on the factors of two in n.  as the shuffling
2650c      can be done by simple interchange, no working array is needed
2660c      decomposed input must be shuffled to take
2670c      care of bit reversal in output.
2680c      example     f0,f4,f2,f6,f1,f5,f3,f7 will
```

FFT (cont'd.)

```
2690c     produce coefficients g0,g1,g2,g3,g4,g5 ....gn
2700c     fourier can then be done in place without
2710c     additional core.
2720c
2730 100    if(ntwo-np1)600,600,110
2740 110    np2hf=np2/2
2750      j=1
2760      do 150 i2=1,np2,non2
2770      if(j-i2)120,130,130
2780 120    i1max=i2+non2-2
2790      do 125 i1=i2,i1max,2
2800      do 125 i3=i1,ntot,np2
2810      j3=j+i3-i2
2820      tempr=data(i3)
2830      tempi=data(i3+1)
2840      data(i3)=data(j3)
2850      data(i3+1)=data(j3+1)
2860      data(j3)=tempr
2870 125    data(j3+1)=tempi
2880 130    m=np2hf
2890 140    if(j-m)150,150,145
2900 145    j=j-m
2910      m=m/2
2920      if(m-non2)150,140,140
2930 150    j=j+m
2940c
2950c     main loop for factors of two.  perform fourier transforms of
2960c     length four, with one of length two if needed.  the twiddle factor
2970c     w=exp(isign*2*pi*sqrt(-1)*m/(4*mmax)).  check for w=isign*sqrt(-1)
2980c     and repeat for w=isign*sqrt(-1)*conjugate(w). note j=sqrt(-1)
2990c
3000      non2t=non2+non2
3010      ipar=ntwo/np1
3020 310    if(ipar-2)350,330,320
3030 320    ipar=ipar/4
3040      go to 310
3050 330    do 340 i1=1,i1rng,2
3060      do 340 j3=i1,non2,np1
3070      do 340 k1=j3,ntot,non2t
3080      k2=k1+non2
3090      tempr=data(k2)
3100      tempi=data(k2+1)
3110      data(k2)=data(k1)-tempr
3120      data(k2+1)=data(k1+1)-tempi
3130      data(k1)=data(k1)+tempr
3140 340    data(k1+1)=data(k1+1)+tempi
3150 350    mmax=non2
3160 360    if(mmax-np2hf)370,600,600
3170 370    lmax=max0(non2t,mmax/2)
3180      if(mmax-non2)405,405,380
3190 380    theta=-twopi*float(non2)/float(4*mmax)
3200      if(isign)400,390,390
3210 390    theta=-theta
3220 400    wr=cos(theta)
3230      wi=sin(theta)
3240      wstpr=-2.*wi*wi
3250      wstpi=2.*wr*wi
3260 405    do 570 l=non2,lmax,non2t
3270      m=1
3280      if(mmax-non2)420,420,410
3290 410    w2r=wr*wr-wi*wi
3300      w2i=2.*wr*wi
3310      w3r=w2r*wr-w2i*wi
3320      w3i=w2r*wi+w2i*wr
3330 420    do 530 i1=1,i1rng,2
3340      do 530 j3=i1,non2,np1
3350      kmin=j3+ipar*m
3360      if(mmax-non2)430,430,440
3370 430    kmin=j3
3380 440    kdif=ipar*mmax
```

FFT (cont'd.)

```
3390 430    kstep=4*kdif
3400        do 520 k1=kmin,ntot,kstep
3410        k2=k1+kdif
3420        k3=k2+kdif
3430        k4=k3+kdif
3440        if(nmax-non2)440,440,480
3450 440    u1r=data(k1)+data(k2)
3460        u1i=data(k1+1)+data(k2+1)
3470        u2r=data(k3)+data(k4)
3480        u2i=data(k3+1)+data(k4+1)
3490        u3r=data(k1)-data(k2)
3500        u3i=data(k1+1)-data(k2+1)
3510        if(isign)470,475,475
3520 470    u4r=data(k3+1)-data(k4+1)
3530        u4i=data(k4)-data(k3)
3540        go to 510
3550 475    u4r=data(k4+1)-data(k3+1)
3560        u4i=data(k3)-data(k4)
3570        go to 510
3580 480    t2r=w2r*data(k2)-w2i*data(k2+1)
3590        t2i=w2r*data(k2+1)+w2i*data(k2)
3600        t3r=wr*data(k3)-wi*data(k3+1)
3610        t3i=wr*data(k3+1)+wi*data(k3)
3620        t4r=w3r*data(k4)-w3i*data(k4+1)
3630        t4i=w3r*data(k4+1)+w3i*data(k4)
3640        u1r=data(k1)+t2r
3650        u1i=data(k1+1)+t2i
3660        u2r=t3r+t4r
3670        u2i=t3i+t4i
3680        u3r=data(k1)-t2r
3690        u3i=data(k1+1)-t2i
3700        if(isign)490,500,500
3710 490    u4r=t3i-t4i
3720        u4i=t4r-t3r
3730        go to 510
3740 500    u4r=t4i-t3i
3750        u4i=t3r-t4r
3760 510    data(k1)=u1r+u2r
3770        data(k1+1)=u1i+u2i
3780        data(k2)=u3r+u4r
3790        data(k2+1)=u3i+u4i
3800        data(k3)=u1r-u2r
3810        data(k3+1)=u1i-u2i
3820        data(k4)=u3r-u4r
3830 520    data(k4+1)=u3i-u4i
3840        kmin=4*(kmin-j3)+j3
3850        kdif=kstep
3860        if(kdif-np2)450,530,530
3870 530    continue
3880        m=nmax-m
3890        if(isign)540,550,550
3900 540    tempr=wr
3910        wr=-wi
3920        wi=-tempr
3930        go to 560
3940 550    tempr=wr
3950        wr=wi
3960        wi=tempr
3970 560    if(m-lmax)565,565,410
3980 565    tempr=wr
3990        wr=wr*wstpr-wi*wstpi+wr
4000 570    wi=wi*wstpr+tempr*wstpi+wi
4010        ipar=3-ipar
4020        nmax=nmax+nmax
4030        go to 360
4040c
4050c     main loop for factors not equal to two.  apply the twiddle factor
4060c     w=exp(isign*2*pi*sqrt(-1)*(j2-1)*(j1-j2)/(np2*ifp1)), then
4070c     perform a fourier transform of length ifact(if), making use of
4080c     conjugate symmetries.
4090c     see differences in math main computer documentation
4100c
```

FFT (cont'd.)

```
4110 600    if(ntwo-np2)605,700,700
4120 605    ifp1=np2
4130      if=1
4140      np1hf=np1/2
4150 610    ifp2=ifp1/ifact(if)
4160      j1rng=np2
4170      if(icase-3)612,611,612
4180 611    j1rng=(np2+ifp1)/2
4190      j2stp=np2/ifact(if)
4200      j1rg2=(j2stp+ifp2)/2
4210 612    j2min=1+ifp2
4220      if(ifp1-np2)615,640,640
4230 615    do 635 j2=j2min,ifp1,ifp2
4240      theta=-twopi*float(j2-1)/float(np2)
4250      if(isign)625,620,620
4260 620    theta=-theta
4270 625    sinth=sin(theta/2.)
4280      wstpr=-2.*sinth*sinth
4290      wstpi=sin(theta)
4300      wr=wstpr+1.
4310      wi=wstpi
4320      j1min=j2+ifp1
4330      do 635 j1=j1min,j1rng,ifp1
4340      i1max=j1+i1rng-2
4350      do 630 i1=j1,i1max,2
4360      do 630 i3=i1,ntot,np2
4370      j3max=i3+ifp2-np1
4380      do 630 j3=i3,j3max,np1
4390      tempr=data(j3)
4400      data(j3)=data(j3)*wr-data(j3+1)*wi
4410 630    data(j3+1)=tempr*wi+data(j3+1)*wr
4420      tempr=wr
4430      wr=wr*wstpr-wi*wstpi+wr
4440 635    wi=tempr*wstpi+wi*wstpr+wi
4450 640    theta=-twopi/float(ifact(if))
4460      if(isign)650,645,645
4470 645    theta=-theta
4480 650    sinth=sin(theta/2.)
4490      wstpr=-2.*sinth*sinth
4500      wstpi=sin(theta)
4510      kstep=2*n/ifact(if)
4520      krang=kstep*(ifact(if)/2)+1
4530      do 698 i1=1,i1rng,2
4540      do 698 i3=i1,ntot,np2
4550      do 690 kmin=1,krang,kstep
4560      j1max=i3+j1rng-ifp1
4570      do 680 j1=i3,j1max,ifp1
4580      j3max=j1+ifp2-np1
4590      do 680 j3=j1,j3max,np1
4600      j2max=j3+ifp1-ifp2
4610      k=kmin+(j3-j1+(j1-i3)/ifact(if))/np1hf
4620      if(kmin-1)655,655,665
4630 655    sumr=0.
4640      sumi=0.
4650      do 660 j2=j3,j2max,ifp2
4660      sumr=sumr+data(j2)
4670 660    sumi=sumi+data(j2+1)
4680      work(k)=sumr
4690      work(k+1)=sumi
4700      go to 680
4710 665    kconj=k+2*(n-kmin+1)
4720      j2=j2max
4730      sumr=data(j2)
4740      sumi=data(j2+1)
4750      oldsr=0.
4760      oldsi=0.
4770      j2=j2-ifp2
4780 670    tempr=sumr
```

FFT (cont'd.)

```
4790      tempi=sumi
4800      sumr=twowr*sumr-oldsr+data(j2)
4810      sumi=twowr*sumi-oldsi+data(j2+1)
4820      oldsr=tempr
4830      oldsi=tempi
4840      j2=j2-ifp2
4850      if(j2-j3)675,675,670
4860 675     tempr=wr*sumr-oldsr+data(j2)
4870      tempi=wi*sumi
4880      work(k)=tempr-tempi
4890      work(kconj)=tempr+tempi
4900      tempr=wr*sumi-oldsi+data(j2+1)
4910      tempi=wi*sumr
4920      work(k+1)=tempr+tempi
4930      work(kconj+1)=tempr-tempi
4940 680     continue
4950      if(kmin-1)685,685,686
4960 685     wr=wstpr+1.
4970      wi=wstpi
4980      go to 690
4990 686     tempr=wr
5000      wr=wr*wstpr-wi*wstpi+wr
5010      wi=tempr*wstpi+wi*wstpr+wi
5020 690     twowr=wr+wr
5030      if(icase-3)692,691,692
5040 691     if(ifp1-np2)695,692,692
5050 692     k=1
5060      i2max=i3+np2-np1
5070      do 693 i2=i3,i2max,np1
5080      data(i2)=work(k)
5090      data(i2+1)=work(k+1)
5100 693     k=k+2
5110      go to 698
5120c
5130c      complete a real transform in the 1st dimension, n odd, by con-
5140c      jugate symmetries at each stage.
5150c
5160 695     j3max=i3+ifp2-np1
5170      do 697 j3=i3,j3max,np1
5180      j2max=j3+np2-j2stp
5190      do 697 j2=j3,j2max,j2stp
5200      j1max=j2+jump2-ifp2
5210      j1conj=j3+j2max+j2stp-j2
5220      do 697 j1=j2,j1max,ifp2
5230      k=1+j1-i3
5240      data(j1)=work(k)
5250      data(j1+1)=work(k+1)
5260      if(j1-j2)697,697,696
5270 696     data(j1conj)=work(k)
5280      data(j1conj+1)=-work(k+1)
5290 697     j1conj=j1conj-ifp2
5300 698     continue
5310      if=if+1
5320      ifp1=ifp2
5330      if(ifp1-np1)700,700,610
5340c
5350c      complete a real transform in the 1st dimension, n even, by con-
5360c      jugate symmetries.
5370c
5380 700     go to (900,800,900,701),icase
5390 701     nhalf=n
5400      n=n+n
5410      theta=-twopi/float(n)
5420      if(isign)703,702,702
5430 702     theta=-theta
5440 703     sinth=sin(theta/2.)
5450      wstpr=-2.*sinth*sinth
5460      wstpi=sin(theta)
5470      wr=wstpr+1.
5480      wi=wstpi
5490      imin=3
5500      jmin=2*nhalf-1
5510      go to 725
5520 710     j=jmin
```

FFT (cont'd.)

```
---
5330      do 720 i=imin,ntot,np2
5340      sumr=(data(i)+data(j))/2.
5350      sumi=(data(i+1)+data(j+1))/2.
5360      difr=(data(i)-data(j))/2.
5370      difi=(data(i+1)-data(j+1))/2.
5380      tempr=wr*sumi+wi*difr
5390      tempi=wi*sumi-wr*difr
5400      data(i)=sumr+tempr
5410      data(i+1)=difi+tempi
5420      data(j)=sumr-tempr
5430      data(j+1)=-difi+tempi
5440 720     j=j+np2
5450      imin=imin+2
5460      jmin=jmin-2
5470      tempr=wr
5480      wr=wr*wstpr-wi*wstpi+wr
5490      wi=tempr*wstpi+wi*wstpr+wi
5500 725     if(imin-jmin)710,730,740
5510 730     if(isign)731,740,740
5520 731     do 735 i=imin,ntot,np2
5530 735     data(i+1)=-data(i+1)
5540 740     np2=np2+np2
5550      ntot=ntot+ntot
5560      j=ntot+1
5570      imax=ntot/2+1
5580 745     imin=imax-2*nhalf
5590      i=imin
5600      go to 755
5610 750     data(j)=data(i)
5620      data(j+1)=-data(i+1)
5630 755     i=i+2
5640      j=j-2
5650      if(i-imax)750,760,760
5660 760     data(j)=data(imin)-data(imin+1)
5670      data(j+1)=0.
5680      if(i-j)770,780,780
5690 765     data(j)=data(i)
5700      data(j+1)=data(i+1)
5710 770     i=i-2
5720      j=j-2
5730      if(i-imin)775,775,765
5740 775     data(j)=data(imin)+data(imin+1)
5750      data(j+1)=0.
5760      imax=imin
5770      go to 745
5780 780     data(1)=data(1)+data(2)
5790      data(2)=0.
5800      go to 900
5810c
5820c     complete a real transform for the 2nd or 3rd dimension by
5830c     conjugate symmetries.
5840c
5850 800     if(ilrng-npi)805,900,900
5860 805     do 860 i3=1,ntot,np2
5870      i2max=i3+np2-npi
5880      do 860 i2=i3,i2max,npi
5890      imin=i2+ilrng
5900      imax=i2+npi-2
5910      jmax=2*i3+npi-imin
5920      if(i2-i3)820,820,810
5930 810     jmax=jmax+np2
5940 820     if(idim-2)850,850,830
5950 830     j=jmax+np0
5960      do 840 i=imin,imax,2
5970      data(i)=data(j)
5980      data(i+1)=-data(j+1)
5990 840     j=j-2
6000 850     j=jmax
6010      do 860 i=imin,imax,np0
6020      data(i)=data(j)
6030      data(i+1)=-data(j+1)
6040 860     j=j-np0
6050c
```

FFT (cont'd.)

```
6260c     end of loop on each dimension
6270c
6280 900    np0=np1
6290      np1=np2
6300 910    nprev=n
6310      return
6320c
6330c     we come here   only in error
6340c
6350 920    write (6, 9601) ndim
6360      return
6370c
6380 930    write (6, 9602) idim, nn (idim)
6390      return
6400c
6410c
6420 9601    format (3(/),10('<*>'),5x,'f o u r t   n o t',
6430&         '   e x e c u t e d',10x,'only',i2,' dimensions')
6440 9602    format (3(/),10('<*>'),5x,'f o u r t   n o t',3x,
6450&         'e x e c u t e d',10x,'length of dimension #',i2,
6460&         ' is only',i4)
6470      end
*
```

AD-A129 690 INTERACTION OF THE RADAR WAVES WITH THE CAPILLARY WAVES 3/3
ON THE OCEAN..(U) KANSAS UNIV/CENTER FOR RESEARCH INC
LAWRENCE REMOTE SENSING L.. S BARKESHLI ET AL. MAY 83
UNCLASSIFIED CRINC/RSL-TR-419-1 N00014-79-C-0533 F/G 17/9 NL

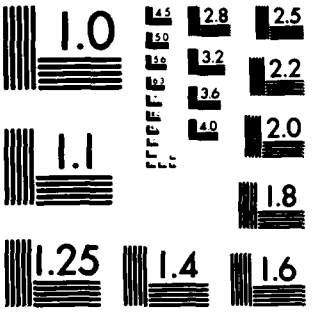

MICROCOPY RESOLUTION TEST CHART
NATIONAL BUREAU OF STANDARDS-1963-A

REFERENCES

Afarani, M., "Directional Properties of Ocean Radar Backscatter—A Harmonic Regression Analysis of AAFE RADSCAT Circle Experiments," Remote Sensing Laboratory Technical Report 186-15, University of Kansas Center for Research, Inc., Lawrence, Kansas, October 1975.

Bass, F.G., I.M. Fuks et al., "Very High Frequency Radiowave Scattering by a Disturbed Sea Surface," IEEE Transactions, vol. AP-16, 1968, pp. 554-567.

Chan, H.L. and A.K. Fung, "Backscattering from a Two-Scale Rough Surface with Application to Radar Sea Return," NASA Contractor Report CR-2327, November 1973.

Chan, H.L. and A.K. Fung, "A Theory of Sea Scatter at Large Incidence Angles," Journal of Geophysical Research, vol. 82, 1977, pp. 3429-3444.

Cox, C. and W. Munk, "Statistics of the Sea Surface Derived from Sun Glitter," Journal of Marine Research, vol. 13, 1954, pp. 198-227.

Donelan, M. and Pierson, W.J., "The Sampling Variability of Estimate of Wind-Generated Gravity Waves,"unpublished paper, 1981.

Fuks, I.M., "Theory of Radiowave Scattering at a Rough Sea Surface," Soviet Radiophysics, vol. 9, 1969, pp. 513-519.

Hasselmann, K., "On the Mass and Momentum Transfer Between Short Gravity Waves and Large-Scale Motions," Journal of Fluid Mechanics, vol. 50, 1971, pp. 189-205.

Jones, W.L., L.C. Schroeder and J.L. Mitchell, "Aircraft Measurements of the Microwave Scattering Signature of the Ocean," IEEE Transactions, vol. AP-25, 1977, pp. 52-61.

Jones, W.L., L.C. Schroeder and J.L. Mitchell, "Aircraft Measurements of the Isotropic Microwave Scattering Signature Over the Ocean for 1975 JONSWAP and 1976 East Coast Missions," NASA TMX-78646, NASA Langley Research Center, Hampton, Virginia, 1978.

Kalmykov, A.I. and V.V. Pustovoytenko, "On Polarization Features of Radio Signal Scattered from the Sea Surface at Small Grazing Angles," Journal of Geophysical Research, vol. 81, no. 12, April 1976, pp. 1960-1964.

Keller, W.C. and J.W. Wright, "Microwave Scattering and the Straining of Wind-Generated Waves," Radio Science, vol. 10, 1975, pp. 139-147.

Keller, W.C. and J.W. Wright, "Modulation of Microwave Backscatter by Gravity Waves in a Wave Tank," NRL Report 7968, Naval Research Laboratory, Washington, D.C., 1976, pp. 1-21.

Kim, Y.S., "Measurement of the Luneberg Lens Cross-Section," Remote Sensing Laboratory Technical Memorandum 419-4, University of Kansas Center for Research, Inc., Lawrence, Kansas, March 1982.

Kwoh, D.S.W. and B.M. Lake, "Microwave Backscatter from Short Gravity Waves: Deterministic, Coherent, Dual-Polarized Study of the Relationship Between Backscatter and Water Wave Properties," presented at the IUCRM Symposium on Wave Dynamics and Radio Probing of the Ocean Surface, May 13-20, 1981, Miami Beach, Florida.

Larson, T.R. and J.W. Wright, "Wind Generated Gravity-Capillary Waves: Laboratory Measurements of Temporal Growth Rates Using Microwave Backscatter," Journal of Fluid Mechanics, vol. 70, 1975, pp. 417-436.

Long, M.W., Radar Reflectivity of Land and Sea, Lexington Books, D.C. Heath and Company, Lexington, Massachusetts 1975.

Longuet-Higgins, M.S., "The Effect of Non-Linearities on Statistical Distributions in the Theory of Sea Waves," Journal of Fluid Mechanics, vol. 17, part 3, 1963, pp. 459-480.

Longuet-Higgins, M.S. and R.W. Stewart, "Radiation Stress in Water Waves: A Physical Discussion with Applications," Deep Sea Research, vol. 11, 1964, pp. 529-562.

Mitsuyasu, H. and T. Honda, "The High Frequency Spectrum of Wind-Generated Waves," Journal of Oceanographical Society of Japan, vol. 30, 1974, pp. 185-198.

Moore, R.K., "Effective Specular Events on Tower and Airborne Measurements of Ocean Backscatter," Remote Sensing Laboratory Technical Memorandum 419-3, University of Kansas Center for Research, Inc., Lawrence, Kansas, January 1982.

Neumann, G. and W.J. Pierson, Principles of Physical Oceanography, Prentice-Hall, Inc., Englewood Cliffs, New Jersey, 1966.

Phillips, O.M., The Dynamics of the Upper Ocean, Cambridge University Press, New York, New York, 1966.

Pierson, W.J. and Fife, P., "Some Nonlinear Properties of Long-Crested Periodic Waves with Lengths Near 2.44 m," Journal of Geophysical Research, vol. 66, 1961, pp. 163-179.

Pierson, W.J. and R.A. Stacy, "The Elevation, Slope and Curvature Spectra of a Wind-Roughed Sea," NASA Contract Report CR-2247, 1973.

Pierson, W.J., "The Theory and Application of Ocean Wave Measuring Systems at and Below the Sea Surface, or the Land, from Aircraft and from Spacecraft," Contractor Report NAS 5-22041, NASA Goddard Space Flight Center, Greenbelt, Maryland, 1975.

Pierson, W.J., Private Communication, 1978.

Plant, W.J. and J.W. Wright, "Growth and Equilibrium of Short Gravity- Capillary Waves in a Wind-Wave Tank," Journal of Fluid Mechanics, vol. 82, 1977, pp. 767-793.

Plant, W.J., W.C. Keller and J.W. Wright, "Modulation of Coherent Microwave Backscatter by Shoaling Waves," Journal of Geophysical Research, vol. 83, 1978, pp. 1347-1352.

Plant, W.J., "Measurement of Ocean Wave--Radar Modulation Transfer Functions," NRL Report (unpublished, 1980).

Valenzuela, G.R., "Depolarization of EM Waves by Slightly Rough Surfaces," IEEE Transactions, vol. AP-15, 1967, pp. 552-557.

Valenzuela, G.R., "Scattering of Electromagnetic Waves from a Tilted Slightly-Rough Surface," Radio Science, vol. 3, 1968, pp. 1057-1066.

Valenzuela, G.R. and M.B. Laing, "Nonlinear Energy Transfer in Gravity- Capillary Wave Spectra, with Applications," Journal of Fluid Mechanics, vol. 54, 1972, pp. 507-520.

Wright, J.W., "Backscattering from Capillary Waves with Application to Sea Clutter," IEEE Transactions, vol. AP-14, 1966, pp. 749-754.

Wright, J.W., "A New Model for Sea Clutter," IEEE Transactions, vol. AP-16, 1968, pp. 217-223.

Wright, J.W., "Detection of Ocean Waves by Microwave Radar: The Modulation of Short Gravity-Capillary Waves," Boundary-Layer Meteorology, vol. 13, 1978, pp.87-105.

Wright, J.W., W.J. Plant and W.C. Keller, "Ocean Wave-Radar Modulation Transfer Functions from the West Coast Experiment," Journal of Geophysical Research, vol. 85, 1980, pp. 4957-4966.

Wu, S.T. and A.K. Fung, "A Noncoherent Model of Microwave Emissons and Backscattering from the Sea Surface," Journal of Geophysical Research, vol. 77, no. 30, 1973, pp. 5917-5929.

CRINC LABORATORIES

Chemical Engineering Low Temperature Laboratory

Remote Sensing Laboratory

Flight Research Laboratory

Chemical Engineering Heat Transfer Laboratory

Nuclear Engineering Laboratory

Environmental Health Engineering Laboratory

Information Processing Laboratory

Water Resources Institute

Technical Transfer Laboratory

Air Pollution Laboratory

Satellite Applications Laboratory